A further restriction, which is only valid for ideally plastic bodies, has been introduced, according to which the magnitude of the yield stress is the same in simple tension and compression. However, this assumption is never met, except, perhaps, only for ideal single crystals. All polycrystalline materials present some small or large difference in yielding under simple tension and compression.

Furthermore, since reversal of one stress influences the sign of J_3 reversing also it, fact which violates the symmetry obligations of the yield criterion, it follows that $f(J_2,J_3)=0$ should be an even function of J_3.

Finally, because of the assumption of isotropy and non-existence of the Bauschinger effect, an interchange in the order of succession of the principal stresses and their opposite values must not influence the yield locus. Therefore, the shape of the yield locus may be fully defined by one of its twelve 30-degree segments limited by a simple axial load and the successive pure shear loading.

Leaving aside in this study Tresca's and Coulomb's yield criteria, which are depending either on the maximum shear stress or on a combination of the maximum shear stress and the hydrostatic stress, we are concentrating to study criteria based on energy assumptions. Among then and the most ancient is the so-called Huber - Mises - Hencky criterion.

It was as early as 1904 that Huber [1] has introduced his yield or brittle-fracture criterion, where he distinguished two cases, when the hydrostatic component of stresses applied to the specimen is either tensile, or compressive. Huber's criterion was based on the distortional component of the elastic energy, for compression, whereas, for tension, the criterion depends on the total elastic energy. Afterwards, von Mises [2], and independently Schleicher [3], have introduced the notion of the *equivalent critical yielding stress*, instead of that of simple shear k, as an arbitrary function of the hydrostatic component of stresses. The criterion was convenient for materials, whose yielding depended on hydrostatic tension or compression, and therefore it presented different critical values for yielding under the different modes of loading.

According to this criterion yielding occurs when the second stress invariant J_2 attains a critical value equal to this energy in simple tension σ_0. Hencky [4] was the first who interpreted this criterion stipulating that yielding begins when the recoverable elastic distortional energy reaches a critical value, equal to the same quantity in simple tension or in pure shear. Then, the J_3-invariant is not involved and, furthermore, it is assumed that hydrostatic tension or compression does not cause any yielding of the material. This may be roughly true only for isotropic metallic specimens when yielding of the overall metallic body is anticipated.

A simpler than Mises's criterion is Tresca's criterion [5], according to which yielding occurs when the maximun shear stress in the body reaches a certain value, that is the respective maximum shear stress in simple tension. Although this criterion is basically not well founded, since it considers only shear stresses creating yielding,

whereas all stresses acting on the body should participate. However, it is frequently used because of its simpicity.

In soils and other materials, for which the hydrostatic component of stresses intereferes significantly in yielding and fracture and where yielding in simple tension is much different to yielding in simple compression, an improvement of the Tresca criterion is the criterion introduced by Coulomb [6] and Mohr [7]. According to this criterion elastic strains are neglected and plastic strain-increments are assumed depending only on the applied stresses. The condition that there is no strain in the z-direction (along the thickness of plane-strain cases) implies a functional dependence of the σ_z-stress on the principal stresses σ_1 and σ_2 along the planes of flow. If the reversal of the stresses assumes a reversal of strain increments, then the σ_z-stress is equal to $(\sigma_1+\sigma_2)/2$ and may be, therefore, eliminated from the yield criterion so that the yielding function is reduced to :

$$f(p, \tau_{max}) = 0 \tag{6}$$

with

$$p = -1/2\,(\sigma_1+\sigma_2) \quad \text{and} \quad t_{max} = 1/2\,(\sigma_1-\sigma_2) \tag{7}$$

where p is the mean compressive stress taking the place of hydrostatic pressure and τ_{max} is the maximum shear stress. Then, the yield criterion may be represented by a locus referred to coordinate axes $1/2\,(\sigma_1+\sigma_2)$ and $1/2\,(\sigma_2-\sigma_1)$. This yield locus is closed on the tension side, if it is assumed that a pure hydrostatic tension may alone produce yielding. Then, Tresca's yield condition with $\tau_{max}=\pm k$, where k is the maximum shear stress in yielding in a state of pure shear, may be assumed as a special case of Mohr's yield condition, when f is independent of p, and the Mohr envelope degenerate, into a pair of parallel lines to the normal-stress σ-axis.

Coulomb-Mohr's criterion is not the only criterion depending on the hydrostatic component of stresses. In this study such criteria will be established and discussed and important results will be derived concerning the behaviour in yielding and fracture of real materials.

Although from the early tests of failure of materials it has been realized that the yield stress in simple tension never coincided with the yield stress in simple compression, it was assumed, at least for the ductile metals, where this difference was not so important, that a complete symmetry of the yield locus exists in the tension and compression spaces. Than, Tresca's and Mises' yield conditions were accepted as describing universally the plastic behaviour of ductile substances [6]. However, in brittle materials, where the ratio of the yield stress in simple compression σ_{0C} is much different to the yield stress in simple tension σ_{0T}, it was accepted that a *Mohr-Coulomb* type of yield locus described the plastic behaviour of these substances [7,8].

Although the *Mohr-Coulomb*, or *internal friction*, criterion fitted satisfactorily the results for nonmetallic geological materials, the agreement established between experimental results and the theory was mainly attributed to the large scatter of experimental results and the lack of such results in the third and most critical quadrant of the principal stress space.

Multiaxial failure criteria were historically developed to characterize the biaxial failure of materials. They represent the maximum stress, maximum shear, maximum strain, maximum strain energy, and distortion energy theories of failure, and may be portrayed as failure loci in a principal stress plane. The simplest of the biaxial criteria represent polygonal failure loci. Generalization to three dimensions is straightforward, and leads, for the simpler criteria, to three-dimensional polygonal failure surfaces in the principal stress space [9]. On the other hand, Tschoegl [10] and independently Theocaris [11] have introduced failure criteria for isotropic bodies, which are based on failure tensor polynomials and which contain all three principal stresses in a symmetric mode. This restricts application of these criteria to isotropic bodies and refers the corresponding failure surfaces to the principal-stress space, as surfaces of revolution around the space diagonal. The space diagonal $\sigma_1=\sigma_2=\sigma_3$, has equal direction cosines $\xi_1=\xi_2=\xi_3=1/\sqrt{3}$ with the positive principal stress axes.

The requirement that the surface should be open in the compressive octant, because hydrostatic compression at moderate pressures cannot lead to failure, restricts the choice of surfaces to *quadrics*. This restriction leaves the cone and the circular paraboloid as the only failure surfaces with the cylinder as special case of both these surfaces. For the two parameters defining a *quadric surface* we can conveniently select the failure stress in simple tension, σ_{0T}, and in simple compression, σ_{0C} [11].

2. THE QUADRIC FAILURE SURFACES FOR ISOTROPIC MATERIALS

2.1 The Conical failure locus

This failure criterion corresponds to the well-known Coulomb criterion [7,12] :

$$|\tau| + \mu\sigma = \tau_0 \qquad (8)$$

where σ and τ are the normal and shear stresses across the plane of failure, τ_0 is the failure stress, amd μ is the so-called coefficient of internal friction. The Coulomb criterion is usually applied to biaxial stressing and τ_0 is then taken as the maximum shear stress. In a triaxial state of stress the simplest modification, which involves the three principal stresses symmetrically, is obtained by considering the τ stress as the octahedral shear stress σ_{ns}, and σ-stress as the mean normal stress σ_{nn}. The criterion can then be stated as :

$$\sigma_{ns} + \mu\sigma_{nn} = \sigma_0 \qquad (9)$$

where σ_0 is a material constant. Eq.(9) is also known as the *Drucker criterion* [13]. This criterion is frequently expressed in the form :

$$\sqrt{I_2} + \beta I_1 = \sigma_Y \qquad (10)$$

where $\beta=\mu/\sqrt{\sigma}$ and $\sigma_Y=\sqrt{3/2}\ \sigma_0$.

The failure surface in the principal stress space for this criterion is a cone with symmetry axis the hydrostatic axis and whose angle at its apex is equal to 2α. Angle α is given by $tg\alpha=\mu$. The intersection of the cone with the $\sigma_2=\sigma_3$ plane is shown in Fig.1.

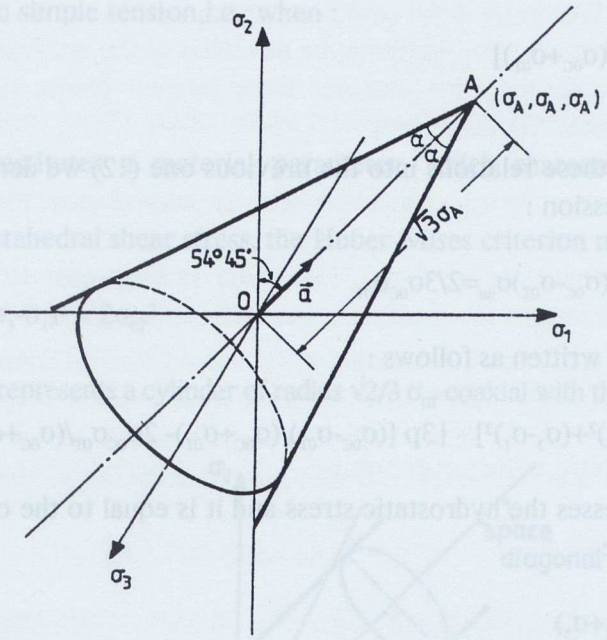

Fig.1 - The conic failure surface.

The apex of the cone A has coordinates $\sigma_A=\sigma_0/\mu$ on the principal stress axes. The cone intersects the positive and negative axes at σ_{0T} and $-\sigma_{0C}$, respectively, where σ_{0C} is the failure stress in simple compression and it is generally larger than σ_{0T} the failure stress in simple tension. For $\sigma_{0C}=\sigma_{0T}$ the cone reduces to a cylinder and Eq. (9) may therefore be regarded as a modification of the Huber-Mises criterion, introducing into it the mean normal stress, weighted by μ.

It is worth noting that Eq.(9) represents a linear combination of the octahedral shear and normal stresses. Expressing μ and σ_0 in terms of an angle 2α and the co-ordinates $\sigma_A=\sigma_A=\sigma_A$ of the apex of cone in the principal stress space Eq.(9) takes the form :

$$\sigma_{ns} ctg\ \alpha + \sigma_{nn} = \sigma_A \quad (11)$$

Inserting Eq.(9) into relation (11) we find :

$$(\sigma_1-\sigma_2)^2+(\sigma_2-\sigma_3)^2+(\sigma_3-\sigma_1)^2-(\sigma_1+\sigma_2+\sigma_3-3\sigma_A)^2 tg^2\alpha=0 \quad (12)$$

This relation represents a cone, coaxial with the hydrostatic axis. It can be readily shown that the co-ordinates σ_A of the apex of the cone and its angle are expressed by [10,11] :

$$\sigma_A = 2\sigma_{0C}\sigma_{0T}/3(\sigma_{0C}-\sigma_{0T})$$

$$tg\alpha = \sqrt{2}\ [(\sigma_{0C}-\sigma_{0T})/(\sigma_{0C}+\sigma_{0T})] \quad (13)$$

Then, introducing these relations into the previous one (12) we derive for the failure criterion the expression :

$$1/\sqrt{2}\ [(\sigma_{0C}+\sigma_{0T})\sigma_{ns}+(\sigma_{0C}-\sigma_{0T})\sigma_{nn}=2/3\sigma_{0C}\sigma_{0T} \quad (14)$$

which may also be written as follows :

$$1/2\ [(\sigma_1-\sigma_2)^2+(\sigma_2-\sigma_3)^2+(\sigma_3-\sigma_1)^2] - \{3p\ [(\sigma_{0C}-\sigma_{0T})/(\sigma_{0C}+\sigma_{0T})- 2\sigma_{0C}\sigma_{0T}/(\sigma_{0C}+\sigma_{0T})]\}^2=0 \quad (15)$$

where $p=\sigma_{nn}$ expresses the hydrostatic stress and it is equal to the octahedral normal stress σ_{nn} given by:

$$p = \sigma_{nn} = 1/3\ (\sigma_1+\sigma_2+\sigma_3) \quad (16)$$

Similarly, the octahedral shear stress, σ_{ns}, is expressed by [5] :

$$\sigma_{ns}^2 = 1/q\ [(\sigma_1-\sigma_2)^2+(\sigma_2-\sigma_3)^2+(\sigma_3-\sigma_1)^2] \quad (17)$$

Moreover, the ratio of the yield or failure stresses in simple compression σ_{0C} and in simple tension σ_{0T} is denoted by :

$$R = \sigma_{0C}/\sigma_{0T} \quad (18)$$

Quantity R is called the *strength differential factor* of the isotropic material.

Relation (10) expresses the equation of a conical failure criterion in terms of the $\sigma_1,\sigma_2,\sigma_3$-principal stresses and the failure stresses σ_{0T} and σ_{0C} for simple tension and compression.

It can be readily shown from relations (13) that when R = 1 and $\sigma_{0C}=\sigma_{0T}$ the apex angle, α, of the cone becomes zero and the distance of the apex $\sqrt{3}\sigma_A$ becomes infinite. This means that the Coulomb-cone degenerates into the Huber-Mises cylinder (9). This criterion is frequently used to represent the yielding of highly ductile materials [3].

In materials failing at small deformations, for which the infinitesimal theory of elasticity is admissible, the cylindrical yield locus is associated with the distortional strain energy. This may not be valid for materials, which undergo large deformation before failure. In this case the theory leading to a cylindrical surface may be referred to as the octahedral shear stress theory, as proposed by Nadai [12]. According to this theory, the material fails when the octahedral shear stress, σ_{ns}, is equal to $\sqrt{2}/3$ times the failure stress in simple tension,i.e., when :

$$\sigma_{nn} = \sqrt{2}/3\ \sigma_{0T} \tag{19}$$

The σ_{0T}-stress constitutes a material parameter, which characterizes the failure behaviour.

Introducing the octahedral shear stress, the Huber-Mises criterion may be stated as :

$$(\sigma_1-\sigma_2)^2+(\sigma_2-\sigma_3)^2+(\sigma_3-\sigma_1)^2 = 2\sigma_{0T}^2 \tag{20}$$

Equation (20) represents a cylinder of radius $\sqrt{2}/3\ \sigma_{0T}$ coaxial with the hydrostatic axis.

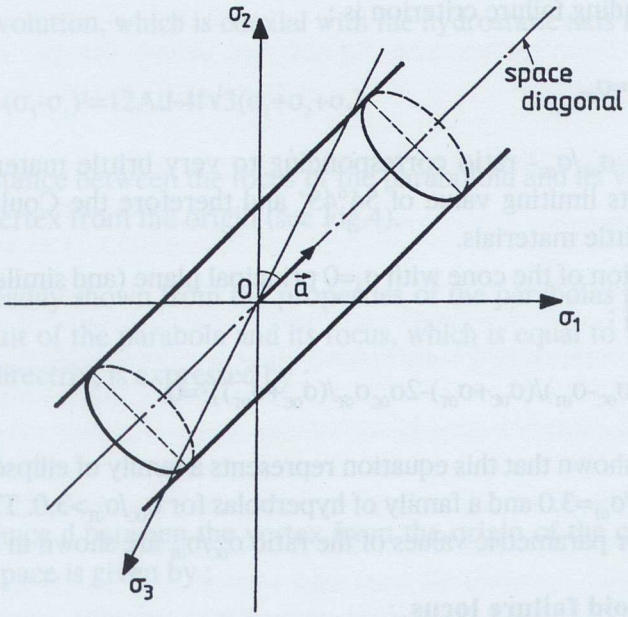

Fig.2 - The cylindrical failure surface

Figure 2 presents the intersection of the cylinder with the plane of symmetry containing the σ_3-axis and the space diagonal. The cylinder cuts the principal stress axes at $\pm\sigma_{0T}$ and the crierion assumes that the failure stress in uniaxial tension and compression are equal. Equation (20) expresses also the fact that failure depends on the octahedral shear stress alone and the octahedral normal stress σ_{nn} is without influence.

The intersection of the failure surface with anyone of the co-ordinate planes yields a failure curve representing, in the plane of the two principal stresses, the associated failure criterion in biaxial loading. The intersection of the cylinder with $\sigma_1=0$ plane is an ellipse, whose major axis lies along the projection of the space diagonal on the $\sigma_1=0$ plane.

Moreover, when $\sigma_{0C}=3\sigma_{0T}$,and therefore $\sigma_A=\sigma_{0T}$, we derive that $tg\alpha=1/\sqrt{2}$, which yields $\alpha_{0T}=35°15'$. This angle is the complementary angle to the angle of the direction cosines of the hydrostatic axis, defining the direction of the octahedral normal stress. For this critical angle the cone disposes three tangent planes parallel to the co-ordinate planes $\sigma_1=\sigma_2$, $\sigma_2=\sigma_3$and $\sigma_3=\sigma_1$.

On the other hand, for $\sigma_{0C}/\sigma_{0T}\rightarrow\infty$ the apex angle becomes $\alpha=54°45'$, which is the complementary one to the α_{0T} and, in this case, the cone dispose three tangent planes parallel to the principal σ_1-, σ_2- and σ_3-axes. Then, the distance of the apex of the cone from origin becomes $\sqrt{3}\sigma_A=2/\sqrt{3}\sigma_{0T}$. This cone corresponds to a totally brittle material. The equation for this limiting cone, with semi-angle $\alpha=54°45'$, becomes :

$$3(\sigma_1\sigma_2+\sigma_2\sigma_3+\sigma_3\sigma_1)- 12p_{0T}+4\sigma_{0T}^2=0 \qquad (21)$$

and the corresponding failure criterion is :

$$1/\sqrt{2}\ (\sigma_{ns}+\sigma_{nn})=2/3=\sigma_{0T} \qquad (22)$$

For values of the σ_{0C}/σ_{0T}- ratio corresponding to very brittle materials the angle α tends rapidly to its limiting value of 54°45' and therefore the Coulomb criterion is justified for all brittle materials.

The intersection of the cone with $\sigma_3=0$ principal plane (and similarly for the other two planes) yields :

$$\sigma_1^2-\sigma_1\sigma_2+\sigma_2^2- \{3p(\sigma_{0C}-\sigma_{0T})/(\sigma_{0C}+\sigma_{0T})-2\sigma_{0C}\sigma_{0T}/(\sigma_{0C}+\sigma_{0T})\}^2=0 \qquad (23)$$

It may be readily shown that this equation represents a family of ellipses for $\sigma_{0C}/\sigma_{0T}<3.0$, a parabola for $\sigma_{0C}/\sigma_{0T}=3.0$ and a family of hyperbolas for $\sigma_{0C}/\sigma_{0T}>3.0$. The conic sections of this criterion for parametric values of the ratio σ_{0C}/σ_{0T} are shown in Fig.3.

2.2 The paraboloid failure locus

The paraboloid failure criterion constitutes a linear combination of a term depending on

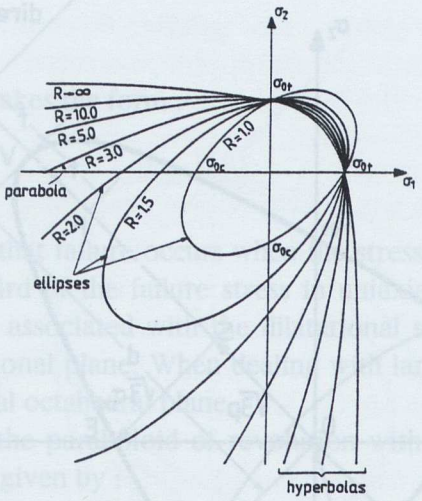

Fig.3 - Conic sections for the conic failure criterion for parametric values of R

the mean normal stress and the square of the octahedral shear stress. It is an attracting compromise among all other criteria because it avoids the physically unlikely angular apex of the cone in the first octant of principal stress space. The equation for a paraboloid of revolution, which is coaxial with the hydrostatic axis is given by [11] :

$$(\sigma_1-\sigma_2)^2+(\sigma_2-\sigma_3)^2+(\sigma_3-\sigma_1)^2=12Ad-4f\sqrt{3}(\sigma_1+\sigma_2+\sigma_3) \qquad (24)$$

where f is the distance between the focus of the paraboloid and its vertex, and d is the distance of the vertex from the origin (see Fig.4).

It may be readily shown from the properties of the parabolas that the distance f between any point of the parabola and its focus, which is equal to the distance of its vertex from its directrix, is expressed by :

$$A = (\sigma_{0C}-\sigma_{0T})/2\sqrt{3} \qquad (25)$$

whereas the distance d between the vertex from the origin of the co-ordinates in the principal stress space is given by :

$$d =\sigma_{0C}\sigma_{0T}/\sqrt{3}(\sigma_{0C}-\sigma_{0T}) \qquad (26)$$

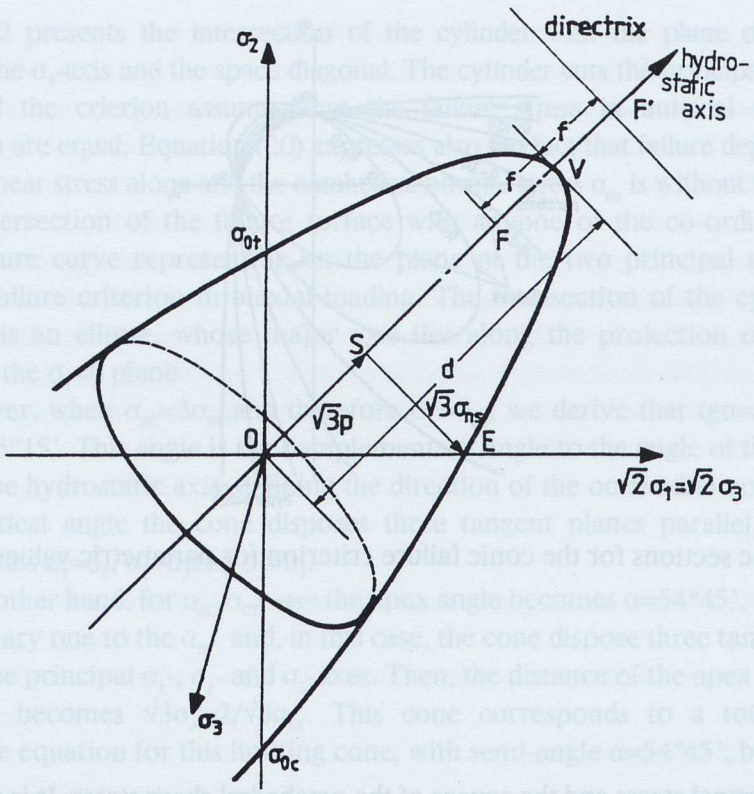

Fig.4 - The elliptic paraboloid failure surface. The intersection of the paraboloid failure surface with the plane $\sigma_1=\sigma_3$.

Then introducing these values into Eq.(24) we derive for the equation of the paraboloid the expression :

$$(\sigma_1-\sigma_2)^2+(\sigma_2-\sigma_3)^2+(\sigma_3-\sigma_1)^2+6p(\sigma_{0C}-\sigma_{0T})-2\sigma_{0C}\sigma_{0T}=0 \quad (27)$$

whereas the corresponding failure criterion takes the form :

$$\sigma_{ns}^2+2/3(\sigma_{0C}-\sigma_{0T})\sigma_{nn}-2/q\ \sigma_{0C}\sigma_{0T}=0 \quad (28)$$

This criterion in terms of J_2 -and I_1-invariants is expressed by :

$$3J_2+(\sigma_{0C}-\sigma_{0T})I_1=\sigma_{0C}\sigma_{0T} \quad (29)$$

Figure 4 presents also the intersection of the paraboloid with the $\sigma_1=\sigma_3$ plane. For $\sigma_{0C}=\sigma_{0T}$ the focus is receding to infinity and the paraboloid, just as the cone, transforms into a cylinder.

On the other hand, the paraboloid degenerates into the principal octaherdal plane for $\sigma_{0C}/\sigma_{0T}\rightarrow\infty$. Its equation becomes :

$$\sigma_1+\sigma_2+\sigma_3=\sigma_{0T} \tag{30}$$

and the failure criterion takes the form :

$$\sigma_{nn}=1/3\sigma_{0T} \tag{31}$$

Relation (31) states that failure occurs when the stress normal to the octahedral plane is equal to one-third of the failure stress in uniaxial tension. In small strain theory the plane can be associated with the dilatational strain energy and is often referred to as the dilatational plane. When dealing with large deformations it is best referred to as the principal octahedral plane.

The intersection of the paraboloid of revolution with the $\sigma_3=0$ plane yields an ellipse whose equation is given by :

$$\sigma_1^2-\sigma_1\sigma_2+\sigma_2^2+3p(\sigma_{0C}-\sigma_{0T})=\sigma_{0C}\sigma_{0T} \tag{32}$$

This ellipse degenerates into a straight line for $\sigma_{0C}/\sigma_{0T}\to\infty$. In this case we have :

$$\sigma_1+\sigma_2=\sigma_{0T} \tag{33}$$

Figure 5 presents the intersections of the paraboloids of revolution with the $\sigma_3=0$ plane of parametric values of the σ_{0C}/σ_{0T}-ratio varying between unity and infinity.

It is worthwhile now giving the distance $\sqrt{3}\sigma_F$ of the locus of the paraboloid from the origin. This quantity is given by :

$$\sqrt{3}\sigma_F=1/2\sqrt{3}\{(4\sigma_{0C}\sigma_{0T}-\sigma_{0C}^2-\sigma_{0T}^2)/(\sigma_{0C}-\sigma_{0T})\} \tag{34}$$

Finally, the following remarks concerning the applicability of these three types of criteria seems to be in order :

i) The Mises-Hencky failure criterion depends only on the octahedral shear stress and it is represented by a cylidrical surface with axis the hydrostatic axis. It is convenient only for materials which obey the equality $\sigma_{0C}=\sigma_{0T}$. Since none of the engineering materials follows this assumption this criterion is convenient only for monocrystals and very ductile materials.

ii) The other two criteria, the conic and the paraboloid of revolution, depend on both the octahedral shear and the normal stresses. Therefore, they take into consideration not only the influence of the distortional part of the strain energy, but also its dilatational part. Moreover, these criteria are better adapted to the real behaviour of the engineering substances, since they take care, in a rational way, of the existing differences in the failure charcteristics of the materials when they are subjected either to simple tension, or to simple compression. Such differences cannot be encountered

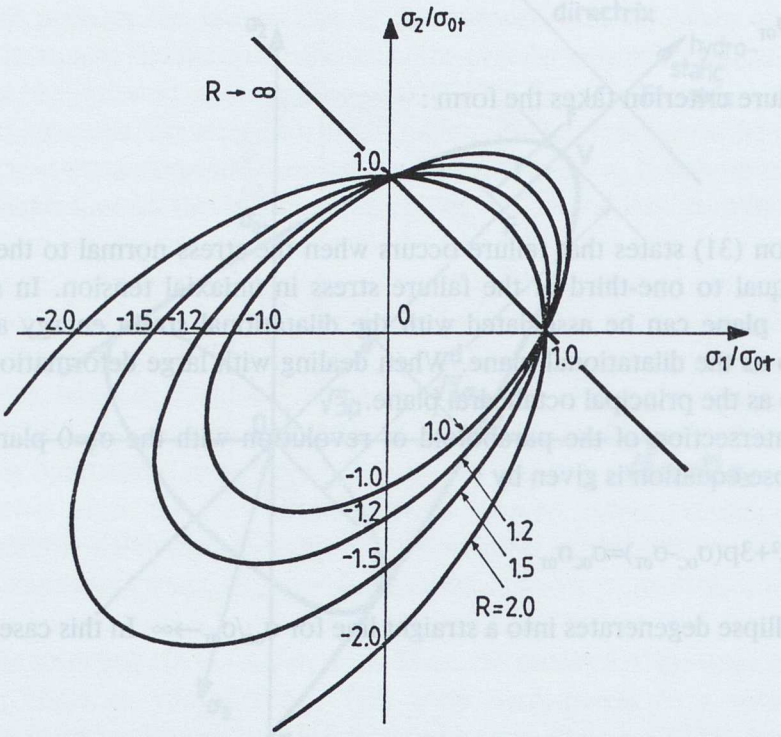

Fig. 5 - Intersections of the elliptic paraboloid failure surface with the σ_3=0 plane for parametric values of R.

either by the Mises-Hencky or the Tresca types of yield or failure criteria.

iii) Comparing the Coulomb cone, expressed by relation (19), or its intersection with one principal stress plane expressed by relation (23), with the respective relationships for the paraboloid given by Eqs.(27) and (32), it becomes clear that the expressions for the paraboloid are much simpler than those of the Coulomb criterion. Therefore, the paraboloid failure surface criterion constitutes the simplest variant of a general criterion which describes with high accuracy an extremely wide class of experimental data.

The paraboloid failure criterion avoids the physically unlike fact that real materials under an hydrostatic tensile loading dispose a unique failure point, the apex of their failure locus. Based on theoretical considerations for the failure envelope in the Coulomb-Mohr theory it has been shown (see Ref.[6], chapt.XI.3 pp.294-300) that only for certain conditions fulfilled in the compression zone of loading there is a real contact between the failure stress circles and the failure envelope. Moreover, experimental evidence with brittle materials [14] indicated clearly that the angular apex of the cone in the Coulomb-Mohr criterion is rather physically improbable, and the failure behaviour of substances in this zone of loading fits better a smooth curve resembling the respective zone of an paraboloid of revolution.

We shall see in the following that such a criterion based on a paraboloid surface

fits well the existing experimental evidence with a variety of substances and explains satisfactorily their failure behaviour, thus presenting a considerable versatility and adaptility to become a generalized failure criterion.

2.3 Experimental evidence for failure criteria of the paraboloid type

Extensive experimental evidence on metallic, polymeric and geological materials has indicated a clear dependence of their yield loci on their respective strength differential factors R. The very meticulous early experiments by Coffin [15] on gray cast-iron, a very brittle material, with $\sigma_{0C}=100\text{x}10^3$ psi and $\sigma_{0T}=33\text{x}10^3$ psi and Grassi and Cornet [15] with $\sigma_{0C}=96\text{x}10^3$ psi and $\sigma_{0T}=28.5\text{x}10^3$ psi gave, both of them, a value for R=3.0. Figure 6 presents the yield locus of these materials normalized to the yield stress σ_{0T} in simple tension. It is clear from this figure that all experimental results fit excellently the paraboloid failure criterion.

Figure 6 presents the same conical section of the paraboloid but now with a strength differential factor R=3.0 in the plane $\sigma_3/\sigma_{0T}=0$. In this principal plane it is valid that $\sigma_1/\sigma_{0T}=\sigma_2/\sigma_{0T}=1.0$, whereas $-\sigma_1/\sigma_{0T}=-\sigma_2/\sigma_{0T}=-3.0$. Although there are not sufficient data in the compression-compression quadrant, it is clear that the materials follow such a form of criterion.

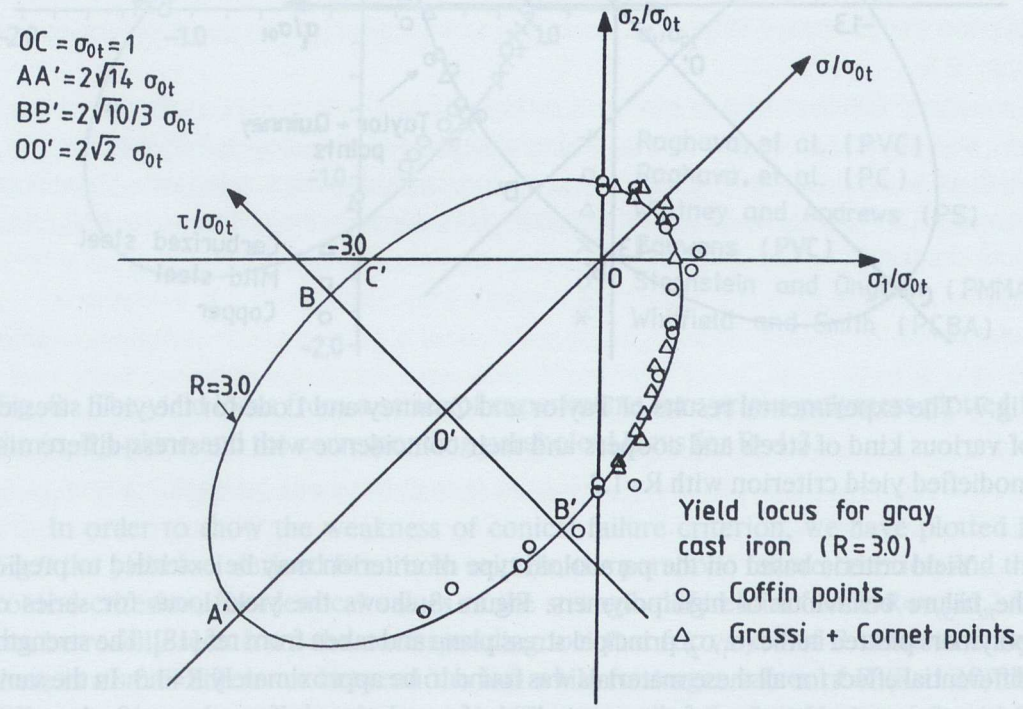

Fig.6 - The yield locus for gry cast-iron with R=3.0 and the experimental points derived from tests of Coffin & Grassi and Cornet.

On the other hand, concerning the yielding mode of various ductile materials, the most famous experiments by Taylor and Quinney [16] indicate clearly that aluminum and copper, with R approaching unity, obey satisactorily the Mises yield criterion. However, mild-steel specimens deviate considerably with all the existing experimental points lying consistently outside the Mises yield locus [6]. It can then readily be proven that these values obey a paraboloid criterion with a strength differential factor equal R=1.30. Figure 7 presents the results of Taylor and Quinney, as well as the equally important results of Lode [17] for various types of steels and copper, which again show an excellent agreement with the paraboloid type of criterion with R=1.30.

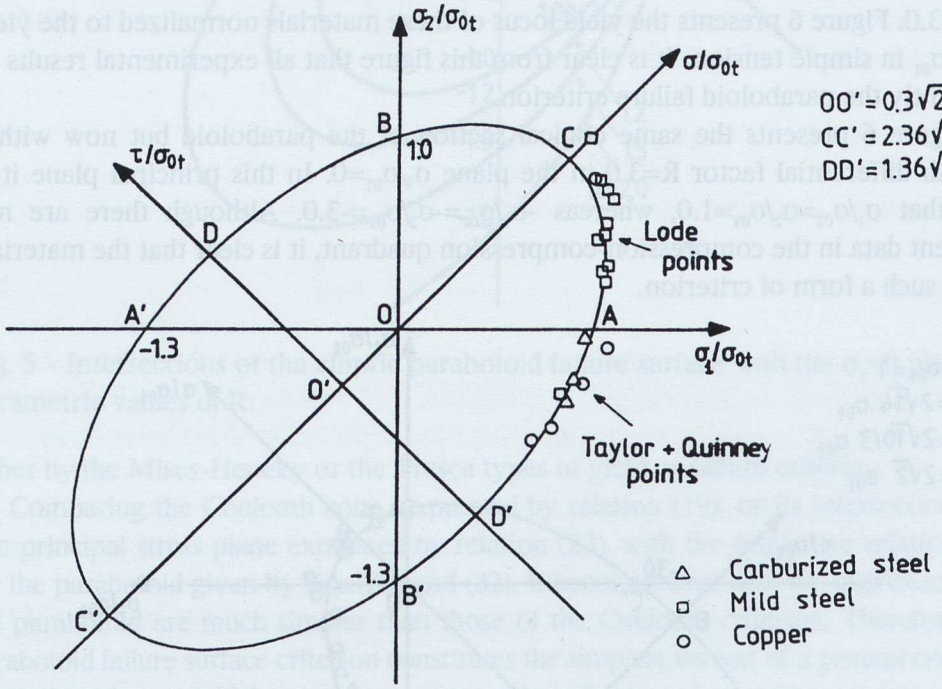

Fig.7- The experimental results of Taylor and Quinney and Lode for the yield stresses of various kind of steels and coopers and their coincidence with the stress-differential modiefied yield criterion with R=1.3

Yield criteria based on the paraboloid type of criterion may be extended to predict the failure behaviour of high polymers. Figure 8 shows the yield locus for series of polymers plotted in the (σ_1,σ_2) principal stress plane and taken from ref.[18]. The strength-differential effect for all these materials was found to be approximately R=1.3. In the same figure the conical section of the paraboloid of revolution surface the σ_3=0 plane was plotted for R=1.30 and represented by a continuous ellipse. It is clear from this figure that again the paraboloid of revolution failure criterion corroborates all experimental results.

On the other hand, experiments executed by Spitzig et al. [19] on various types of steels, presenting strength differential ratios $\sigma_{0C}/\sigma_{0T}=1.055$, fit the conical type of criterion. The values for the tangent of the semi-angle, α of the apex of the cone were found to be tg $\alpha=0.026$ and 0.028 respectively, whereas the distance $\sqrt{3}\,\sigma_A$ of the apex of the cone from the origin of the co-ordinates, multiplied by the factor $\sqrt{3}/2$ R, were given as $\sqrt{2}\,R\sigma_A=1.480$ and 1.066 MPa. However, from the respective values of σ_{0C} and σ_{0T} these quantities are 1.47 MPa and 1.070 MPa respectively. Although the theory by Spitzig et al., based on the conical failure criterion, yields satisfactory results, these results, with ratios σ_{0C}/σ_{0T} of the order of R=1.10, correspond to yielding loci, which differ only slightly between theories and, therefore, they are not decisive for the selection of the correct criteria.

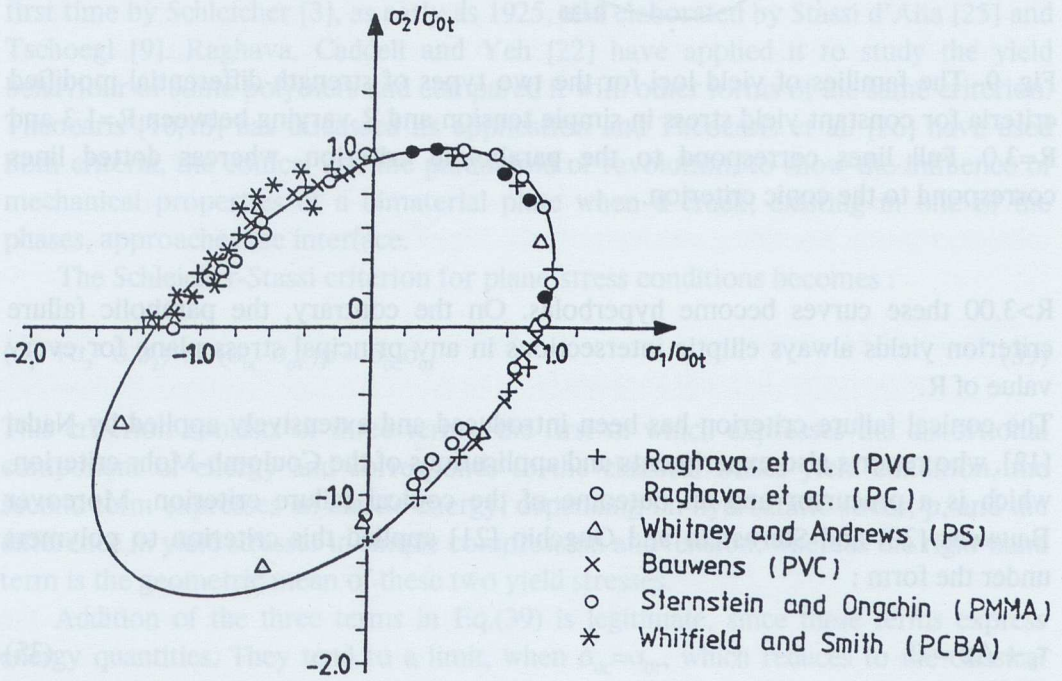

Fig. 8 - The yield locus from a series of experiments for various polymers plotted in the (σ_1,σ_2)-plane and the corresponding paraboloid locus for R=1.3.

In order to show the weakness of conical failure criterion, we have plotted in Fig.9 the yield loci derived from both criteria, the parabolic failure criterion and the conical criterion, for identical values of the strength-differential factor $R=\sigma_{0C}/\sigma_{0T}$. It can be readily seen from the corresponding loci that for values of R close to unity, there is a small difference between the loci while for larger values of R (R>1.10) the differences increase and they become significant, so that, for brittle materials with R approaching values of 3.00, the ellipses of the conical failure criterion degenerate into a parabola passing through the points (1, 0), (0, 1) and (0,-3),(-3, 0), whereas for

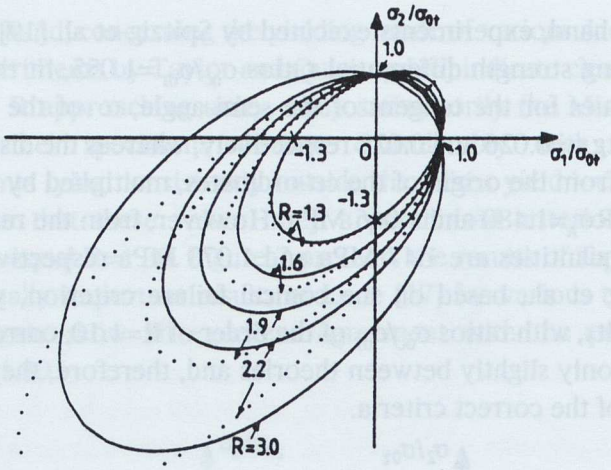

Fig. 9- The families of yield loci for the two types of strength-differential modified criteria for constant yield stress in simple tension and R varying between R=1.3 and R=3.0. Full lines correspond to the paraboloid criterion, whereas dotted lines correspond to the conic criterion.

R>3.00 these curves become hyperbolas. On the contrary, the parabolic failure criterion yields always elliptic intersections in any principal stress plane for every value of R.

The conical failure criterion has been introduced and extensively applied by Nadai [12], who reports also experiments and applications of the Coulomb-Mohr criterion, which is a precursor and an outcome of the conical failure criterion. Moreover Bauwens [20] and Sternstein and Ongchin [21] applied this criterion to polymers under the form :

$$\tau_n + Ap = C \qquad (35)$$

where τ_n is the octahedral shear stress, which is directly related to the second stress invariant J_2, p is the mean normal stress, and A and C are real constants, with the constant C, having dimensions of stress. As it is pointed out by Raghava et al.[22], eq.(35) is another expression of the relationship :

$$\sqrt{3}\, J_2^{1/2} + aI_1 = c \qquad (36)$$

in which it was also taken into account that the odd dependence of any failure and yield criterion on the J_3-stress invariant is insignificant, and it may therefore be neglected.

In this relation (36) the quantity α is the so-called mean stress coefficient and the constant c expresses the basic strength of the material [23]. This criterion for

constant values of α and c coincides with the Drucker-Prager criterion for soils [24].

The constants A and C in the criterion of Eq. (35) are expressed by :

$$A = (\sigma_{0C}-\sigma_{0T})/(\sigma_{0C}+\sigma_{0T}) \quad \text{and} \quad C = \sigma_{0C}\sigma_{0T}/(\sigma_{0C}+\sigma_{0T}) \tag{37}$$

which, when compared with relations (16) and (17) of the conical failure criterion, yield :

$$A = \sqrt{2}/2 \ \text{tg}\alpha \quad \text{and} \quad C = 3/2\sqrt{2}\ \sigma_A \text{tg}\ \alpha \tag{38}$$

In the same context the paraboloid of revolution criterion was suggested for the first time by Schleicher [3], as early as 1925, and elaborated by Stassi d'Alia [25] and Tschoegl [9]. Raghava, Caddell and Yeh [22] have applied it to study the yield behaviour of some polymers and compared it with other forms of the same criterion. Theocaris [10,18] has discussed its application and Theocaris et al. [26] have used both criteria, the conical and the paraboloid of revolution, to show the influence of mechanical properties of a bimaterial plate when a crack, existing in one of the phases, approaches the interface.

The Schleicher-Stassi criterion for plane-stress conditions becomes :

$$(\sigma_1^2 + \sigma_2^2 - \sigma_1\sigma_2) + 3\ (\sigma_{0C}-\sigma_{0T})p = \sigma_{0C}\sigma_{0T} \tag{39}$$

This criterion consists of three terms, the first of which expresses the distortional component of energy and corresponds to the classical Mises yield condition, the second term expresses an elastic energy, depending on hydrostatic stress, p, and the difference in yield stresses in simple compression and tension, whereas the right-hand term is the geometric mean of these two yield stresses.

Addition of the three terms in Eq.(39) is legitimate, since these terms express energy quantities. They tend to a limit, when $\sigma_{0C}=\sigma_{0T}$, which reduces to the classical Mises yield condition for ductile materials. Moreover, for $\sigma_{0C} \gg \sigma_{0T}$, when it may be assumed that $\sigma_{0T}/\sigma_{0C} \to 0$, Eq. (39) represents an ellipse, which is equal in size to the typical Mises ellipse, with $\sigma_{0C}=\sigma_{0T}$, and it passes through the origin of coordinates in a $(\sigma_1/\sigma_{0C}, \sigma_2/\sigma_{0C})$-diagram, as well as through the points (-1, 0) and (0, 1). All other ellipses, if they are referred to the same yield stress in simple compression σ_{0C}, are smaller in size than these two limit curves and they pass, through the points (-1, 0) and (0, -1). Figure 10 presents the family of the yield-loci according to the Schleicher-Stassi criterion when normalized to the same yield stress in simple compression. It is clear from this figure that the ellipses for R=1.0 and R=Ξ are equal. Contrariwise, Fig. 11 which presents a similar family of yield loci, but for the same yield stress in simple tension, contains ellipses, whose sizes increase progressively as R is increasing, but all ellipses pass through the points (1, 0) and (0, 1) in the σ_1/σ_{0T}, σ_2/σ_{0T} principal stress space.

Comparing the yield loci resulting from the two models and the experimental data available for various materials it may be concluded that, whereas the Schleicher-Stassi criterion corroborates satisfactorily the existing experimental evidence with various materials, the Nadai-Bauwens-Sternstein criterion deviates significantly, especially in the critical compression-compression quadrant.

Furthermore, a noticeable difference between the two types of criteria exists, which influences considerably the reliability of their results. Indeed, the Nadai-Bauwens-Sternstein failure criterion, derived from the conical criterion, as it is expressed by relation (28), considers an algebraic addition of stresses, which are not collinear. The octahedral shear stress, τ_n, lies always on the deviatoric plane, whereas the hydrostatic component, p, is always normal to this plane. Therefore, any algebraic addition of these stresses is meaningless. Their addition is explained if we consider from relation (15) that only the component of octahedral shear stress multiplied by the ctg α becomes collinear to σ_{nn}-stress and therefore it can be added to it. On the contrary, addition of the terms in Eq.(32) is legitimate, since these terms express energy components, which are scalar quantities. This is another reason to consider this criterion and therefore the paraboloid of revolution criterion, as a reliable criterion describing satisfactorily the failure mode of engineering substances.

2.4 The void-formation process and its influence to failure

It has been lately shown that the influence of the hydrostatic component of stresses on yielding is directly related to the mechanism of local void nucleation and growth in regions of high-concentration. Therefore, the void nucleation and development is followed by a bulk dilatancy, or, inversely, in materials containing intitialy voids, due to their structure, a void closure is developed during volume contraction. Both procedures have a result to change drastically the yield behaviour of the material.

Many models have been recently introduced, which are based on the development of voids and their influence on the yield criterion of the materials. The McClintock model [27] assumes that a mechanism of localization of deformation, which starts from some discontinuity of the substance (macrovoid, grain boundary, crack) is developed along within a narrow shear band, due to the progressive reduction of hardening of the material as the loading of the material along a zone ahead of the dincontinuity increases, because of the progressive softening of the material by the increasing porosity at the dincontinuity. Then, the material along this zone is damaged to such an extent that microvoids begin to appear with increasing load. Further loading induces the formation of a population of voids, usually in an enclave, which ultimately coalesces with its neighbour void concentrations and produces a propagation of the discontinuity.

This process is preceded by an incubation period for cavity nucleation, which is always short, followed by a rapid development and spreading out of the void zone.

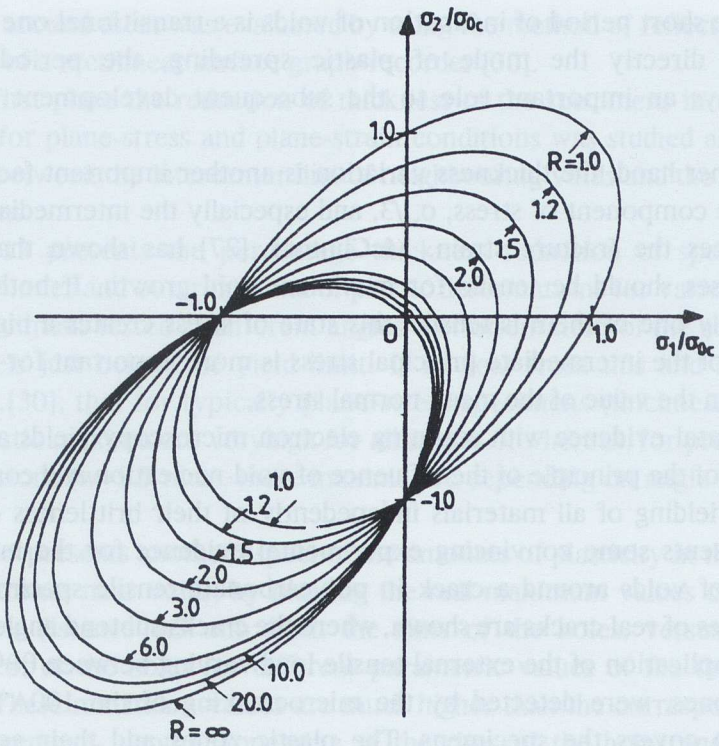

Fig. 10 - The family of the strength-differential modiefied yield criteria with R varying between unity and infinity for the same yield-stress in uniaxial compression.

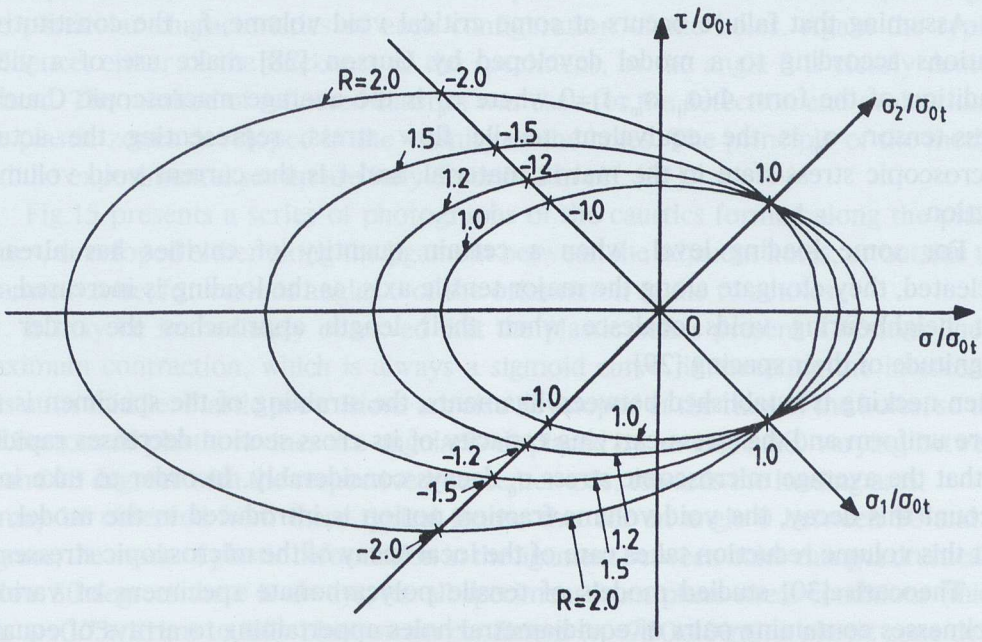

Fig.11 - The family of the strength-differential modiefied yield criteria with R varying between unity and R=2.0, for the same yield-stress in uniaxial tension in the (σ,τ)-plane.

Thus, while the short period of incubation of voids is a transitional one and it does not influence directly the mode of plastic spreading, the period of cavity nucleation plays an important role to the subsequent development of regional yielding.

On the other hand, the thickness variation is another important factor because the hydrostatic component of stress, $\sigma_{kk}/3$, and especially the intermediate principal stress, influences the fracture strain. McClintock [27] has shown that the three principal stresses should be tensile for maximum void growth. If both transverse stresses, or only one of them is tensile, this state of stress creates a big difference, since the role of the intermediate principal stress is more important for plane stress conditions, than the value of the mean-normal stress.

Experimental evidence with scanning electron microscopy yields ample proof of the validity of the principle of the influence of void-nucleation and coalescence to the mode of yielding of all materials indepedently of their brittleness or ductility. Figure 12 presents some convincing experimental evidence for the initiation and development of voids around a crack in polycarbonate tensile specimens. In this figure four cases of real cracks are shown, where the cracks subtend angles θ with the direction of application of the external tensile load varying between $\theta=90°$ and 15°. The plastic zones, were detected by the microcracking of the 100A° aluminium coating, which covers the specimens. The plastic zones and their geometry are obvious from these figures where the cracking of the coating presents families of principal strain trajectories.

Assuming that failure occurs at some critical void volume, f_C, the constitutive relations according to a model developed by Gurson [28] make use of a yield condition of the form $\Phi(\sigma_{ij}, \sigma_m, f)=0$ where σ_{ij} is the average macroscopic Cauchy stress-tensor, σ_m is the equivalent tensile flow stress, representing the actual macroscopic stress-state in the matrix material, and f is the current void volume-fraction.

For some loading level, when a certain quantity of cavities has already nucleated, they elongate along the major tensile axis, as the loading is increased, so that neighbouring voids coalesce when their length approaches the order of magnitude of their spacing [29].

When necking is established between ligaments, the straining of the specimen is no more uniform and the stress-carrying capacity of its cross-section decreases rapidly, so that the average microscopic stress σ_{ij} decays considerably. In order to take into account this decay, the void-volume-fraction notion is introduced in the model, so that this volume reduction takes care of the local decay of the microscopic stresses.

Theocaris [30] studied models of tensile polycarbonate specimens of various thicknesses containing pairs of equidiametral holes appertaining to arrays of equally spaced performations, taking the place of neighbour microvoids in the material. The thickness reduction in the intercenter zone between holes, as well as the stress

distribution around them was evaluated by using the method of reflected caustics and the plotting of a rectilinear surface graph-recorder [30].

In the first place the reduction of thickness of the specimens in the in-between void zones for plane-stress and plane-strain conditions was studied as a function of the angle θ between the intercenter line of neighbouring voids and the loading axis of the specimen.

Figure 13 presents the percentage thickness reduction of specimens at the zones of the inner and outer maxima of plastic deformations for various thicknesses w of the specimens tested at different angles θ of orientation of the holes for tensile loading levels just below the yield limit. It is clear from this and similar figures given in ref.[30], that for typically plane-stress specimens (thickness below w=1.5 mm) the plastic maxima are veryhigh for all angles θ, whereas, for prevailing plane-strain conditions (w=9.5 mm), these maxima are depending on angle θ and they are very low.

Figure 14 presents another aspect of the amounts of plasticity in the outer squid-like, plastic zones near voids, by plotting the real maximum values of outer plastic enclaves at a distance 0.5 mm from the rims of the holes, versus the angle of orientation, θ, of the holes for different parametric values of the thickness of the specimens. These maximum-values are much higher than the corresponding relative maxima percentage- depths, appearing at the rims of the holes and presented in Fig.12. Although all specimens were loaded with identical overall tensile stresses at infinity, the shapes, forms and sizes of the plastic zones are different, depending on the particular characteristics of each configuration of the holes. Again the typical influence, either of the thickness of the specimens, or the angle θ is clearly demonstrated. The method of reflected caustics was used for the detection and evaluation of the plastic zones developed in the vicinity of the holes. The principle of the method and the experimental set-up are fully described in ref. [31].

Fig.15 presents a series of photographs of the caustics formed along the plastic zones, developed either along the ligament between the adjacent holes, or outside this ligament-zone, for various angles θ of the orientation of the two holes.

It may be immediately observed that the plastic zones present a bottom line of maximum contraction, which is always a sigmoid curve, intersecting the intercenter axis at its middle. Plastic protrusions are also developed at the rims of the holes, so that the bottom of plastic ravines are angularly displaced by an angle Δθ, varying between 10 and 18 degrees with the respective intercenter axis, towards the loading axis.

It may be observed from these typical figures that for an angle θ between 50 and 55 degrees, the mode of plastic deformation in the ligament between holes changes drastically. Below 50 degrees there is always, for all specimens from plane-stress conditions (thickness $w=0.75\times10^{-3}$m) to fully plane-strain conditions ($w=9.50\times10^{-3}$m), a plastic zone developed between holes. Above 55 degrees the plastic deformation changes mode, presenting plastic asymmetric zones on both sides of each hole. These squid-like plastic zones ex-

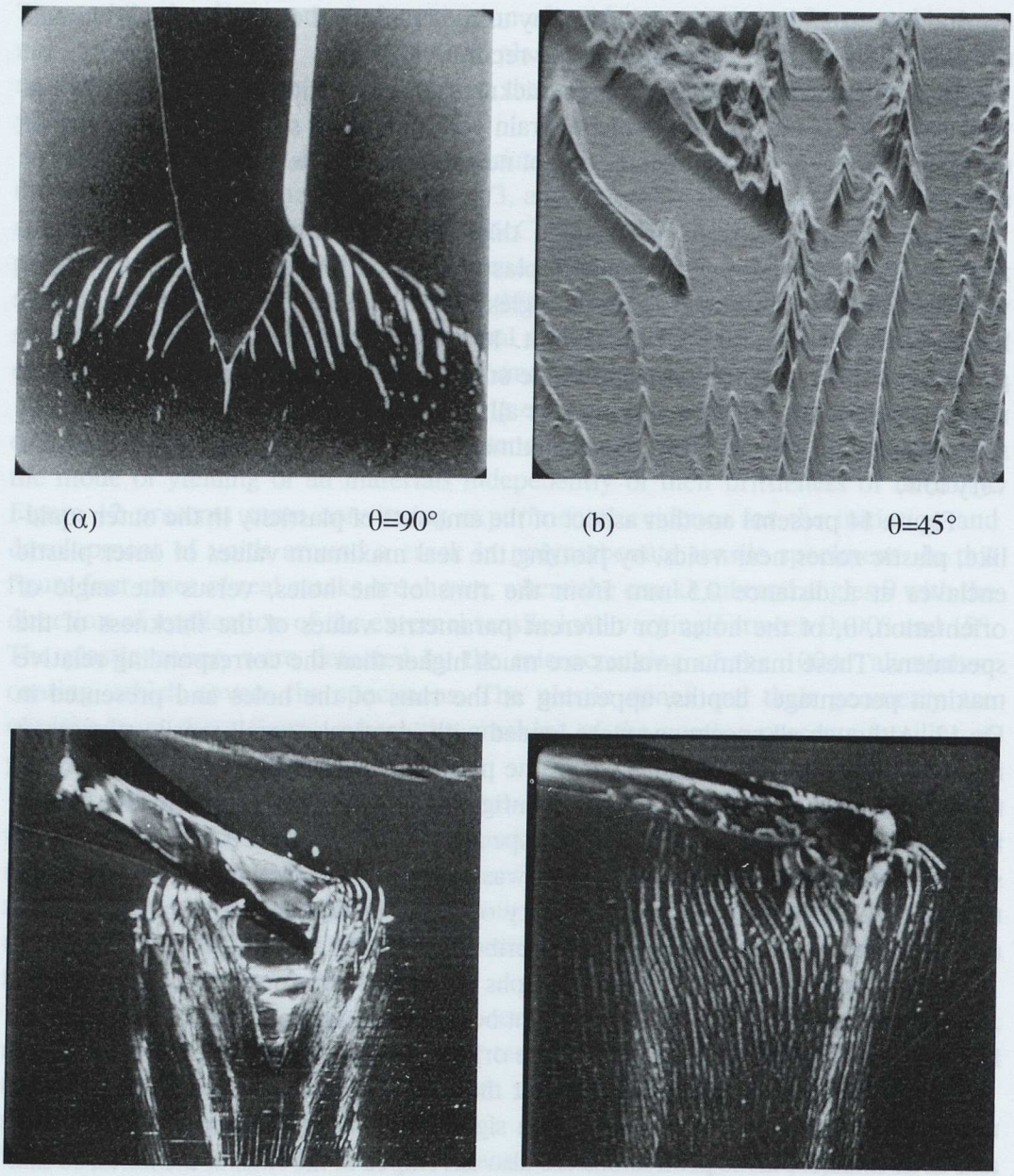

Fig.12 - A series of scanning electron micrographs showing the plastic zones developed around the crack-tips in polycarbonate plates containing oblique cracks with angles θ=90°, 45°, 30° and 15°. The development of voids in these plastic zones is obvious in some of these figures.

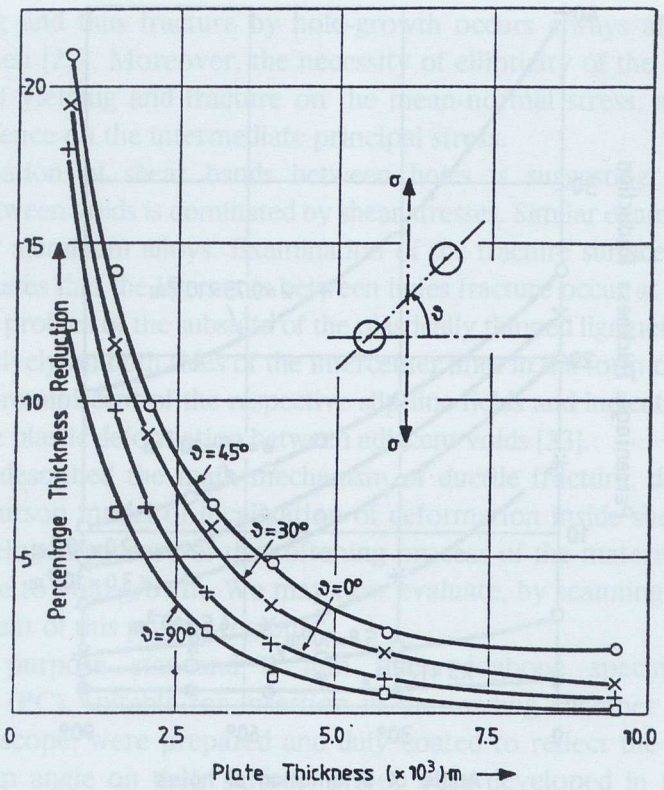

Fig.13 - The percentage maximum reduction of the thickness of the specimens at the plastic zones developed outside the intercenter zone between holes, versus the specimen thickness for different angles of inclination of the intercenter line.

tend to different lengths, and unsymmetrically on both sides of the central part of holes, forming an angle with the respective radial directions. This change of mode development of the plastic enclaves around holes remains unchanged, if the thickness of the specimens is increased, and the state of deformation changes from plane-stress to plain-strain.

From this experimental study it may be concluded that all voids, developed in the vicinity of cracks participate in the fracture mechanism of the plate. Those, which are oriented with angles θ smaller than 55 deg., contribute to the failure process by creating plastic bridges between voids, which afterwards evolute and create probable paths of crack propagation by kinks. The voids which are forming between the holes for angles greater than 55 deg. develop squid-like external plastic enclaves, which are oriented almost parallely to the crack-axis and they may coalesce with neighbouring voids. These voids also facilitate the prospective extension of the crack, since they create transverse bridges between neighbouring voids.

This kind of deformation is developed in plates with clusters of voids under uniaxial tensile loading at the zome of the cloud of voids. Since the elastic- and the

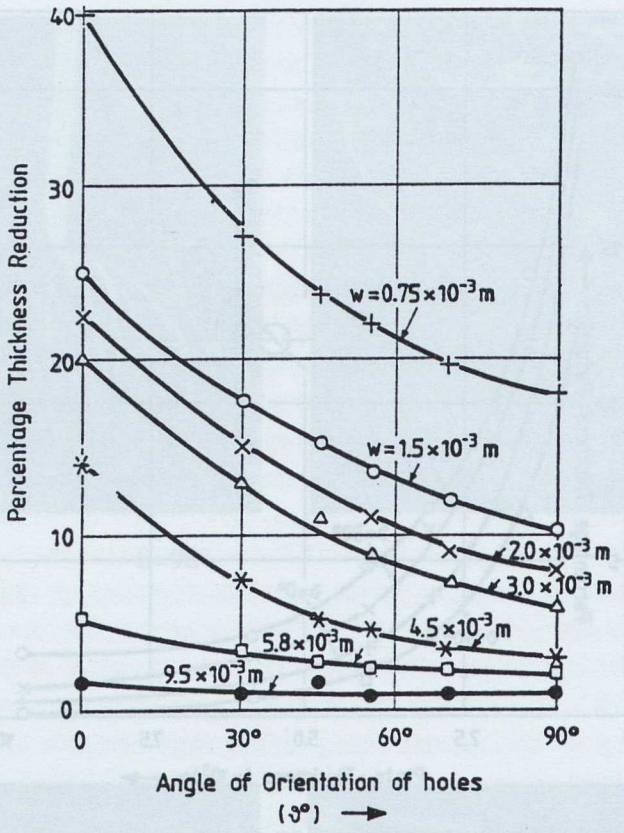

Fig.14 - The percentage maximum reduction of the thickness of the specimens at the plastic zones outside the intercenter zone between holes versus the angle of orientation of the holes for different parametric values of the thickness of the specimen, from plane-stress to plain-strain conditions.

plastic-stress fields in front of a crack, are generally biaxial for plane-stress, or triaxial for plain strain, and in the general case, the intermediate components of stresses in the plane of the plate contribute significantly to the mode of crack propagation. This is achieved by providing an additional stress field of smaller intensity, but oriented by 90 deg.to the main σ_y-stress field, which is participating to the development of voids in regions, where the main stress field, because of its orientation ($\theta \geq 55°$), cannot create plastic ligaments between adjacent voids, provided it is an overall tensile field. Although the experimental evidence presented in the previous figures is based on the plastic straining of a glassy polymer, qualitatively the same phenomena are expected to appear for crystalline metallic specimens, provided their mode of fracture is similar. This series of results corroborates the findings by McClintock, who has introduced the condition that the holes should remain open

during loading and thus fracture by hole-growth occurs always after necking of a tensile specimen [27]. Moreover, the necessity of ellipticity of the holes implies the dependence of yielding and fracture on the mean-normal stress, and especially its strong dependence on the intermediate principal stress.

The formation of shear bands between holes is suggesting that the link-up mechanism between voids is dominated by shear stresses. Similar examples are reported in ref. [32] for aluminum alloys. Examination of the fracture surface profiles in these examples indicates that the ligaments between holes fracture occur at angles $\theta\Theta60$ deg. Moreover, the profiles of the substata of the plastically thinned ligaments between holes deviate successively on both sides of the intercenter lines in the form of sigmoid curves, a fact which is reminiscent of the respective slip-line fields and indicating a progressive influence of the plastic deformation between adjacent voids [33].

We have described the main mechanism of ductile fracture, developed by the McClintock-Gurson model of localization of deformation inside shear bands. These bands are developed because of the softening process of the material, by increasing its porosity due to void growth. We may now evaluate, by scanning electron microscopy, this extent of this porous region.

For this purpose standand 1 mm thick dogbone specimens, made of polycarbonate (PC), suitable for insertion in the loading chamber of the scanning electron-microscope, were prepared and duly coated to reflect the electron bundle impinging at an angle on their surface. Holes were developed in the plastic zone when the tensile load was slowly increasing under isothermal conditions in the loading chamber of microscope. A number of holes started to develop on the surface and very rapidly tended asymptotically to a limiting population of holes in the plastic zone for impending development of a kink in the crack. A typical curve of the increase of the void surface, versus applied tensile stress is given by the graph of Fig.16. The limiting stress of $5x10$ N/m^2 applied to the specimen was at the threshold of crack initiation. Similar curves have been given by Gurson in his Fig.3 of ref. [34].

Figure 17 presents a series of electron-micrographs, taken in a z-modulation arrangement of the instrument, which indicate the topography of the plastic zones around the progressing crack tip and the position and size of the voids developed in this zone. It is clear from this series of photographs that, at the beginning, a small number of surface voids are developed. As the loading is increasing, the number of voids increases rapidly to some limit and simultaneously their depth is increased considerably, especially at the vicinity of the tip and the flanks of the crack. Their shape on the lateral faces of the specimen is approximately circular, tending to elliptic. When they penetrate inside the specimen they take conical forms. This is a clear indication that inside the specimen in the plane-strain zone the void-density is drastically reduced. Then, the void distribution, based on calculations of the surface-void population, constitutes an upper limit. The real void population should be certainly smaller. Then, the value of void volume density calculated by counting the

number at the average surface of the void should be reduced. The void volume-density f_{app}, calculated on the surface, at the limit load was found to be f_{app} =0.014. This is reduced to :

$$f=0.010 \quad (40)$$

2.5 The Gurson-Theocaris failure criterion based on void formation and coalescence

A failure criterion based on the McClintock-Gurson model, describing failures by void evolution and coalescence, was correlated with the paraboloid of revolution criterion and in this way was totally and safely defined.

The McClintock-Gurson failure model [27,28], based on a description of failure void nucleation and coalescence for the initiation and propagation of cracks in a material, is expressed by a yield condition, which is based on an upper-bound rigid-plastic solution for spherically symmetric deformations, applied around a spherical inclusion. This condition is expressed by :

$$\sigma_e^2 + 2q_1 f\sigma_m^2 ch(q_2\sigma_{kk}/2\sigma_m)-(1+q_3 f^2)\sigma_m^2=0 \quad (41)$$

where σ_e is, as usual, the macroscopic effective Mises stress, given by $\sigma_e^2=1/2\ s_{ij}s_{ij}$, with s_{ij} the deviatoric components of stresses, whereas $\sigma_{kk}/3$ is the hydrostatic stress.

While Gurson assumed values for the constants $q_i(i=1,2,3)$ given by $q_1= q_2= q_3=1$, it was found by Tvergaard [35] that a better fitting of results can be achieved, when the influence of neighbouring voids to a central pair of voids is considered, for periodically arranged cylindrical voids in a matrix. If this influence is taken into account in a continuum model without initial voids, these constants should take the values :

$$I_1=1.5, \quad q_2=1.0 \quad \text{and} \quad q_3= q_1^2=2,25 \quad (42)$$

Moreover, σ_m is the equivalent tensile flow stress, representing the actual macroscopic stress state in the voided matrix material, disregarding local stress concentrations, and f is the current void volume-fraction. Quantity f is the volume fraction of small-scale voids, created between the larger voids. At the beginning of loading f is taken equal to zero and, as the loading is increasing, the quantity f is increasing from zero to provided that the material is subjected to a state of stress with tensile stresses predominant. Moreover, it is reasonable to accept that for an initially compact material, which is subjected to a triaxial compression state of stress there is only an insignificant increase of the nucleation and development of voids. Therefore, for a state of plane stress with $\sigma_1= \sigma_2=-\sigma$ and $\sigma_3=0$ the values of f must remain equal to zero.

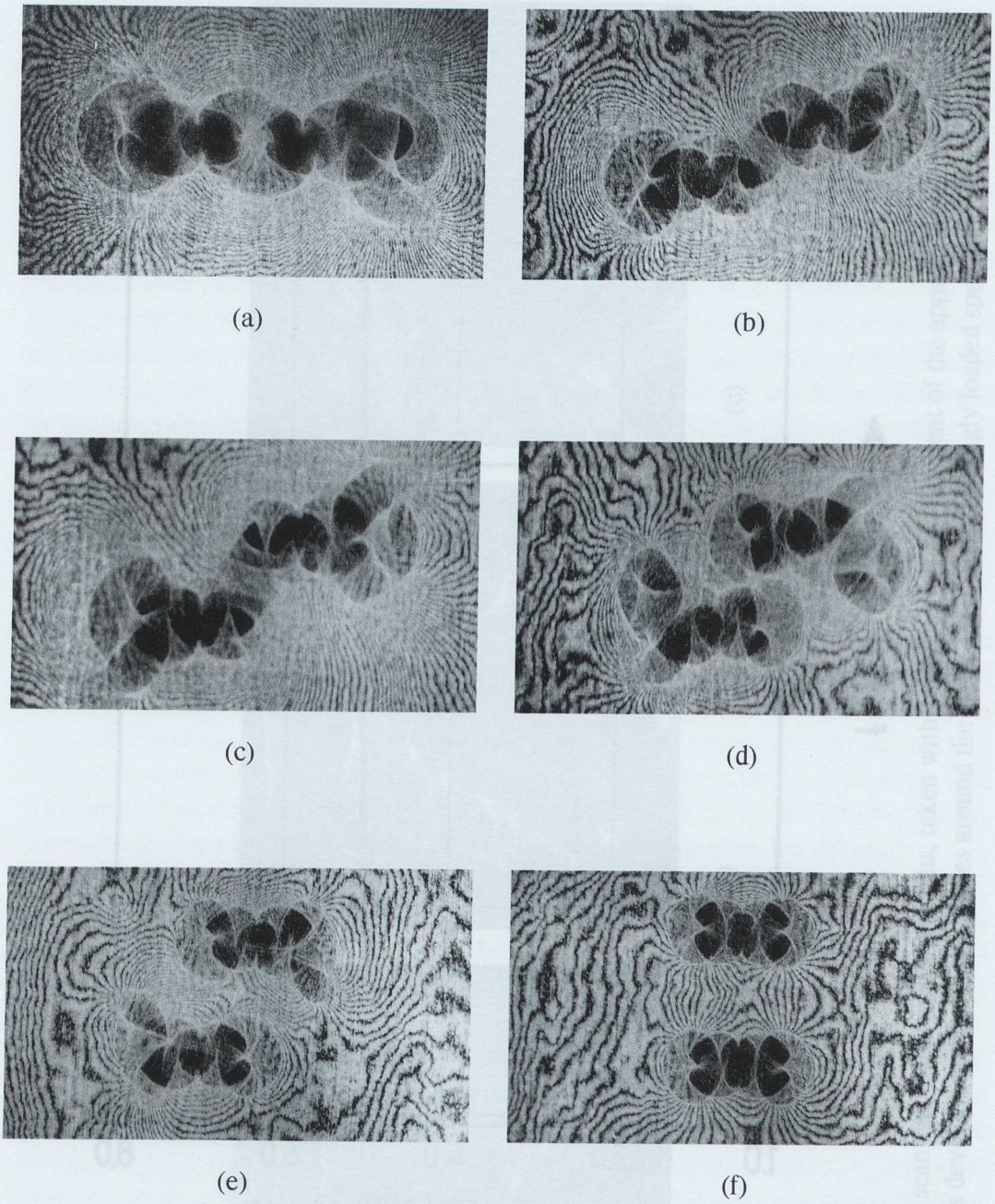

Fig.15 - Series of photographs of reflected caustics developed at the intercenter zone and the outer neighbourhood of two interacting holes lying inside the plastic zone developed around the trip of a crack for various orientations of their intercenter axis.

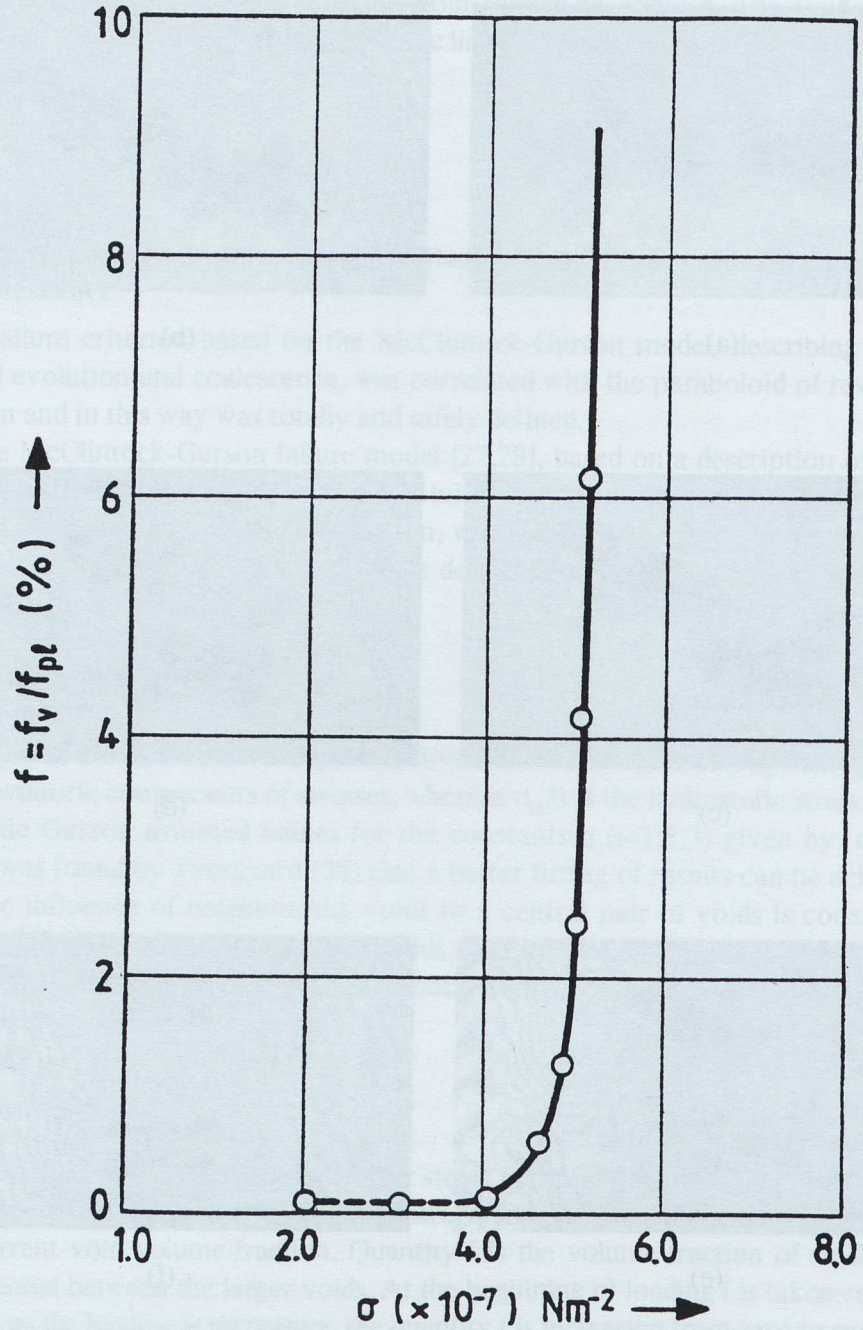

Fig.16 - The evolution of the volume void-fraction, f, expressed as the ratio of the volume surface, f_v covered by voids, normalized to the size of the plastic zone f_{pe}, around the crack tip, versus the externally applied σ-stress of a cracked specimen made of PC.

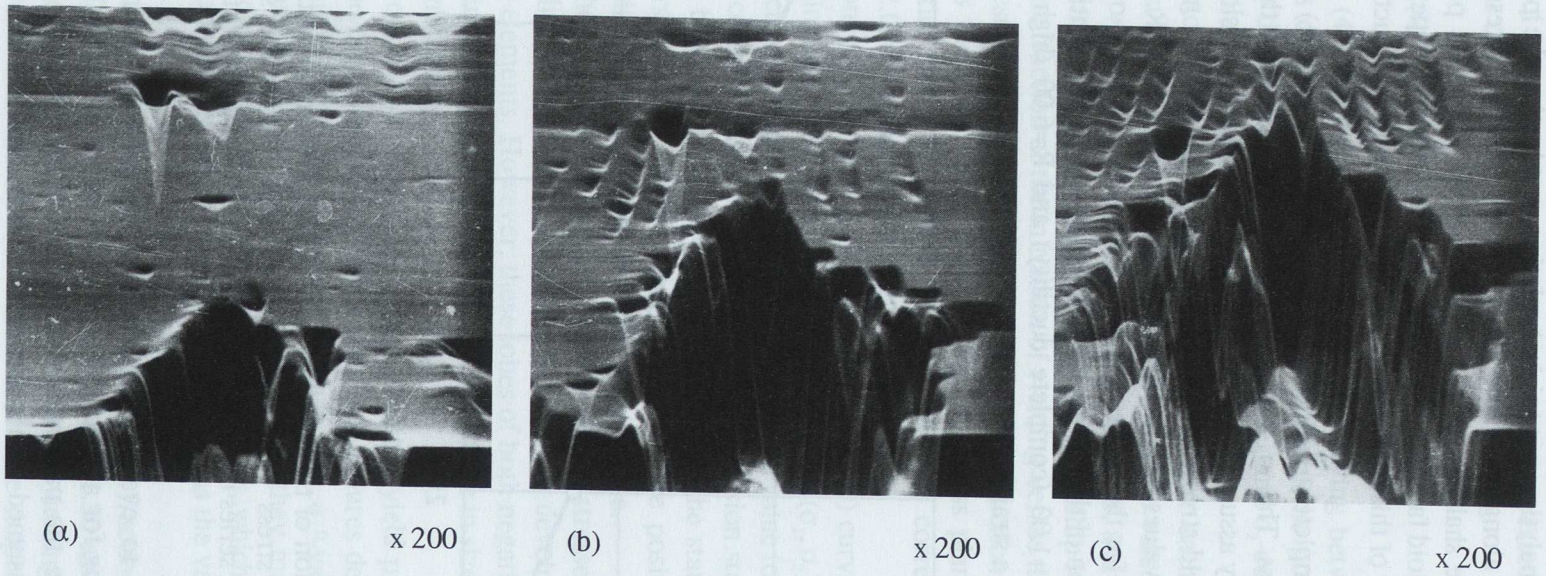

Fig.17 - A series of scanning electron micrographs, taken with z-modulation arrangement of the apparatus, and indicating the population of voids developed in the plastic zones around the crack tip of an increasingly loaded specimen.

Since all semi-analytic or empirical relations evaluating the parameter f fail to yield reliable results along the whole domain of the principal stress plane for plane-stress conditions, we shall try to evaluate the variation of this parameter on data based on the paraboloid failure criterion. This is because large experimental evidence indicates the validity of this criterion for the whole spectrum of ductility or brittleness of materials [42-71].

In order to completely define the criterion of relation (41) it is necessary to evaluate the σ_m-stress. The σ_m-equivalent tensile flow stress of the voidless matrix material is defined by assuming that in the compression-compression zone of loading with $|\sigma_1|=|\sigma_2|$, the yield stress of the material corresponds to and gives the σ_m-stress. Then, for various values of the strength differential factor, R, we evaluate the respective σ_m-stress for the points of the respective loci where $(-\sigma_1)=(-\sigma_2)$. Figure 18 presents the variation of the σ_m-stress versus the strength differential factor, R, in the interval between R=1.00 (complete ductility) and R=6.00 (high brittleness). This curve appears to be a straight line.

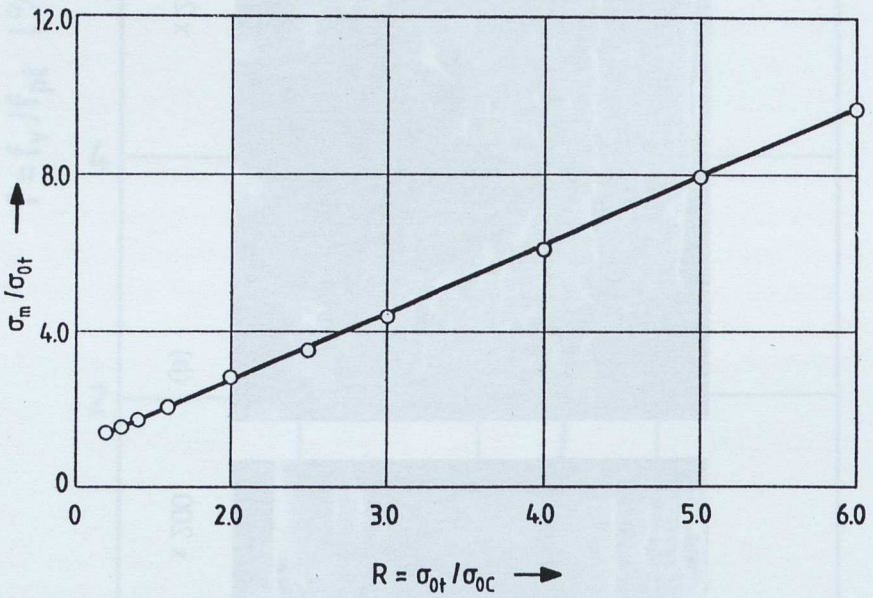

Fig.18 - The variation of the σ_m-equivalent tensile flow stress in the matrix material, disregarding local stress variations due to voids, versus the strength-differential parameter, R, for a series of materials from ductile (R0=1) to brittle ones (R>5.0).

In order now to evaluate the variation of the void-volume fraction at the initiation of yielding for any combination of the components of stresses in the (σ_1, σ_2)-plane we define the particular value of R for the material. For the paraboloid failure criterion assumed as a generalized failure criterion we introduce in it the

particular value of R into its plane-stress relationship expressed in polar co-ordinates (ϱ,θ), which takes the form :

$$\varrho^2(1-\sin 2\theta/2)+\sigma_{0T}(R-1)\varrho(1+\sin 2\theta)^{1/2}=R\sigma_{0T}^2 \qquad (43)$$

Solving relation (43) for parametric values of θ, varying between zero and 2π we define the values of ϱ, corresponding to each value of the polar angle θ and from these values of ϱ the corresponding values of the σ_1- and σ_2-components of stresses for yielding or failure ($\sigma_1=\varrho\cos\theta$, $\sigma_2=\varrho\sin\theta$).

Introducing now the pairs of stresses corresponding to each value of θ and ϱ into Eq.(41) we obtain a relationship between σ_m and f. For the value of σ_m corresponding to the respective value of R, defined from graph of Fig.18, and limiting ourselves to solutions for positive f's we derive from Eq.(41) a relationship $f=\varphi(\theta)$ of the variation of the void-volume fraction at the initiation of yielding versus the polar angle θ.

Figure 19 presents the variation of the void-volume fraction for initiation of yield or failure, versus the polar angle θ in the (σ_1, σ_2)-stress plane, for values of the strength differential factor R varying between R=1.00, corresponding to perfect ductility, and R=2.00 for quasi-brittle materials.

It is clear from this figure that, for R=1.00, the $f=\varphi(\theta)$ curve is degenerated into one point coinciding with the origin of co-ordinates in the (σ_1, σ_2)-plane. For values of R>1.00 cusp-like curves are developed presenting a zero value for $\theta=5\pi/2$. Indeed, for this point, which corresponds to a compression-compression state of stress the void formation should be equal to zero. On the other hand, the state of maximum void formation appears at $\theta=\pi/4$, where $\sigma_1=\sigma_2$ and both are positive, thus increasing isotropically the size of voids without distorting their shape.

Moreover, there are zones, where both principal stresses are negative and, contrariwise to what it was believe up-to-now, voids may develop under such modes of stressing of the elements. However, these lobes of both negative principal stresses are limited zones in the $f=\varphi(\theta)$ diagrams, and they increase in size, as R, and therefore the brittleness is increasing.

Whereas all loci of $f=\varphi(\theta)$ corresponding to initial yield present a cusp point, coinciding with the origin of the (σ_1, σ_2)-coordinates, failures developed beyong the initial yielding, that is for higher values of σ_m than the σ_m^0-value for initiation of yielding, correspond to $f=\varphi(\theta)$ curves, which, although they maintain their overall shape as quasi-cardioid curves, they present blunted cusps, which no more start from the origin of the coordinates, but recede from this point, as the values of the σ_m-stress increase.

Figure 20 presents the variation of the void-volume fraction, f, around a crack tip, versus the polar angle θ in the (σ_1, σ_2)-plane for R=1.30 and for initial yielding $\sigma_m=1.50\ \sigma_{0T}$. Moreover, the subsequent extensions of yielding, corresponding to values σ_m/σ_{0T} between 1.70 and 2.50 are also traced. The shapes of cardioid-curves

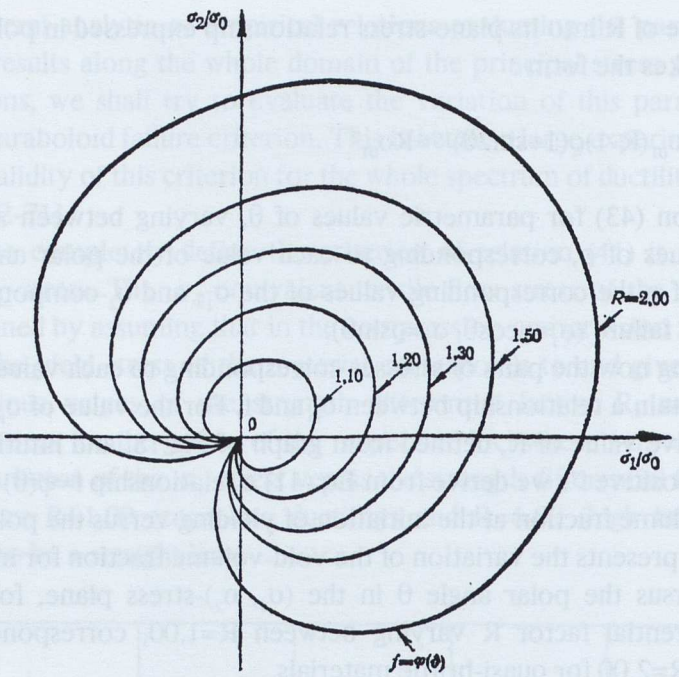

Fig.19 - The variation of the void-volume fraction for initial yielding, f, around a crack tip, versus the polar angle θ in the (σ_1, σ_2)-plane for parametric values of the strength-differential parameter, R, between R=1.0 (ductile materials) and R=2.00 (semibrittle materials).

indicate that, as plasticity is progressing, negative values for both principal σ_1- and σ_2-stresses may develop voids and thus may participate in the plastic deformation of the solid by void nucleation and overall dilatation of the zone surrounding the crack tip.

In this chapter yield and failure criteria for initially isotropic bodies were examined by using an inductive procedure of presenting the various forms of primative yield criteria, as they appeared chronologically in the literature. This mode of presentation exhibits the advantage to follow the evolution in time of the concept of yielding and failure of materials used in constructions. However, it is an imperative need for more sophisticated criteria, which take into consideration, in a rational and equilibrated manner, the influence of the various stress- and strain-components, on the formulation of a realistic failure criterion which, based on a sound phenomenological framework, can define a mathematical model, which can anticipate correctly and accurately failure for any combination of loading of any kind of material. The universality of this criterion constitutes an additional proof of its soundness.

The advent of modern materials with high anisotropic and eventual non-homogeneous properties compels and enforces on the necessity of developing more sophisticated forms of criteria, which are designed to fulfill fundamental require-

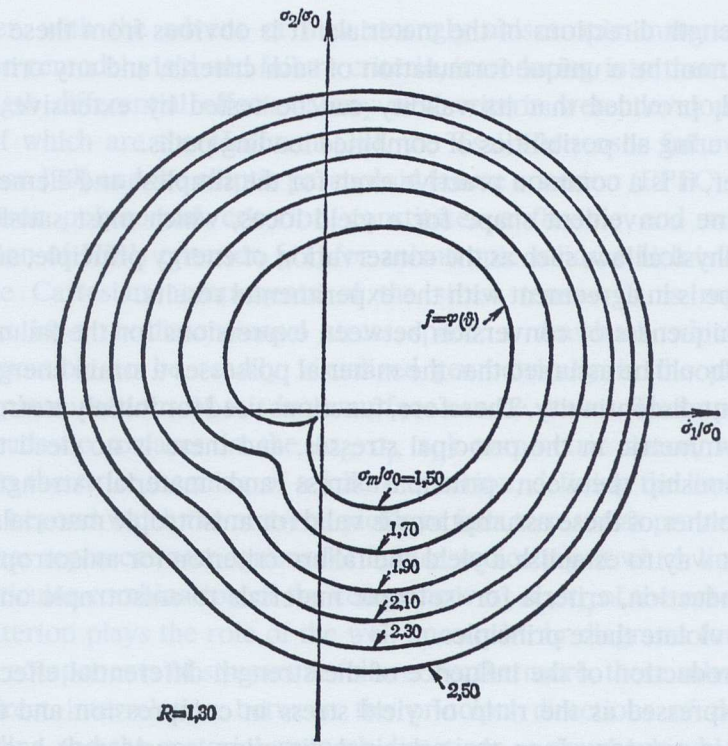

Fig.20 - The variation of the void-volume fraction, f, around a crack-tip, versus the polar angle θ in the (σ_1, σ_2)-plane for R=1.30 and various steps of loading corresponding to σ_m between σ_m/σ_{ot}=1.50 and σ_m/σ_{ot}==2.50.

ments, such as the invariancy of the coordinate axes, combined with the flexibility to yield failure envelopes, which are in agreement with accepted failure mechanisms. Such modern failure criteria are based on simple form-invariant expressions of tensor polynomial functions.

3. CRITERIA BASED ON FAILURE TENSOR POLYNOMIALS FOR THE ORTHOTROPIC BODIES

3.1 Introduction

Suitable failure criteria for anisotropic materials should be again phenomenological and therefore their mathematical models should fulfill the requirements to be invariant to the coordinate system to which they are referred, to be flexible to model any yield and failure envelope, to be single sheet surfaces, in order to yield a unique solution for each simple loading path and to be unambiguously defined along the

principal strength directions of the materials. It is obvious from these requirements that there cannot be a unique formulation of such criteria, and any criterion may be proved valid, provided that its validity can be tested by extensive experimental evidence covering all posibilities of combined loading paths.

However, it is a common practive even for the simplest and elementary criteria to select some convenient shape for a yield locus, which must satisfy beforehand some basic physical law, such as the conservation of energy principle, and then verify that this shape is in agreement with the experimental results.

Since uniqueness of conversion between expressions for the failure criterion is required, it should be assumed that the material possesses a strain energy function up to an incipient discontinuity. Therefore, functions used for initialy isotropic materials should be symmetric in the principal stresses, and there is no need to specify the phase relationship between principal stress and material strength directions. However, neither of these assumptions is valid for anisotropic materials.

The best way to establish a yield and failure criterion for anisotropic bodies is to extend by induction, criteria for isotropic materials to anisotropic ones keeping in mind not to violate these principles.

The introduction of the influence of the strength differential effect on the yield criterion (expressed as the ratio of yield stress in compression and the respective yield stress in tension along the principal direction considered) has resulted in a change to the already established classical yield criteria [2,5] and resulted to a destruction of the invariancy of the criteria in the stress space. Thus, the acceptance of the invariancy of any failure criterion may be considered as a tribute paid to the objective of simplicity of results and a facility of calculations. On the other hand, neglect of acceptance of the strength differential effect introduces large errors especially with materials whose strength differential parameters take large values and they are tested outside the first tension-tension quadrant of the failure locus expressed in the principal stress space.

On the other hand, introduction of the influence of the strength differential effect into the failure criterion heals the breach between theoretical expression of the failure criterion and the respective experimental results, but introduces complications in the use of the criterion. Indeed, in order to take into consideration the strength differential effect it is necessary to introduce into the criterion expressions containing linear terms of stresses. This implies that the invariancy of the failure locus is destroyed and it becomes imperative to take into consideration the relative position of the principal strength axes of the material with respect to the principal stress axes developed by the external loading mode of the material. Then, each test of either of these principal frames should be connected to the other by the well known relations, expressed by the rotation matrices, which yield the proper mode of loading of the material relative to the principal strength directions of the materials.

However, with the advent of new strongly anisotropic materials it became imperative to remodel yield and failure criteria, introducing into them the influence of the strength differential effects. Many new criteria were developed, the most important of which are the Hoffman [38], the Tsai-Wu tensor failure polynomial (TFP) criterion [39] and the elliptic paraboloid failure criterion (EPFC) [42-50].

The tensor polynomial criterion constitutes a flexible and mathematically elegant version of Hill's criterion [41] for anisotropic solids, which is formulated in terms of the Cartesian components of the stress tensor. It is represented by hypersurfaces in a six-dimensionsal stress space, a drawback which makes the criterion impossible to be readily visualized geometrically in the physical stress space. Only plane sections of this hypersurface can be drawn. These plane sections represent quadratic surfaces in the $(\sigma_x, \sigma_y, \tau_{xy})$ parametric space, which do not correspond to the strict meaning of a failure criterion, defining the limits of loading of a material beyond which the material yields or fails to resist as previously. Indeed, these subspaces represent nomograms for failure, indicating at which limit a material fails for a paticular combination of the component $\sigma_x, \sigma_y, \tau_{xy}$ of the external loading. Thus, this criterion plays the role of the well known Mohr diagrams for the limiting values of the components of stresses at failure. Furthermore, these subspaces do not provide a direct interrelation between the principal directions of the externally imposed loading and the material strength directions, a drawback which causes the necessity of meticulous and delicate experiments for its definition.

The Hoffman criterion [38] constitutes a simple and well defined failure criterion taking care of the strength differential phenomena of the materials in the correct way. The criterion resulted from Hill's quadratic form by simply adding to it the missing linear terms of normal stresses. It yields satisfactory results concerning the strength orientation properties of the materials, as well as the prediction of plane-stress failure loci. However, since the establishment of this criterion is only empirical, no attempt was made to interrelate the properties of the surfaces describing the criterion with the material properties at failure. Although Hoffman in his concluding remarks [38] states that *"no physical significance is to be attributed to this fracture condition neither can it be considered complete"*, a deeper study of the properties of the failure surface anticipated by this criterion under certain stability conditions proves the contrary, that there is a sound physical significance for this fracture condition which is also a complete and a general one. This misunderstanding was ensued since Hoffman presumably was interested just to complete the second degree polynomial introduced by Hill for his criterion [38].

It has been established in the previous chapter that the failure locus for isotropic materials presenting the strength differential effect (SDE) is a paraboloid of revolution, which has an axis of symmetry coinciding with the hydrostatic axis $\sigma_1=\sigma_2=\sigma_3$. The intersections of the paraboloid of revolution failure surface with the principal stress axes $\sigma_1, \sigma_2, \sigma_3$ yield failure stresses σ_{0T} or σ_{0C} depending on which part

of the stress axis (positive or negative) is piercing the paraboloid. It was further shown that all well known experimental evidence with such materials fits excellently the yield loci derived by the intersections of this failure surface and the respective stress planes considered, thus supporting strongly the validity and the efficiency of this criterion.

The paraboloid of revolution failure surface was extended to encompass the case of orthotropic materials. For the category of transversely isotropic materials the paraboloid of revolution becomes an elliptic paraboloid, (EPFS), with its axis of symmetry now parallel to the hydrostatic axis, displaced from it by a quantity depending exclusively on the geometric mean of the failure stresses in tension and compression along the strong direction of the material, as well as on the difference of the SDE along the strong and weak directions. Moreover, all intersections of the paraboloid by planes parallel either to the deviatoric plane, or to the principal stress planes, are ellipses, thus guaranteeing that all plane failure loci are closed curves, except the intersections of the EPFS by the principal diagonal planes [42-67].

The theory concerning the EPFS was further extended to encompass the general orthotropic material [68-71]. It was shown that even for the general orthotropic material the failure locus is an elliptic paraboloid with an axis of symmetry that remains parallel to the hydrostatic axis. While this axis for transversely isotropic materials lies on the principal diagonal plane (σ_3,δ_{12}) defined by the strong principal axis σ_3 and the bisector δ_{12} of the angle formed by the σ_1- and σ_2-axes on the transverse plane, for orthotropic materials, the axis of symmetry lies outside this plane, whereas the elliptic paraboloid presents some angular displacement about this axis, so that its planes of symmetry intersect the principal diagonal planes of the stress space. The same features appear for transversely isotropic materials when the material is off-axis loaded, so that the principal strength axes of the material subtend an arbitrary angle with the principal directions of external loading. It was then established that the influence of the anisotropy of the material and its strength differential effect are intertwined, and mutually influence the structure of the failure locus of an anisotropic material. By using experimental data of similar or related materials an attempt was made to disclose these intimate relationships between the anisotropy of a material and its strength differential effect.

3.2 Historical Review

Failure criteria are based on Hill's well known theory for anisotropic metals [41]. Hill's criterion is based on Mises' first attempt to formulate yielding and failure for anisotropic solids [72]. However, Hill's criterion neglects the effect of the strength differences in tension and compression, which are apparent to all solids. A progress in the criteria for anisotropic bodies was done by Hoffman's criterion, which presents a further improvement on Hill's criterion by incorporating the

strength differential effect. This was achieved by adding the linear terms in the quadratic expression of Hill's criterion [38]. However, this addition resulted in a destruction of the tensorial invariancy of Hill's criterion, but gained the advantage of describing correctly the yielding behavior of real engineering materials. Then, the old generation of yield criteria sacrificed the exactness to the altar of simplicity and convenience of using the advantages of the tensor invariancy and thus abolishing the inclusion in these criteria of important universal phenomena of the mechanical behavior of the materials, such as the Bauschinger effect and others based on the strength differential effect.

From these criteria only the Coulomb, or internal friction, yield and fracture criterion was incorporating the strength differential effect, as early as from 1773 [7] by introducing in the criterion the influence of the first stress invariant and thus relating the dilatational component of energy to the distortional component and recognizing its importance in the mode of yielding of the materials. This was imperative since the Coulomb criterion was called to describe a fracture criterion for brittle materials, where the strength differential parameter R takes important values and thus influences considerably the yielding behavior of such materials.

Overpassing the typical yield and failure criteria, which neglect the influence of the first stress invariant and are based on the approximation of stress invariancy, we review the two basic criteria developed recently which are convenient for anisotropic substances. This remodelling of the failure criteria was mainly based on Hill's criterion for anisotropic materials [41] and its modification by Hoffman's criterion [38].

These criteria which are based on energy balance considerations are mainly the Tsai-Wu tensor failure polynomial (TFP) [39] and the elliptic paraboloid failure surface [45]. Both are variations of the same basic principle and they are described by quadric surfaces thus presenting a fundamental property to comply with basic physical laws.

The tensor polynomial criterion constitutes a flexible and mathematically elegant version of a criterion formulated by means of a series of Cartesian components of the stress tensors. It is represented by hypersurfaces in the six-dimensional stress space, which is impossible to be conveniently visualized geometrically in the physical stress space. Only plane sections of this hypersurface were possible to be studied, which represent quadric surfaces in the Cartesian $(\sigma_x, \sigma_y, \tau_{xy})$-parametric space. However, even these subspaces do not yield a direct interrelation between the externally applied load to the body and the material strength directions. This constitutes a drawback of the criterion necessitating meticulous and delicate experiments and an extensive study based on Weibull's distribution theory, in order to define with certitude the appropriate values of the characteristic parameters defining this failure locus. However, this criterion is an excellent instrument for evaluating with high accuracy the influence of the variation of one failure component to the values of the remaining ones. Thus, the tensor polynomial criterion constitutes for the anisotropic bodies what the Mohr circles yield graphically for the isotropic materials.

The elliptic paraboloid failure surface (EPFS) as a failure criterion was introduced by the author [42]-[72] first to describe the most general failure surface for isotropic materials [40]. It was shown that for isotropic materials presenting the strength differential effect, defined by the strength differential parameter $R=\sigma_{0C}/\sigma_{0T}$, where σ_{0C} and σ_{0T} are the yield stress in compression and tension respectively, the EPFS is reduced to a paraboloid of revolution surface, as this which was described by Tschoegl [10].

The paraboloid of revolution failure surface becomes an elliptic paraboloid surface for orthotropic materials, where six strength parameters, three for tension and three for compression along the principal strength axes of the material define three different strength differential parameters $R_3=\sigma_{C3}/\sigma_{T3}$, $R_2=\sigma_{C2}/\sigma_{T2}$ and $R_1=\sigma_{C1}/\sigma_{T1}$. For transversely isotropic materials, where $R_1=R_2$ (the σ_3-axis is assumed as the strong axis of the transversely isotropic material) the failure surface changes to an elliptic paraboloid surface. It has been shown that the elliptic paraboloid presents some symmetry with respect to the principal strength axes having as plane of symmetry the principal diagonal plane (σ_3,δ_{12}), where σ_3 is the strong axis and δ_{12} is the bisector of the right angle $(\sigma_1 0\sigma_2)$ along the plane of isotropy. This symmetry results in a simplification of the expressions for the various plane sections of the surface by characteristic planes, as they are the principal strength planes (σ_3,σ_1), (σ_3,σ_2), (σ_2,σ_1) the deviatoric plane and its parallel planes $(\sigma_1+\sigma_2+\sigma_3)=k$ (k=0,1,2, ...,n) and the principal diagonal plane (σ_3,δ_{12}).

A property, which is maintained in the isotropic, the transversely isotropic, as well in the orthotropic materials, is that the axis of symmetry of the failure surface (either a paraboloid of revolution, or an elliptic paraboloid) coincides or is parallel to the hydrostatic axis in the stress space, besides the fact that all failure surfaces are paraboloids. This comes from the fact that independently of the isotropy or anisotropy of the material the consequences from an arbitrary external hydrostatic loading $(\sigma_1=\sigma_2=\sigma_3)$ should be independent of direction and therefore the hydrostatic axis should be an axis of symmetry of the failure surface.

3.3 Failure criteria based on tensor polynomials

The isotropic failure theory, generalized to cover also anisotropic failure, is based on the hypothesis, which is largely supported experimentally [75], that isotropic materials can withstand infinitely large amounts of *hydrostatic compression* (or tension) without failing. Thus, a *safe loading path* exists in the 6D-Euclidean space of symmetric stress tensors which, for isotropic solids, coincides with the direction of the 2nd rank *spherical tensor,* $\mu\mathbf{1}(\mu\in R^-)$. It must be clearly stated that *only either hydrostatic compression constitutes a safe triaxial loading path* and not *hydrostatic tension,* or the inverse, under which materials fail always [73]. Then, the failure criterion depends on the hydrostatic pressure and an indirect proof of it, is the strength differential effect manifested, more or less, by every solid. The above hypothesis,

graphically represented in the 3D principal stress space, is satisfactorily interpreted by an isotropic failure surface, which is a paraboloid of revolution with the hydrostatic axis $\sigma_1=\sigma_2=\sigma_3$, as a symmetry axis, whereas the open end of the paraboloid is oriented towards the direction of hydrostatic compression, or tension [11].

Such a generalization of these concepts for failure of *orthotropic solids* was undertaken in refs.[42-50], by means of the geometric interpretation of the failure surface in the principal stress space. It was shown that the failure surface for orthotropic materials is an *elliptic paraboloid* with a symmetry axis parallel to the hydrostatic axis and displaced from the origin of the coordinate system by an amount depending on the degree of strength anisotropy of the material. The failure condition expressed in terms of principal stress components, σ_i, was shown to have the general form of the quadric surface equation, that is :

$$H_{ij}\sigma_i\sigma_j + h_i\sigma_i - 1 = 0 \qquad (i, j = 1, ..., 3) \tag{44}$$

where the tensor H_{ij} and the vector h_i are appropriately defined in terms of the basic strength properties of the material. Such a formulation of the anisotropic failure criterion is restricted to a material symmetry up to orthotropy at most, and it is also confined for loading cases for which principal stress axes coincide with material symmetry axes. For all other loading cases, which most commonly arise in fiber composite laminates, eq.(44) must be extended [68-71].

Then, the quadric surface equation (44), if extended in terms of the Cartesian components of the stress tensor, takes the following tensorial expression :

$$f(\sigma) = \boldsymbol{\sigma} \cdot \mathbf{H} \cdot \boldsymbol{\sigma} + \mathbf{h} \cdot \boldsymbol{\sigma} - 1 = 0 \tag{45}$$

where **H** and **h** denote 4th and 2nd-rank *failure tensors* respectively.

The postulate upon which the anisotropic failure criterion of eq.(45) is formulated stipulates the existence of a safe triaxial loading path, which means that the failure hypersurface must not be intersected by some stress-tensor direction. While for isotropic materials it is generally accepted and experimentally proved that the hydrostatic loading constitutes safe triaxial loading path, for anisotropic materials this safe triaxial loading path is parallely displaced by a well defined constant amount of strain energy taking care of the influence of anisotropy, which makes the safe axis to be displaced by a well-defined invariant amount of stress, depending on the anisotropy of the material and expressed by the distance between the hydrostatic axis and the axis of symmetry of the hypersurface.

The values of the failure function $f(\boldsymbol{\sigma})$ for the initially anisotropic elastic solid with respect to the tensor $\boldsymbol{\sigma}$ must be path independent as long as the material does not fail under the loading mode $\boldsymbol{\sigma}$. Since the stress tensor is considered symmetric, *path independence* of function $f(\boldsymbol{\sigma})$ is guaranteed by the *symmetric failure tensors* **H** and **h**.

Moreover, the tensorial character of function $f(\boldsymbol{\sigma})$ implies the *form-invariancy,* of eq.(45) and its holding for any coordinate system transformation. Besides, the linear polynomial term, $\mathbf{h}.\boldsymbol{\sigma}$, accounts for the strength differential effect and thus, eq.(45), after a proper determination of failure tensors **H** and **h**, may constitute a valid generalization of the paraboloidal failure surface criterion for anisotropic solids.

The form of eq.(45) does not impose any restriction on the symmetry class of the anisotropic medium and thus the 4th rank failure tensor **H** may possess at most 21 independent components. Symmetry properties of tensor **H** follow those of elastic compliance 4th-rank tensor **S**. The 2nd-rank failure tensor, **h**, may have, in general, six independent components, whereas, for specially orthotropic media, or of increased symmetry, tensor **h** becomes *axisymmetric* degenerating to a *spherical* tensor for the isotropic medium.

Inner products, denoted by dots, transform relation (45) in the natural Cartesian notation as follows :

$$f(\sigma_{ij}) = H_{ijkl}\sigma_{ij}\sigma_{kl} + h_{ij}\sigma_{ij} - 1 \qquad (i, j, k, l = 1, ..., 3) \tag{46}$$

whereas the same relation in contracted Cartesian notation is given by :

$$If(\sigma_i) = H_{ij}\sigma_i\sigma_j + h_i\sigma_i - 1 \qquad (i, j = 1, ..., 6) \tag{47}$$

The necessary and sufficient condition for the failure hypersurface of eq.(45) to be convex and open-ended is that tensor **H** must be positive semi-infinite, which means that:

$$\boldsymbol{\sigma} \cdot \mathbf{H} \cdot \boldsymbol{\sigma} \geq 0, \quad (\forall\, \boldsymbol{\sigma}>0) \tag{48}$$

Then, a necessary condition to be satisfied by the contracted components of the 4th-rank tensor **H** is given by :

$$H_{ii}H_{jj}-H_{ij}^2 \geq 0 \qquad (i,j = 1, ...,6) \tag{49}$$

The convexity of the failure hypersurface, together with its open end along a triaxial path of normal stresses, postulates which are assured by the validity of the inequality (48), implies that any single stress component leads to failure at a critical value σ_i^{cr}, which is defined by :

$$H_{ii}(\sigma_i^{cr})^2 \pm h_i\sigma_i^{cr} - 1 = 0 \qquad (i = 1, ..., 6) \tag{50}$$

with the minus (-) sign holding for the *opposite loading.*

By solving the twelve equations (50), it is derived that the *strength differential tensor,* **h,** is completely determined together with the *"main diagonal"* components of tensor **H.**

Then, the normal components of the failure tensors are expressed by :

$$H_{ii} = 1/\sigma_{Ti}\sigma_{Ci} \qquad (i \leq 3) \tag{51}$$

$$h_i = (1/\sigma_{Ti}) - (1/\sigma_{Ci}) = (\sigma_{Ci}-\sigma_{Ti})\, H_{ii} \tag{52}$$

whereas for shear components are given by :

$$H_{ii} = 1/\sigma_{si}^{+}\sigma_{si}^{-} \qquad (i > 3)$$

$$h_i = (1/\sigma_{si}^{+}) - (1/\sigma_{si}^{-}) = (\sigma_{si}^{-} - \sigma_{si}^{+})\, H_{ii} \tag{53}$$

In the above relations the repeated index convention does not apply and the σ_{Ti} and σ_{Ci} - stresses express the tension (T) and compression (C) failure stresses in the i-direction. Furthermore, the σ_{si}^{+}, σ_{si}^{-} -stresses express the shear strengths, positive or negative, in the i-plane ($i > 3$) and the usual contracted notation of Cartesian indices is used, meaning, that index 4 corresponds to natural indices 23, index 5 to 13 and index 6 to 12. For the orthotropic materials, when the coordinate system defining the failure stresses coincides with the material symmetry directions, there is no shear-strength differential effect, that is : $\sigma_{si}^{+} = \sigma_{si}^{-}$

Up to this point, the failure tensor components given in relations (51) to (53) may be determined without recourse to a special phenomenological hypothesis. The evaluation of these components is based upon standard basic requirements, common for all anisotropic failure criteria, which can be expressed by the general form of eq.(45). This leaves the off-diagonal components of the failure tensor **H** (H_{ij}, $i \neq j$) to be derived according to the particular assumptions, which are different for the various criteria.

The open end of the failure hypersurface is mathematically assured by imposing the 4th-rank failure tensor **H** to have a *zero eigenvalue.* Moreover, the hypothesis that hydrostatic stress is a safe loading path is further formulated mathematically by associating the zero eigenvalue of tensor **H** to the 2nd-rank spherical tensor, **1**, which is then an *eigentensor* of **H**. The above implies that the failure hypersurface is a generalized elliptic paraboloid with a symmetry axis parallel to the direction of the spherical tensor, **1**. Since the spherical tensor, **1**, is an eigentensor of the 4th-rank tensor **H** and corresponds to its zero eigenvalue, the following relation holds :

$$\mathbf{H} \cdot \mathbf{1} = 0 \tag{54}$$

or equivalently :

$$H_{ijkk} = 0 \tag{55}$$

The system of six equations (55), if expressed in contracted notation, reads as :

$$\begin{aligned} H_{11} + H_{12} + H_{13} &= 0 \\ H_{12} + H_{22} + H_{23} &= 0 \\ H_{13} + H_{23} + H_{33} &= 0 \\ H_{41} + H_{42} + H_{43} &= 0 \\ H_{51} + H_{52} + H_{53} &= 0 \\ H_{61} + H_{62} + H_{63} &= 0 \end{aligned} \qquad (56)$$

whereas, from the first three equations, one has :

$$H_{ij} = 1/2\,(H_{kk} - H_{ii} - H_{jj}), \qquad (i, j, k \leq 3,\ i \neq j \neq k) \qquad (57)$$

Relations (57) imply that the interaction failure coefficients H_{12}, H_{23} and H_{31} of the elliptic paraboloid failure surface (EPFS), are interrelated with the diagonal components, which are directly defined through relations (51) and (52) with the basic strength data. This is a significant advantage of the EPFS-criterion, which is not met with other similar criteria, as it is the failure tensor polynomial [75]. Indeed, all these criteria are solely based on the experimental evaluation of these off-diagonal coefficients. However, the problem of the optimal experimental determination of the failure tensor components presents unsurmountable difficulties, which were considered by Wu [76]. Complicated and sophisticated experimental techniques were proposed, which were not generally accepted. Thus, several researchers adopted the *zeroing* of the undetermined 4th-rank failure tensor components, which in general assume very small values. This arbitrary choice altered drastically the concepts of the criterion proposed by Tsai and Wu [75] and the resulting failure condition was shown to yield erroneous predictions when compared with 3D-experimental failure data [77]. Only in the various versions of the EPFS-criterion for orthotropic materials, the non-zero components of the failure tensors **H** and **h** are completely determined in terms of the basic strength data through eqs. (51) to (53) and (55) and, thus, the criterion can be directly used, without further need of additional complicated experimental data.

3.4 The EPFS-criterion for the orthotropic material

For the complete definition of the elliptic paraboloid failure surface it is required to visualize a series of its characteristic intersections. Indeed, since intersections by the principal stress planes (σ_i, $\sigma_{(i+1)}$), (i=1,2,3) constist of superficial slices of this failure solid, these intersections may be confusive, since respective intersections belonging to different versions of the criterion present eventually only imperseptible differences. Then, it is well established that for the experimental

verification of the postulates of any failure criterion it does not suffice to compare its predictions with experimental results from two-dimensional failure tests. Further comparison with triaxial failure tests is needed. As more convenient 3D-failure tests should be considered a superposition of hydrostatic compression on uniaxial tension or compression. Such tests correspond to loading modes corresponding to arbitrary intersections of the paraboloid.

For the complete study of the elliptic paraboloid surface four types of intersections are deemed as necessary. These intersections are :

i) The principal diagonal intersections defined by planes containing one principal stress axis and the bisector of the right angle formed by the remaining principal axes.

ii) The deviatoric π-plane which is normal to the hydrostatic axis.

iii) The principal stress plane intersections, which are convenient for the study of the mechanical properties of the anisotropic body when thin plates of the material under plane-stress conditions are to be studied.

iv) The intersections of the EPFS-surface by planes defined by the axis of symmetry of the paraboloid and either principal axis of the ellipse corresponding to the deviatoric plane.

The elliptic paraboloid failure surface for the general orthotropic material, satisfying all the properties previously described, is expressed as follows in the $(\sigma_1,\sigma_2,\sigma_3)$-principal stress space, by a complete polynomial of the second degree, where the σ_3-principal direction corresponds to the strongest direction [68] :

$$H_{11}\sigma_1^2+H_{22}\sigma_2^2+H_{33}\sigma_3^2+(H_{33}-H_{11}-H_{22})\sigma_1\sigma_2+(H_{11}-H_{22}-H_{33})\sigma_2\sigma_3+(H_{22}-H_{33}-H_{11})\sigma_1\sigma_3+$$
$$+h_1\sigma_1+h_2\sigma_2+h_3\sigma_3=1 \qquad (58)$$

This second-degree polynomial, referred to the Cartesian coordinate system 0xyz, where the 0z-axis is parallel to the hydrostatic axis and the (0xy)-plane coincides with the deviatoric plane with the 0y-axis lying on the $(\sigma_3\delta_{12})$-principal diagonal plane,(δ_{12} being the bisector of the $\sigma_1 0\sigma_2$-angle) is expressed by :

$$(H_{11}+H_{22}+H_{33})x^2 + 3/2H_{33}y^2 + \sqrt{3}(H_{11}-H_{22})xy + 1/\sqrt{2}(h_2-h_1)x +$$
$$+1/\sqrt{6}(2h_3-h_1-h_2)y + 1/\sqrt{3}(h_1+h_2+h_3)z = 1 \qquad (59)$$

Figure 21 presents the mapping of the paraboloid in the principal stress space $(0\sigma_1\sigma_2\sigma_3)$, as well as the new Cartesian coordinate systems (0xyz) and (0"x"y"z") corresponding to the already defined system and the Cartesian system whose 0"z"-axis is parallel to the hydrostatic axis (0z), whereas the 0"x" - and 0"y" axes lie again on the deviatoric plane but they are created by an angular displacement on the (0xy)-system so that the new (0"x"y")-system coincides with the principal axes of the elliptic intersection of the EPFS by the deviatoric plane. Then, the deviatoric plane is defined at once by putting in relation (59) the value z=0.

The principal diagonal intersection of the elliptic paraboloid failure surface by the plane (σ_3,δ_{12}), where σ_3 is the strong principal stress axis and δ_{12} is the bisector of the angle $\sigma_1 0\sigma_2$ subtended by the two other principal stress-axes σ_1 and σ_2. For the general orthotropic body the equation of the intersection of the failure locus and the (σ_3,δ_{12})-plane is given by [68] :

$$1/2(H_{11}+H_{22}+2H_{12})\delta_{12}^2+H_{33}\sigma_3^2+\sqrt{2}(H_{13}+H_{23})\delta_{12}\sigma_3+\sqrt{2}/2(h_1+h_2)\delta_{12}+h_3\sigma_3-1=0 \quad (60)$$

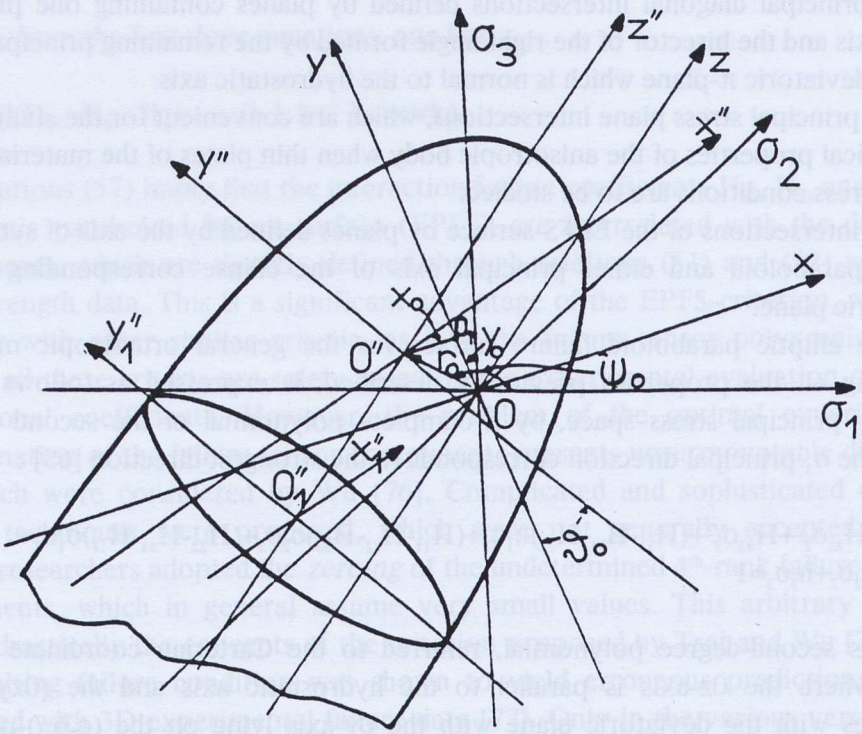

Fig.21 - The elliptic paraboloid failure surface EPFS for the general orthotropic material as it appears in the three dimensionsal $(\sigma_1, \sigma_2, \sigma_3)$-space and its connection with the 0xyz- and 0''x''y''z''-Cartecian frames whose 0z and 0''z''-axes are coincident or parallel to the hydrostatic axis.

The other two principal diagonal intersections of the EPFS-surface by the planes (σ_1,δ_{23}) and (σ_2,δ_{13}) can be readily established from relation (60) by cyclic interchange of the respective indices of the relation (60).

Figure 22 presents the three different principal diagonal intersections of the elliptic paraboloid failure surface for a mildly anisotropic polymer the oriented polycarbonate (PC), which was subjected to three different deformation steps in order to become an oriented anisotropic substance (materials A, B and C).

Expressions (58) to (60) for the elliptic paraboloid failure surface were established by a straightforward application of the theory for second-degree one-sheet surfaces as they have developed in analytic geometry given for example in ref. [78]. For details of calculations deriving these relationship the reader is referred to the extensive literature of articles by the author and his co-workers included in the references of this study [42-71].

The intersection of the EPFS by the deviatoric plane z=z"=0 for the general orthotropic material is given in Fig.23.

It can be shown that this intersection is also an ellipse, provided that the stability condition for the material is satisfied. This condition is expressed by [11] :

$$4H_{11}>H_{33} \tag{61}$$

The center 0" of the ellipse is defined by the polar distance r_0 and the angle ψ_0 indicated in Fig.22, which are expressed by :

$$\begin{aligned} x_0 &= \sqrt{2}/3F\ \{2h_3(H_{11}-H_{22})+h_1(3H_{33}-H_{11}+H_{22})-h_2(3H_{33}+H_{11}-H_{22})\} \\ y_0 &= \sqrt{6}/9F\ \{h_1(5H_{22}-H_{33}-H_{11})+h_2(5H_{11}-H_{22}-H_{33})-2h_3(2H_{11}+2H_{22}-H_{33})\} \end{aligned} \tag{62}$$

with

$$F = \{2(H_{11}H_{22}+H_{22}H_{33}+H_{33}H_{11})-(H_{33}-H_{11})^2-(H_{11}-H_{22})^2-(H_{22}-H_{33})^2$$

$$\tan\psi_0 = \frac{\sqrt{3}}{3}\left\{\frac{h_1(5H_{22}-H_{33}-H_{11})+h_2(5H_{11}-H_{22}-H_{33})-2h_3(2H_{11}+2H_{22}-H_{33})}{2h_3(H_{11}-H_{22})+h_1(3H_{33}-H_{11}+H_{22})-h_2(3H_{33}+H_{11}-H_{22})}\right\} \tag{62}$$

Of great interest are anisotropic materials representing some symmetry in their mechanical properties. These materials are particularly the so-called *transversely isotropic materials* whose strengths in tension and compression along one principal direction are higher or lower than their respective strengths along the two other principal directions, along which the respective strengths are mutually equal. For the transversely isotropic material with σ_{T3}, σ_{C3} as failure limits in tension and compression along the strong direction of the material and $\sigma_{T1}=\sigma_{T2}$, $\sigma_{C1}=\sigma_{C2}$ the respective failure limits along the transverse isotropic plane, relation (60) yielding the shape of the $(\sigma_3\delta_{12})$-intersection of the EPFS is simplified into the equation :

$$(H_{11}+H_{12})\delta_{12}^2+H_{33}\sigma_3^2+2\sqrt{2}H_{13}\delta_{12}\sigma_3+\sqrt{2}h_1\delta_{12}+h_3\sigma_3-1=0 \tag{63}$$

Moreover, the polar distance r_0 representing the additional loading because of the anisotropy of the material is given by :

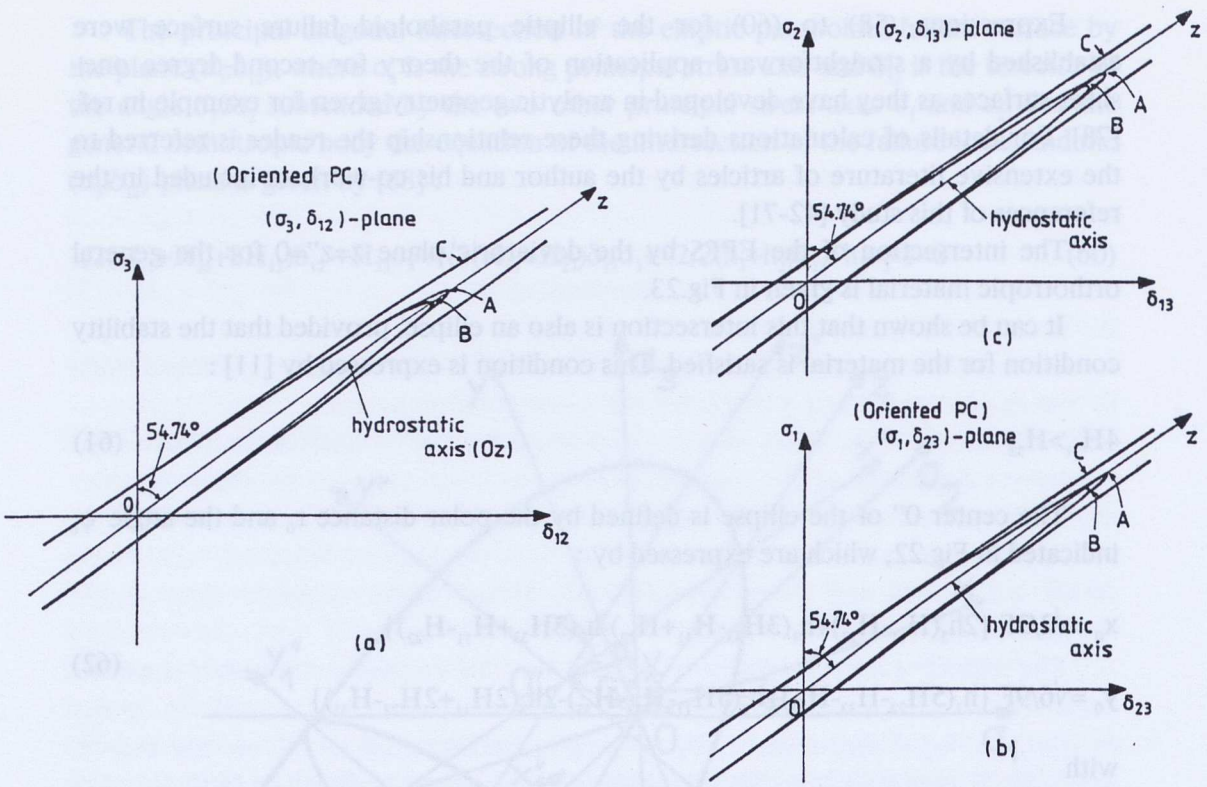

Fig.22 - The intersections of the EPFSs for the three types of oriented polycarbonate (materials A, B, C) by the principal diagonal planes (σ_3,δ_{12}), (σ_1,δ_{23}) and (σ_2,δ_{13}) respectively.

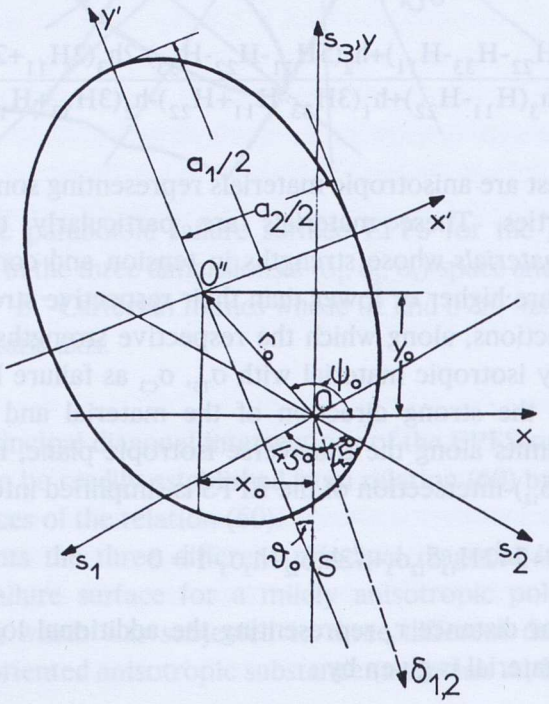

Fig. 23 - The intersection of the EPFSs by the deviatoric plane z=z"=0 for the orthotropic material.

$$x_0=0$$

$$y_0=\frac{\sqrt{6}\,(h_1-h_3)}{9H_{33}} \tag{64}$$

$$\tan\psi_0=\Xi\,,\qquad \psi_0=90^\circ$$

Relations (64) indicate that for the transversely isotropic materials the elliptic section indicated in Fig.22 representing the intersection of the EPFS-surface by the deviatoric plane is symmetric to 0y≡0"y"axis and, therefore, the principal diagonal plane $(\sigma_3\delta_{12})$ is a plane of symmetry of the elliptic paraboloid surface for these materials. This property reduces considerably the complications in evaluating the mechanical behavior of this type of anisotropic bodies, since, in general, the abscissas x_0 for the orthotropic materials are very small as compared to y_0 and, therefore, the approximation of an orthotropic material by its corresponding transversely isotropic one is legitimate.

Another characteristic quantity defining the orientation of the cross section of the EPFS by the deviatoric plane is the angle θ of inclination of the principal axes of the ellipse with respect to the 0xy-system (Fig.22).

This angle is given by, [43] and [45]:

$$\theta=1/2\,\tan^{-1}\left[\sqrt{3}(H_{22}-H_{11})/(2H_{33}-H_{11}-H_{22})\right] \tag{65}$$

which, again for the transversely isotropic material, for which it is valid that $H_{11}=H_{22}$, becomes :

$$\theta=0^\circ \tag{66}$$

The principal semi-axes a_1 and a_2 of the elliptic intersection by the deviatoric plane are expressed by:

$$\left.\begin{matrix}a_1\\a_2\end{matrix}\right\}=\left\{\frac{1-\frac{1}{2\sqrt{2}}(h_2-h_1)x_0-\frac{1}{2\sqrt{6}}(2h_3-h_1-h_2)y_0}{\frac{1}{2}(H_{11}+H_{22}-H_{33})\pm(H_{11}^2+H_{22}^2+H_{33}^2-H_{11}H_{22}-H_{22}H_{33}-H_{33}H_{11})^{1/2}}\right\}^{1/2} \tag{67}$$

with x_0 , y_0 the quantities given by relations (61) and the "plus" sign in (67) corresponding to the a_1-length.

For the transversely isotropic body these principal axes of the ellipse are readily reduced to [47] :

$$\left.\begin{matrix} a_1 \\ a_2 \end{matrix}\right\} = \begin{cases} \left(\dfrac{2}{3H_{33}}\right)^{1/2}\left\{1+\dfrac{1}{H_{33}}\left(\dfrac{h_1-h_3}{3}\right)^2\right\}^{1/2} \\ \left(\dfrac{1}{4H_{11}-H_{33}}\right)^{1/2}\left\{1+\dfrac{1}{H_{33}}\left(\dfrac{h_1-h_3}{3}\right)^2\right\}^{1/2} \end{cases} \tag{68}$$

The ratio of the major axis $2a_1$ to the minor axis $2a_2$ of the elliptic intersection expresses the ellipticity of the paraboloid and it is given by :

$$\lambda = \{3H_{33}/(4H_{11}-H_{33})\}^{1/2} \tag{69}$$

Moreover, the angle θ_0 subtended by the principal axes of the elliptic intersection and the 0xy-system is given by [68] :

$$\theta_0 = 1/2 \tan^{-1}[\sqrt{3}\,(H_{11}-H_{22})/(2H_{33}-H_{11}-H_{22})] \tag{70}$$

which obviously becomes equal to zero for the transversely isotropic body, where $H_{11}=H_{22}$.

Finally, the equation of the EPFS in the 0"x"y"z"-frame is given by :

$$\begin{aligned} &[(H_{11}+H_{22}+H_{33})+(H_{11}^2+H_{22}^2+H_{33}^2-H_{11}H_{22}-H_{22}H_{33}-H_{33}H_{11})^{1/2}]x''^2 + \\ &+ [(H_{11}+H_{22}+H_{33})-(H_{11}^2+H_{22}^2+H_{33}^2-H_{11}H_{22}-H_{22}H_{33}-H_{33}H_{11})^{1/2}]y''^2 + \\ &+ 2/\sqrt{3}\,(h_1+h_2+h_3)z'' = 2+2\,(h_1-h_3/3)^2 + \\ &+ \frac{(h_1-h_2)\,[2h_3(H_{11}-H_{22})+h_1(3H_{33}-H_{11}-H_{22})-h_2(3H_{33}+H_{11}+H_{22})]}{6\,[\,2(H_{11}H_{22}+H_{22}H_{33}+H_{33}H_{11}) - (H_{11}^2+H_{22}^2+H_{33}^2)]} \end{aligned} \tag{71}$$

Now we study the intersections of the EPFS-surface by the three principal-stress planes (σ_3, σ_1), (σ_1, σ_2) and (σ_2, σ_3).

The equation expressing the elliptic intersection of the elliptic paraboloid failure surface, represented in the principal stress space $(\sigma_1, \sigma_2, \sigma_3)$, by the principal plane (σ_3,σ_1) is expressed by :

$$H_{11}\sigma_1^2+H_{33}\sigma_3^2+2H_{31}\sigma_3\sigma_1+h_1\sigma_1+h_3\sigma_3=1 \tag{72}$$

The center of this ellipse is defined by its coordinates (σ_{3M}, σ_{1M}). Figure 24 presents this intersection in the (σ_3,σ_1)-principal stress plane and the coordinates σ_{3M}, σ_{1M} and the angle λ_1 of inclination of the polar radius (0M) are given by [68] :

$$(\sigma_{3M}, \sigma_{1M}) = \left\{ \frac{\frac{1}{2}(h_3H_{31}-h_1H_{33})}{(H_{11}H_{33}-H_{31}^2)} , \frac{\frac{1}{2}(h_1H_{31}-h_3H_{11})}{(H_{11}H_{33}-H_{31}^2)} \right\} \tag{73}$$

$$\lambda_1 = \tan^{-1}(h_1H_{33}-h_3H_{31})/H_{33}(2h_1+h_3) \tag{74}$$

The system of Cartesian coordinates (M- σ_1, σ_3), to which this ellipse is central and symmetric, is defined by the angle θ_1, expressed by :

$$\theta_1 = 1/2\tan^{-1}(2H_{31}/H_{33}-H_{11}) \tag{75}$$

whereas the semi-axes a_{1M} and a_{3M} of the ellipse are given by [17] :

$$a_{1M} = \left(\frac{1}{\bar{a}}\right)^{1/2} \left\{ 1 + \frac{H_{11}h_3^2+H_{33}h_1^2-2h_1h_3H_{31}}{(H_{11}-H_{22})^2+H_{33}(4H_{12}-H_{33})} \right\}^{1/2} \tag{76}$$

$$a_{3M} = \left(\frac{1}{\bar{b}}\right)^{1/2} \left\{ 1 + \frac{H_{11}h_3^2+H_{33}h_1^2-2h_1h_3H_{31}}{(H_{11}-H_{22})^2+H_{33}(4H_{12}-H_{33})} \right\}^{1/2} \tag{77}$$

and

$$\bar{a} = \frac{1}{2}\left\{ (H_{11}+H_{33}) + \left[(H_{33}-H_{11})^2+4H_{31}^2\right]^{1/2} \right\}$$

$$\bar{b} = \frac{1}{2}\left\{ (H_{11}+H_{33}) - \left[(H_{33}-H_{11})^2+4H_{31}^2\right]^{1/2} \right\} \tag{78}$$

The above relations for the transversely isotropic body are reduced to the following equations :

$$(\sigma_{3M}, \sigma_{1M}) = \left(-\frac{(h_1 H_{33}+2h_3 H_{11})}{H_{33}(4H_{11}-H_{33})}, -\frac{(2h_1+h_3)}{(4H_{11}-H_{33})} \right) \tag{79}$$

$$\lambda_1 = \tan^{-1} \frac{(h_1 H_{33}+2h_3 H_{11})}{H_{33}(2h_1+h_3)} \tag{80}$$

$$\theta_1 = \frac{1}{2} \tan^{-1} \frac{H_{33}}{(H_{11}-H_{33})} \tag{81}$$

$$\left.\frac{\bar{a}}{b}\right\} = \frac{1}{2} \left\{ (H_{11}+H_{33}) \pm \left[(H_{11}-H_{33})^2 + H_{33}^2 \right]^{1/2} \right\} \tag{82}$$

and

$$(a_{1M}, a_{3M}) = \left(\frac{1}{\bar{a}, \bar{b}} \right)^{1/2} \left\{ 1 + \frac{H_{11}h_3^2 + H_{33}h_1^2 + H_{33}h_1h_3}{H_{33}(4H_{11}-H_{33})} \right\}^{1/2} \tag{83}$$

It can be derived from the above theory that the elliptic paraboloid failure surface for the general orthotropic material has its axis of symmetry parallely displaced, relatively to the hydrostatic axis, but moving outside the principal diagonal (σ_3,δ_{12})-plane. Only the transversely isotropic materials have their EPFSs whose axes of symmetry lie on the (σ_3,δ_{12})-plane and therefore they are symmetric to this plane, so that any transverse intersection of the EPFS is an ellipse whose principal axes are parallel to the 0x- and 0y- axes.

For the orthotropic materials the respective EPFSs are angularly displaced so that the centers of their transverse elliptic intersection lie outside the (σ_3,δ_{12})-plane and their planes of symmetry, 0"y"z" or 0"x"z" are intersecting the principal diagonal planes along lines parallel to the hydrostatic axis, whose traces on the deviatoric plane are points S (for the 0"y"z"-plane) different than the origin 0. The angle θ_0 subtended by the planes of symmetry with the respective principal diagonal planes is of importance and was given by relation (70).

In Figure 24 the intersection of the EPFS corresponding to an oriented poly-carbonate material by the (σ_3,σ_1)-principal stress plane is presented. The failure strengths in simple tension and compression of the material along the principal directions are given in Table 1 and correspond to material A.

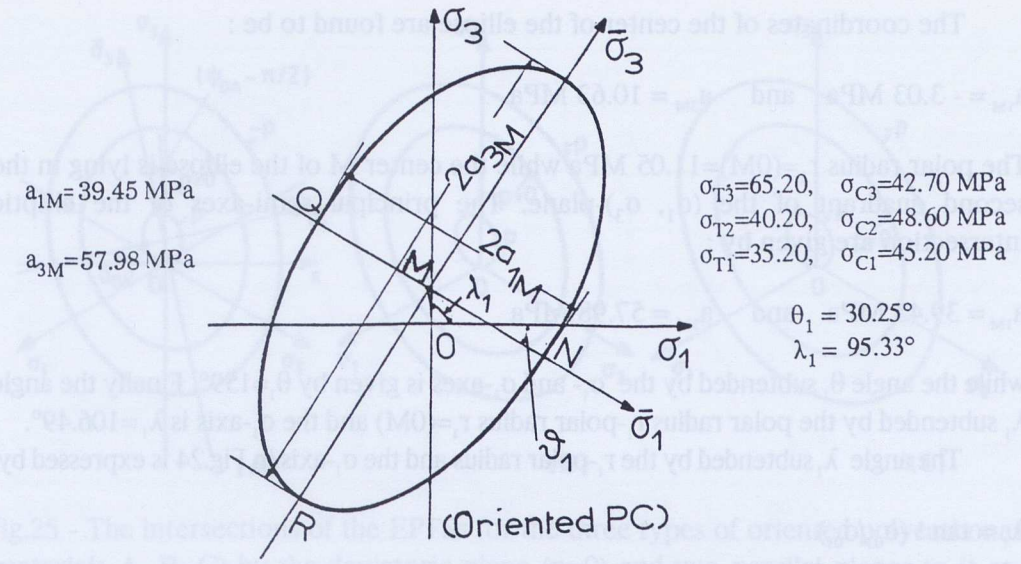

Fig. 24 - The intersection of the EPFS by the (σ_3,σ_1)-principal stress plane for an oriented polycarbonate.

Material	A	B	C
σ_{T3}(MPa)	65.20	65.20	65.20
σ_{C3}	42.70	42.70	42.70
σ_{T2}	42.20	43.60	48.10
σ_{C2}	48.60	54.00	56.30
σ_{T1}	35.20	35.20	35.20
σ_{C1}	45.20	45.20	45.20

Table 1 - The values of the principal strengths in tension and compression for three types of oriented polycarbonate named A, B and C.

The coordinates of the center of the ellipse are found to be :

$a_{1M} = -3.03$ MPa and $a_{3M} = 10.63$ MPa

The polar radius $r_1=(0M)=11.05$ MPa while the center M of the ellipse is lying in the second quadrant of the (σ_1, σ_3)-plane. The principal semi-axes of the elliptic intersection are given by :

$a_{1M} = 39.45$ MPa and $a_{3M} = 57.98$ MPa

while the angle θ_1 subtended by the σ_1- and σ_1-axes is given by $\theta_1=159°$. Finally the angle λ_1 subtended by the polar radius r_1-polar radius $r_1=(0M)$ and the σ_1-axis is $\lambda_1=106.49°$.

The angle λ_1 subtended by the r_1-polar radius and the σ_1-axis in Fig.24 is expressed by:

$$\lambda_1 = \tan^{-1}(\sigma_{03}/\sigma_{01})$$

The other two intersections of the EPFS by the principal stress planes (σ_2,σ_3) and (σ_1,σ_2) may be readily derived by cyclic interchange of the respective indices and coefficients. However, since σ_{T2} and σ_{C2} stresses are the intermediate failure strengths, the differences between σ_{T3}, σ_{C3} and σ_{T2}, σ_{C2} and, on the other hand, σ_{T1}, σ_{C1} and σ_{T2}, σ_{C2} are always smaller than the respective differences between σ_{T3}, σ_{C3} and σ_{T1}, σ_{C1}. Then, the elliptic intersection in the (σ_3,σ_1)-principal stress plane presents the strongest anisotropy and therefore it constitutes the most important intersection concerning the phenomena of anisotropy of the material.

3.5 Application of the EPFS-theory to a typical orthotropic material

As a typical example of application of the EPFS-theory to an orthotropic material three types of an oriented polycarbonate were used, whose strengths in simple tension and compression are given in table 1.

Figure 25 presents the intersections of the EPFS for the three types of oriented polycarbonate (materials A, B, C) by the deviatoric plane (p=0) and two parallel planes to it at a distances z=±p respectively, where the quantity p is given by :

$$p=d_0=\sqrt{3}/(h_1+h_2+h_3) \qquad (84)$$

Since the quantity p expresses the distance between the origin 0 and the point where the hydrostatic axis is piercing the EPFS, it is obvious that for z=p the elliptic intersection of the EPFS by this plane should pass through the origin 0.

Table 2 summarizes the values of the coordinates x_0, y_0 of the center of the ellipse representing the intersection of the EPFS by the deviatoric plane, the lengths a_1 and a_2 of its principal axes and the values of the angle θ_0 and ψ_0 subtended by the

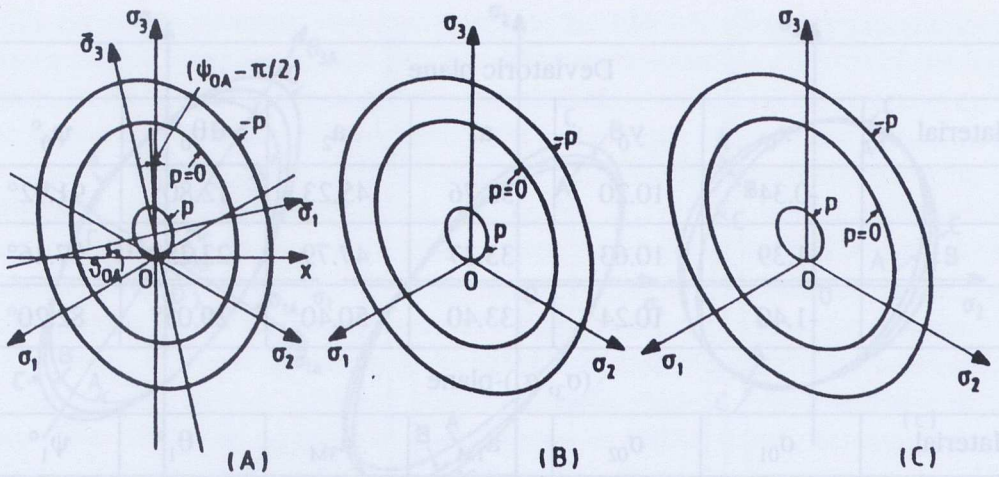

Fig.25 - The intersections of the EPFSs for the three types of oriented polycarbonate (materials A, B, C) by the deviatoric plane (p=0) and two parallel planes to it at a distances z=±p respectively ($p=\sqrt{3}/h_1+h_2+h_3$).

σ_1-principal axis and the 0x-axis of the Cartesian frame and, on the other hand, by the polar distance r_0=(00") of the center of the ellipse and the same 0x-axis.

It is clear from these figures that a variation of the failure strengths along the intermediate axis of anisotropy of the material does not influence significantly the size and orientation of the EPFS at the deviatoric plane. Furthermore, if one compares these ellipses with the elliptic intersection along the π-plane for the same materials he may realize that the small angular displacements of the orthotropic material relatively to its counterpart of the transversely isotropic one, which is of an angle smaller than $\theta_0^{max}=30°$ does not influence considerably the size and the shape of the elliptic cross-section at the π-plane.

Figure 26 presents the elliptic intersections of the EPFSs for the three types of polycarbonate with the (σ_3, σ_1)-, (σ_2, σ_1)- and (σ_3, σ_2)- principal stress planes.

It is worthwhile indicating the following remarks :

(i) Variation of the intermediate strengths σ_{T2} and σ_{C2} does not influence considerably the shapes and orientations of the intersections of the EPFSs and the (σ_3, σ_1)-plane. While the ellipses become more oblong as the strengths σ_{T2} and σ_{C2} move from the limits of σ_{T1}, σ_{C1} towards the limit of σ_{T3}, σ_{C3} , the angles θ_1 of inclination of these ellipses with respect to the $0\sigma_1$-axis do not change considerably remaining of the order of 30 deg.

(ii) Similarly, the intersections of the EPFSs with the (σ_2, σ_1)-plane present small variations in angles and lengths of their principal axes.

Deviatoric plane						
Material	x_0	y_0	a_1	a_2	$\theta_0°$	$\psi_0°$
A	-0.34*	10.20	32.76	45.23	12.80°	91.92°
B	-1.39	10.63	33.37	47.79	23.25°	97.46°
C	-1.40	10.24	33.40	50.40	29.05°	82.20°
(σ_3, σ_1)-plane						
Material	σ_{01}	σ_{02}	a_{1M}	a_{3M}	$\theta_1°$	$\psi_1°$
A	-0.99	10.59	36.92	68.88	30.25°	95.33°
B	0.059	11.30	36.02	75.83	32.22°	89.70°
C	0.93	12.05	35.47	81.72	33.23°	85.60°

* *All quantities except angles in Mpa's.*

Table 2 - The values of the principal axes of the elliptic intersections of the EPFSs, as well as their orientation and position, for three types of oriented polycarbonate (A,B,C) by the deviatoric π-planes and the (σ_3, σ_1)-principal stress planes.

(iii) Comparing this group of ellipses with the respective intersections of the EPFS of the corresponding material, which is transversely isotropic and described in Ref. [50, Figs. 5 and 7], one may state a striking similarity between the ellipses of Fig.26a of this work and Fig. 7 of Ref. [50]. For the transversely isotropic material we have :

a_{3M}=62.40 MPa, a_{1M}=38.20 MPa, θ_1=27° ψ_1=101.10°

whereas for the material A we have respectively :

a_{3M}=68.88 MPa, a_{1M}=36.92 MPa, θ_1=30.25° ψ_1=95.33°.

On the other hand, the differences in the (σ_1,σ_2)-plane of ref.[50], which is the isotropic plane for the respective transversely isotropic material, between the transversely isotropic material and its respective fully isotropic material, indicated in Fig.5 of ref.[50], are significant, whereas the differences in size and oriantation between the transversely isotropic material and the orthotropic one are much smaller.

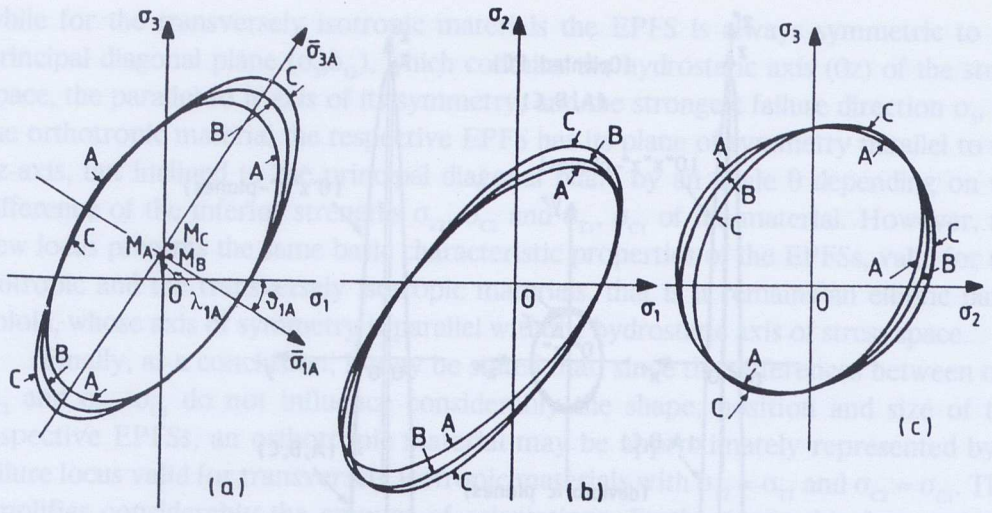

Fig. 26 - The elliptic intersections of the EPFSs for the three types of oriented polycarbonate (materials A, B, C) by the principal-stress planes (σ_3, σ_1), (σ_2, σ_1) and (σ_3,σ_2).

(iv) These remarks suggest that, for convenience, it is acceptable to assume that an orthotropic material is satisfactorily described by the respective transversely isotropic material and proceed in the design, since the differences between these two materials do not influence the overall behaviour of the orthotropic material.

(v) The shapes of the intersections of the EPFSs of the three materials by the third (σ_2,σ_3)-principal stress plane present a rounded elliptic one to counter balance the excess in ellipticity of the respective intersections with the (σ_3,σ_1)-plane relatively to the transversely isotropic case.

For the general orthotropic material the EPFS has its planes of symmetry 0"y"z" and 0"x"z", which are oblique relatively to principal stress and principal diagonal planes. These obliquenesses are represented by angles θ_1 and ψ_1. It is therefore of interest to plot the intersections of the EPFSs for the materials A,B and C and the three principal diagonal planes (σ_3,δ_{12}), (σ_1,δ_{23}) and (σ_2,δ_{13}). These intersections are plotted in Figs. 27 (a,b,c).

It is clear from these figures that, although the EPFSs for the orthotropic materials are obliquely positioned relatively to the principal stress- and diagonal-planes, subtending angles with the first group of the order of 30 degrees, the intersections of the EPFSs by the principal diagonal planes are parabolas almost symmetric to the hydrostatic axis, 0z, in the stress space. This fact indicates that, although the EPFS of a certain orthotropic material is obliquely positioned relatively to the principal diagonal planes, it presents some kind of symmetry according to which the hydrostatic axis remains always close to the axis of symmetry of the particular failure locus of the material.

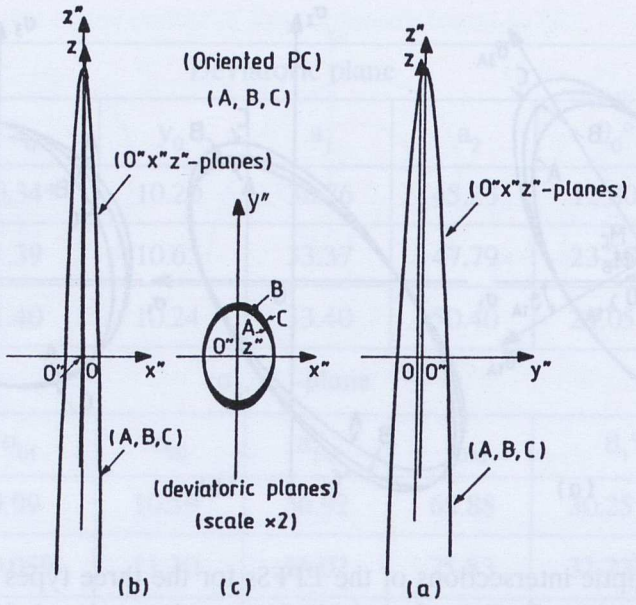

Fig. 27 - The intersection of the EPFSs for the three types of oriented polycarbonate (materials A, B,C) by the planes of symmetry 0"y"z", 0"x"z" and the deviatoric plane 0"x"y".

It is interesting pointing out that an increase of the intermediate failure strength of the material (σ_{T2},σ_{C2}), while does not influence significantly its failure behaviour for loadings lying close to the deviatoric plane, it creates a large difference at the regions of vertices of the EPFSs. Indeed, as the intermediate strengths increase, in the interval between the lowest strengths σ_{T1},σ_{C1} and the highest ones σ_{T3},σ_{C3}, the vertex of the respective EPFS is rapidly receding along the 0z-axis toward the possitive infinity, thus resembling more and more to the conical or Coulomb-Mohr criterion for brittle materials. Then, this rapid movement of the vertex of the EPFS indicates the strong influence of the hydrostatic component of the stress tensor to the failure behaviour of the material.

Finally, in Fig.27 the intersections of the EPFSs for the three types of oriented PC with their planes of symmetry 0"y"z" (Fig.27a), 0"x"z" (Fig.27b) and by the deviatoric planes, 0"x"y" (Fig.27c) were plotted in order to compare these symmetric intersections of the EPFSs with their respective intersections of Fig.22. It is clear that the maximum deviation between the 0z- and 0"z"-axes happens on the 0"y"z"-section, whereas for the 0"x"z"-intersection the two axes almost coincide. The differences of the same axes in the intersections of Fig.22 are in-between these extreme distances. The intersections of EPFSs by the deviatoric plane shown in Fig.27c presents another aspect of the same phenomenon.

Then, it may be concluded that the elliptic paraboloid failure surface continues to represent satisfactorily the general failure locus of any orthotropic material. However,

while for the transversely isotropic materials the EPFS is always symmetric to the principal diagonal plane (σ_3,δ_{12}), which contains the hydrostatic axis (0z) of the stress space, the parallel to it axis of its symmetry, and the strongest failure direction σ_3, for the orthotropic material the respective EPFS has its plane of symmetry parallel to the 0z-axis, but inclined to the principal diagonal plane by an angle θ depending on the difference of the inferior strengths σ_{T2}, σ_{C2} and σ_{T1}, σ_{C1} of the material. However, the new locus presents the same basic characteristic properties of the EPFSs, valid for the isotropic and the transversely isotropic materials, that is it remains an elliptic paraboloid, whose axis of symmetry is parallel with the hydrostatic axis of stress space.

Finally, as a conclusion, it may be stated that, since the differences between σ_{T2}, σ_{C2} and σ_{T1}, σ_{C1} do not influence considerably the shape, position and size of the respective EPFSs, an orthotropic material may be approximately represented by a failure locus valid for transversely isotropic materials with $\sigma_{T2} \approx \sigma_{T1}$ and $\sigma_{C2} \approx \sigma_{C1}$. This simplifies considerably the amount of calculations. Furthermore, this fact explains why real orthotropic materials are treated in the vast literature of the subject as transversely isotropic materials without large deviations between theory and experimental evidence.

3.6 The properties of the elliptic paraboloid failure surface.

The validity of the elliptic paraboloid failure surface criterion was checked in the numerous publications by the author cited at the end of this study [42-71] with the abundant experimental evidence existing in the literature for transversely isotropic and orthotropic materials. However, all the existing experimental evidence concerns the failure behavior of these materials subjected to a biaxial mode of loading. No sufficient experimental evidence exists concerning the effect of hydrostatic compression on the failure properties of anisotropic solids, except the results of Caddell and Kim [79] for the moderately anisotropic oriented polycarbonate. These experimental results are given in Fig.27 together with the theoretical prediction of the EPFS-criterion. The failure locus shown in this figure is a parabola and corresponds to the intersection of the elliptic paraboloid failure surface in the principal stress space, $(\sigma_1,\sigma_2,\sigma_3)$, by the main diagonal plane $(\sigma_1 = \sigma_2)$ referred to the $(\sigma_3\ \delta_{12})$-coordinate frame.

Figure 27 indicates the predictions of the EPFS-criterion, called (EPFS-1), which approximate satisfactorily the effect of hydrostatic pressure on the failure behavior of oriented polycarbonate. On the other hand, the predictions by the extensively used *failure tensor polynomial* criterion introduced by Tsai and Wu [39], who stated that all interaction terms H_{ij} are independent of the diagonal components of tensor H and should be defined by experimental tests, are also indicated in Fig.27 by the curves assigned as (EPFS-2), by assuming the validity of the Tsai-Hahn empirical condition $H_{ij} = -1/2\ (H_{ii}H_{ij})^{1/2}$ [80]. It is clear from this figure that the use of this

assumption, which is very popular in applications, results in large errors between theory and experiments when the material is subjected to a triaxial loading mode, although, when the results of the two criteria are compared in the principal (σ_1,σ_3)-plane, almost coincide [77].

It should be born in mind that the Tsai-Wu approach [39], where all stress interaction terms in the tensor polynomial function should be experimentally determined, is merely a curve- fitting process by a quadratic polynomial. Therefore, it constitutes a failure condition with statistical features, since for the determination of the stress interaction terms a large number of strength tests is required. Moreover, either the Tsai-Hahn assumption, or the acceptance that all off-diagonal terms are equal to zero [81], which yields an ellipsoid failure surface indicated in Fig.27 by the closed curve designated as (EFS), are unrealistic and should be avoided.

On the other hand, applications of the EPFS-criterion to several, either orthotropic, or transversely isotropic materials, either homogeneous, or composites, have proved that the coincidence of the predictions of this criterion with the existing experimental results is much better than any other criterion and especially with the tensor failure polynomial criterion, which yielded up-to-now the best of approximations with the results of tests in biaxial loading modes [42-71].

The position of the EPFS in the principal stress space presents a particular interest since it allows the separation of the orthotropic materials into two categories the tension-strong (T-strong) and the compression strong (C-strong) materials, depending on what octant in the stress space the open part of the paraboloid is lying. This can be defined by the position of the vertex of the paraboloid relatively to the deviatoric plane. Then the distance between the deviatoric plane and the vertex of the EPFS designated by d' and the distance of the same plane from the point of piercing of the hydrostatic axis 0z the EPFS, designated by d, are of interest. These distances are expressed by [11,47]:

$$d' = \frac{\sqrt{3}\left\{1+\frac{1}{9}(h_1-h_3)^2\right\}}{H_{33}(h_1+h_2+h_3)} \tag{85}$$

and :

$$d = \sqrt{3}/(h_1+h_2+h_3) \tag{86}$$

It is obvious from relations (85) and (86) that, since the numerators of both expressions are always positive, the sign of quantities d and d' depends on the sum $(h_1+h_2+h_3)=tr\mathbf{h}$ [47]. Then, if the quantity $(h_1+h_2+h_3)$ is positive the vertex of the paraboloid lies in the tension-tension-tension octant of the principal stress space and

therefore the EPFS opens toward the negative z'-axis. An orthotropic material with such a type of failure surface is classified as compression strong material (C-strong). On the contrary, if $(h_1+h_2+h_3)$ is negative the vertex of the paraboloid lies on the negative part of the z'-axis of symmetry and therefore the EPFS is open to the tension-tension-tension octant. The material in this case is classified as tension-strong (T-strong) material.

Figure 28 presents the (σ_3,δ_{12})-principal diagonal intersection of the elliptic paraboloid failure surface for a typical C-strong transversely isotropic material. The δ_{12}-coordinate axis coincides with the bisector of the angle $\sigma_1 0\sigma_2$ on the isotropic plane of the principal stress space. The distances d and d' are indicating the respective distance between the deviatoric plane 0xy normal to the (σ_3,δ_{12})-plane and the points of piercing the paraboloid by either the hydrostatic axis (0z) or the symmetry axis (0'z'). The angles subtended by either the hydrostatic axis or the symmetry axis and the $0\delta_{12}$-axis are equal to 35.26°, whereas the same axes subtend angles with the σ_3-strong axis equal to 54.74°.

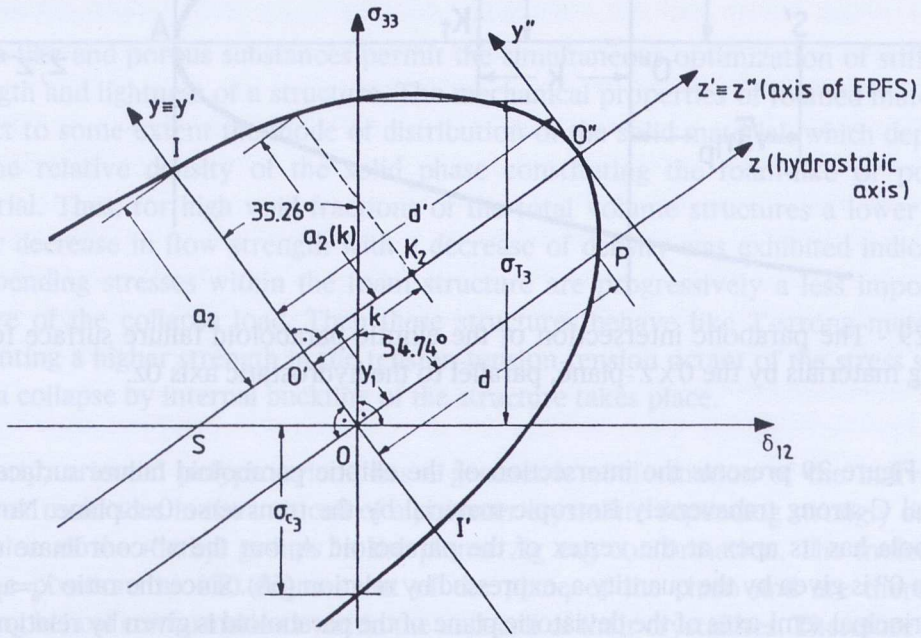

Fig.28 - The intersection of the elliptic-paraboloid failure surface by the principal diagonal plane $(\sigma_{33},\delta_{12})$ for C-strong transversely isotropic materials (δ_{12} is the bisector of the $(\sigma_{11}0\sigma_{22})$-angle in the $(\sigma_{11},\sigma_{22})$ principal stress plane).

The distance $y_1 \equiv \eta_p$ given by eq.(64) for the transversely isotropic material is given by the (00')-segment. This distance is a characteristic quantity of the anisotropy of the material, which is related to the necessary elastic energy consumed by the external loading to overcome the elastic energy of anisotropy of the material [82-89].

Examining now the other principal cross-section of the elliptic paraboloid failure surface it may readily be proven that this cross-section is also a parabola. For reasons of simplicity we give the shape of this parabolic intersection by the 0xz-plane for a typical transversely isotropic body, thus avoiding the complications in the forms of these sections for the orthotropic material, where the axes of symmetry are inclined to the initial 0xyz-frame.

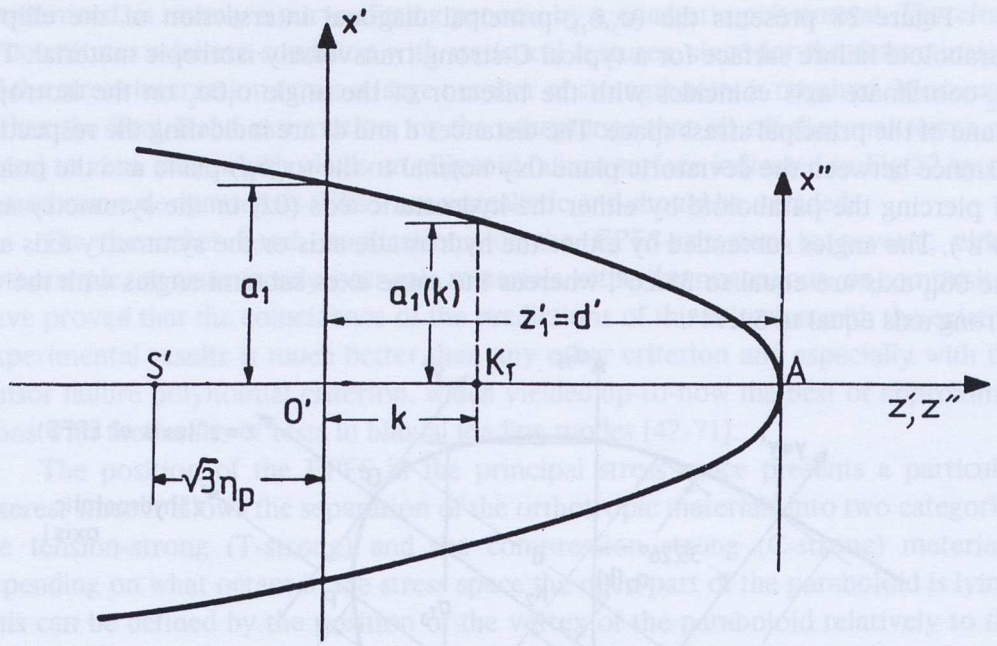

Fig. 29 - The parabolic intersection of the elliptic-paraboloid failure surface for C-strong materials by the 0'x'z'-plane, parallel to the hydrostatic axis 0z.

Figure 29 presents the intersection of the elliptic paraboloid failure surface of a typical C-strong transversely isotropic material by the transverse 0xz-plane. Now the parabola has its apex at the vertex of the paraboloid A, but the x"-coordinate at the origin 0" is given by the quantity a_1 expressed by relation (68). Since the ratio $\lambda_0=a_2/a_1$ of the principal semi-axes of the deviatoric plane of the paraboloid is given by relation (69) where $a_1<a_2$, it is obvious that this parabola is much more shallow than the parabola representing the intersection of the EPFS by the 0"y"z"-plane of symmetry, which coincides with the $(0\sigma_3\delta_{12})$-plane for the transversely isotropic materials. The ratio λ_0 expresses the degree of shallowness of the EPFS-surface. This coefficient, which is called the *prolateness parameter* of the elliptic paraboloid is equal to unity for the isotropic materials, where the paraboloid is a surface of revolution. As the anisotropy of the material is increased the value of λ_0 is diminishing and the EPFS becomes more and more shallow. For highly anisotropic materials the shape of the EPFS becomes very flattened and takes the form of a crashed sigar (expression common in the U.S.A.).

The distance 0's' along the 0"z"-axis, defining the point where the 0"z"-axis of symmetry is piercing the transverse plane $(0\sigma_1\sigma_2)$, is given by :

$$(0's') = \sqrt{3}\,\eta_p = \frac{\sqrt{2}}{3H_{33}}(h_1\text{-}h_3) \tag{87}$$

Most of the orthotropic solids and compact materials are C-strong materials, since they are capable to sustain large compressive stresses without failure. However, there is a restricted category of materials, which behave like T-strong ones. In these substances the solid material is distributed in little columns or beams forming the cell edges in cellular open-cell foam-like solids, where clusters of microvoids intervene between molecules or crystals, thus creating structures, which may be either isotropic or more frequently orthotropic. Most polymers can be readily foamed and techniques exist for doing the same thing with ceramics and glasses, even with metals, in modern technologies.

Foam-like and porous substances permit the simultaneous optimization of stiffness, strength and lightness of a structure. The mechanical properties of foamed materials reflect to some extent the mode of distribution of the solid material, which depends on the relative density of the solid phase constituting the foam-like or porous material. Thus, for high void fractions of the total volume structures a lower than linear decrease in flow strength with a decrease of density was exhibited indicating that bending stresses within the foam structure are progressively a less important feature of the collapse load. Then these structures behave like T-strong materials presenting a higher strength in the tension-tension-tension octant of the stress space until a collapse by internal buckling of the structure takes place.

Similarly, oriented polypropylene has a geometric conformation of the individual polymer molecules in the unit cell of a polymer crystallite depending strongly on the repulsion of the methyl groups in the planar zig zag conformation. The molecules assume positions at 120 degrees out of the plane of the chain and are therefore forming helical conformations within the unit-cell of their crystallites. Therefore low-density oriented polypropylene influenced by the spring-like cells presents a T-strong behavior as it has been proved in refs.[11] and [53].

Likewise, paper sheats, which consist of networks of fibers placed at different random arrangements, whose properties, nature and frequency of bonds between them influence the properties of the paper sheets belong in the same category. Indeed, fibers are actually filament-wound composite systems, whose cell walls are composed of a number of different layers, the fibrils, which are aggregates of cellulose molecules with cellobiose as the basic repeating unit, arranged either in an orderly, or in a

random fashion. The fibrils themselves are arranged in a regular fashion differing within the various layers of the cell-wall and they are held together by the hemicellulose and lignin matrix material.

Such conglomerates contain a great number of microvoid clusters distributed randomly inside the structure and this reduces considerably the specific density of the material. The bonded fibers act like springs largely interconnected. It is therefore to be expected that low density paper sheets behave like T-strong anisotropic materials, as it is clearly indicated in ref.[49].

Similar results have been found in a study of foamy materials [51] where the failure modes of three types of polyurethane foams with densities varying between d_1=64kg/m^3, d_2 = 96 kg/m^3 and d_3 = 192 kg/m^3 were studied. Whereas the low density material (d_1) may be considered as a open cell rigid foam, the other two substances correspond to closed-cell cellular solids. All these materials are transversely isotropic bodies whose failure loci are completely determined by their failure stresses in tension and compression along the three principal stress directions. It was clearly proved that as the density of the cellular solid is increased the mode of failure of the material changes from a T-strong material to a C-strong one. In-between the material passes through a quasi-isotropic status, where the axis of symmetry of the respective EPFS almost coincides with the hydrostatic axis.

On the contrary, elastic compact solids, whose porosity is insignificant, present always a C-strong behavior independently if they are rigid homogeneous solids, or composite materials. As an example, an oriented polycarbonate studied in [79] behaves as a moderately anisotropic C-strong material, as all the fiber reinforced composites studied in refs. [42-71].

In the following we consider transversely isotropic materials obeying the stability condition (61). This means that we consider only well-behaving transversely isotropic materials whose ratios $R_L=\sigma_{C3}/\sigma_{T3}$ and $R_T=\sigma_{C1}/\sigma_{T1}$, defining the two *principal strength differential factors,* and ratio $R_{LT}=\sigma_{T3}/\sigma_{T1}$, defining the *tensile coefficient of anisotropy* of the material, take values that are in agreement with the features of typical materials used in applications. Assuming that $\sigma_{C1}>\sigma_{T1}$, a fact which is always valid in anisotropic materials used in constructions, we investigate the sign the quantity tr**h**, since the signs of R_T and R_{LT} are always positive, because it is valid that $R_T\geq 1.0$, $R_{LT}\geq 1.0$. The quantity [50,53] :

$$\mathrm{tr}\mathbf{h} = (h_1+h_2+h_3) \tag{88}$$

which for the transversely isotropic material becomes :

$$\mathrm{tr}\mathbf{h} = (2h_1+h_3)$$

may be written in terms of R_L, R_T, R_{LT} as follows :

$$\mathrm{tr}\mathbf{h} = \frac{2}{\sigma_{T3}}\left[R_{LT}\left(\frac{1}{R_T} - 1\right) + \frac{1}{2}\left(\frac{1}{R_L} - 1\right)\right] \tag{89}$$

The sign of the quantity tr**h**, as it is already mentioned, defines the orientation of the EPFS for each transversely isotropic material. A positive value for tr**h** indicates a C-strong material, whereas a negative one, a T-strong material. In the first case the EPFS has its open end oriented toward the compression-compression-compression octant, whereas in the second case the EPFS is oriented toward the tension-tension-tension octant. The values of tr**h**=0 are of interest since for tr**h**=0 the EPFS degenerates into an elliptic cylinder, resembling the Mises yield condition for anisotropic materials, which, as is known, neglects the strength differential effect.

However, in the general case of EPFS, where the strength differential effect is significant and is taken into account, selection of the appropriate values for R_L, R_T and R_{LT} to reduce the failure locus into an elliptic cylinder indicates a weakness and instability of the material, since in this case it is not possible to decide which one of the two types of failure surfaces it should follow.

Putting tr**h**=0, a manifold in the (R_L, R_T, R_{LT})-space may be defined which characterizes all weak transversely isotropic materials and separates the restricted (R_L, R_T, R_{LT})-space into two regions, on either side of each limiting curve corresponding to either C-strong (upper part) or T-strong (lower part) materials. Then, it is convenient to give in the (R_L, R_T)-plane the parametric family of curves with the quantity R_{LT} as parameter. This was done for a series of either mildly anisotropic or strongly anisotropic transversely isotropic materials and fiber composites, with curves $R_L = f(R_T)$. The parameters of these curves were plotted for individual values of R_{LT} in Fig. 30.

These materials were either oriented polycarbonate, Boron-Aluminium, Boron-Epoxy, Carbon-Epoxy, Glass-Epoxy or Kevlar 49 fibre composites, with the characteristic failure strengths as given in Table 3. Values for R_T smaller than unity indicate T-strong materials.

Material	σ_{T3}(Mpa)	σ_{C3}(Mpa)	σ_{T1}(Mpa)	σ_{C1}(Mpa)	$R_T=\sigma_{C1}/\sigma_{T1}$
PC(oriented)	65.20	42.70	35.20	45.20	1.284
PP(oriented)	34.00	25.90	14.40	9.20	0.639*
Bo-epoxy [14]	1296.21	2489.08	62.05	310.26	5.000
Ca-epoxy	1043.00	698.00	43.10	142.24	5.000
Keviar 49 [14]	1379.00	276.00	29.60	138.00	4.660
Boron-Al [16]	965.30	1379.00	102.05	222.02	2.176
* *A value for R_T<1.00 indicates a T-strong material.*					

Table 3 - The values of principal strengths of various orthotropic materials

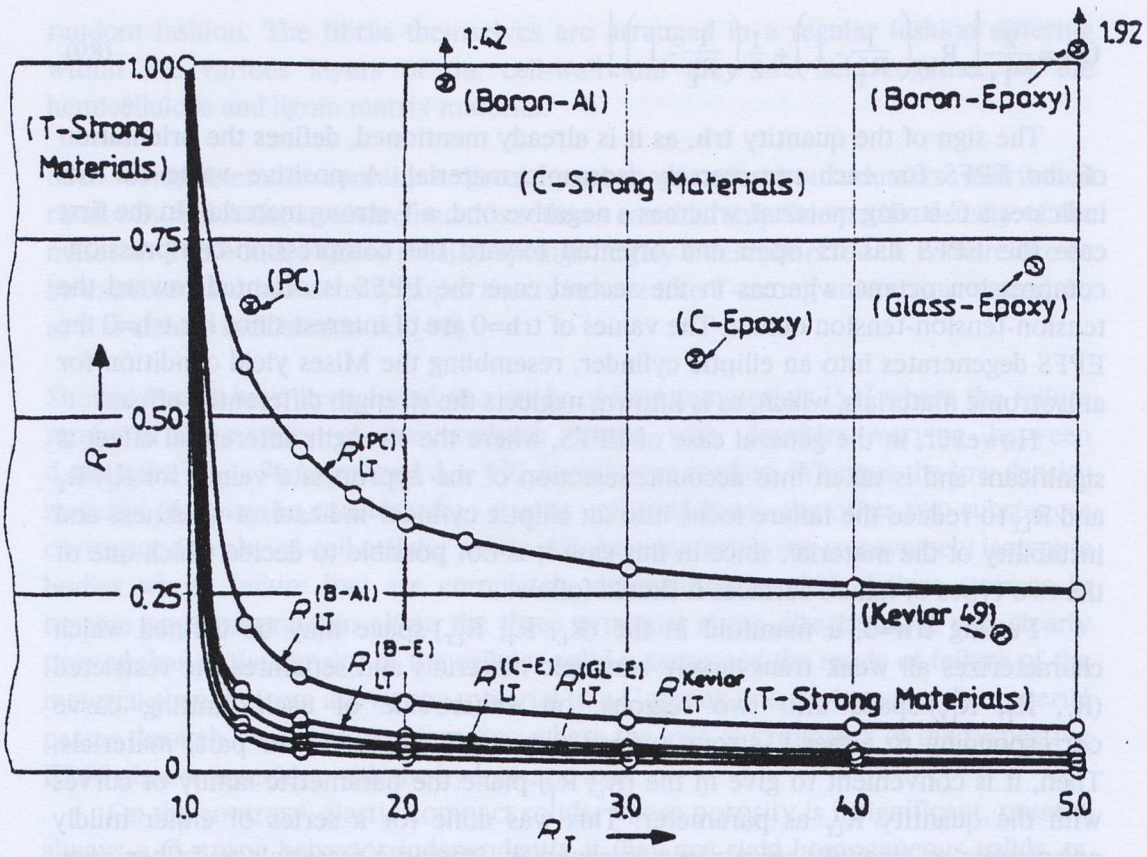

Fig. 30 - The variation of the strength differential parameter along the strong direction, R_L, against the transverse direction R_T, for different values of the parameter of anisotropy, R_{LT}, for a series of fiber composites.

The relationship expressing this parametric family of curves is given by :

$$\frac{1}{R_L} = (1 + 2R_{LT}) - \frac{2R_{LT}}{R_T} \qquad (90)$$

It was assumed in plotting the curves of Fig.30 that the parameter R_{LT} was kept constant and equal to its value for each individual material plotted and only the quantities R_L with R_T are varying between unity and a large number (say five).

It is interesting pointing out that all curves $R_L=f(R_T)$ pass through the point $R_L=R_T=1.0$, which defines the theoretically ideal isotropic material. This point presents equal strengths along its respective tensile and compressive principal directions. Indeed, for $R_T=R_L=1.0$, the failure surface degenerates into the Mises cylinder :
$x^2 + y^2 = 2/3\ \sigma_0^2$

where σ_0 is the yield or failure strength for ideally isotropic materials.

It is also clear from this nomogram that any combination of R_L, R_T and R_{LT}-values corresponding to points lying above each respective limiting $R_L=f(R_T)_{RLT}$ curve for each particular material, indicates a C-strong material, whereas points beneath this curve represent a T-strong material.

Since the region of weak behaviour of the material is restricted around its respective $R_L=f(R_T)_{RLT}$ curve, the position of each material in the (R_L, R_T)-plane and its distance from the respective $R_L=f(R_T)$ curve indicates the degree of the efficient performance of the material. The position of performance of the transversely isotropic materials study in table 3 are indicated in Fig.30 by oblique crosses. The distances along the ordinates between these points and the respective transient $R_L=f(R_T)$ curves indicate the degree of efficiency of the materials. Thus, the Boron-epoxy and the Boron-aluminium composites indicate a very satisfactory performance, whereas glass-epoxy and graphite-epoxy show a rather reduced quality. The minimum distance appears for Kevlar 49, for the fiber composites and for oriented polycarbonate and the homogeneous materials.

The region $R_T<1.0$ in Fig.30 belongs exclusively to T-strong materials, but these materials present a peculiar behavior, since their transient curves cannot exceed the limit for which the R_L-ratio becomes negative. Then, the interval of variation of R_T is restricted between $R_T=1.0$ and $R_T=2R_{LT}/(1+2R_{LT})$. In this limited interval small variations of R_T create large variations in R_L, which for $R_T=2R_{LT}/(1+2R_{LT})$ tend to infinity. Such large values for the longitudinal strength differential factor are unattainable. The actual positions of the T-strong materials in the (R_L,R_T)-diagram are always inside the safe zone for these materials.

For example, oriented polypropylene with $\sigma_{T3}=34.0$ MPa, $\sigma_{C3}=25.9$ MPa, $\sigma_{T1}=14.40$MPa, and $\sigma_{C1}=9.20$ MPa, and coefficients $R_L=0.761$, $R_T=0.639$ and $R_{LT}=2.361$ presents a transient $R_T=f(R_L)$ curve varying between $R_L=1.0$ (for $R_T=1.0$) and $R_L=\infty$ for $R_T=0.825$. However, its position with $R_L=0.761$ and $R_T=0.639$ in the (R_L,R_T)-diagram is deeply inside the second quadrant (for $R_T<1.0$) of Fig.30 and lies far away from the position of its $R_L=f(R_T)_{RLT=2.361}$-curve and therefore it presents a safe mechanical behavior.

3.7 Experimental verification of EPFS

It has been shown that the elliptic paraboloid failure surface for transversely isotropic materials is symmetric to the principal diagonal plane containing the σ_3-strong principal axis and the bisector δ_{12} of the right angle $\sigma_1 0\sigma_2$ on the transverse isotropic plane of the material. The intersection of the EPFS with this plane is a parabola having its vertex in the tension-tension-tension octant for C-strong materials and in the compression-compression-compression octant for the T-strong mate-

rials. All other sections of the quadratic surface not containing its axis of symmetry, which is parallel to the hydrostatic axis of the principal stress space, are ellipses. Ellipses are also the intersections of the EPFS by planes parallel to the deviatoric plane. The situation is more complicated for orthotropic materials because of the angular displacement of the symmetry planes of their failure surfaces about the hydrostatic axis of the material.

Of all these intersections, the most important for the study of the validity of the failure locus are the intersections by the deviatoric π-plane and those by the principal stress planes. For transversely isotropic materials two such intersections are important, those by the (σ_3,σ_1)- or (σ_3,σ_2)- planes (which are identical) and the intersection by the plane, (σ_1,σ_2), of isotropy of the material.

Figure 31 presents the intersection of the elliptic paraboloid failure surface of a graphite-epoxy fiber composite by the principal diagonal (σ_3,δ_{12})-plane and its normal (x'0'z')-plane. Both these intersections are parabolas with openings that have a ratio given by the quantity λ_0. In the same figure the elliptic intersection of the EPFS by the deviatoric π-plane is given by K_s, L_s, K'_s, L'_s-curve. The axis of symmetry of the paraboloid, which is parallel to the hydrostatic axis, lies at a distance $y_1=\eta_p$, which depends exclusively on the strength differential parameters and the parameter of anisotropy of the material. Figure 32 presents the intersection of the EPFS for the graphite-epoxy fibre composite of Fig.31 by the principal (σ_3,σ_1)-plane. This intersection is an ellipse with centre M, and lengths and orientation of its principal axes as defined in the figure.

For strongly anisotropic materials, the shape of EPFS resembles a *sword's sheath* (a very flattened paraboloid) and its intersection by the (σ_3,σ_1)-plane an oblong ellipse almost parallel to the principal σ_1- and σ_3-axes. This explains why the maximum principal stress σ_3 along the fibre direction constitutes a satisfactory approximate criterion for failure of strongly anisotropic fibre composites.

Since triaxial tests are difficult to execute, so as to yield reliable results, biaxial tests remain the only tests along the principal planes (σ_3,σ_1) or (σ_3,σ_2) for the verification of the influence of orthotropy on the elliptic failure (σ_2,σ_1)-locus of the plane of isotropy of material. Although the change of the shape of the elliptic locus along the isotropic (σ_1,σ_2)-plane is very sensitive to the influence of orthotropy of the material, up to now no test along this plane has been executed.

Figure 33 presents the intersections of the EPFSs for oriented polycarbonate (C-strong material) and for oriented polypropylene (T-strong material) by the (σ_1,σ_2)-planes of isotropy. The ellipses corresponding to the transversely isotropic material (curves 1) and to the respective isotropic materials presenting the same strength differential parameter (curves 2) were plotted in these diagrams. Moreover, and for comparison, the ellipses for the respective isotropic materials were also plotted for the case where R=1.0 ($\sigma_T=\sigma_C$). It is clear from these plottings that although in both

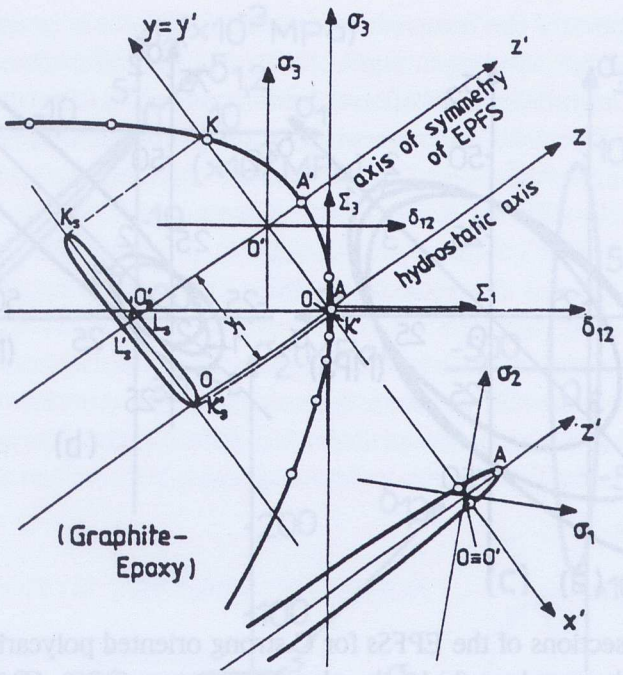

Fig. 31 - The intersections of the EPFS for a graphite-epoxy fiber composite by the principal diagonal (σ_3,δ_{12})-plane and its normal one (0'x'z').

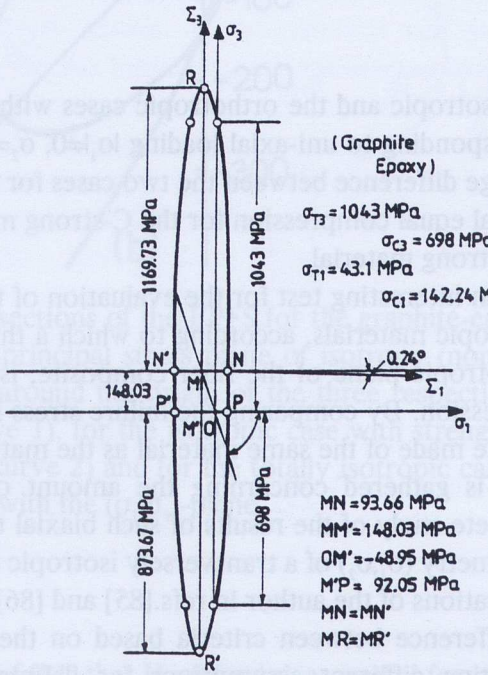

Fig. 32 - The intersection of the EPFS for the graphite-epoxy fiber composite of Fig. 31 by the principal stress (σ_3,σ_1)-plane.

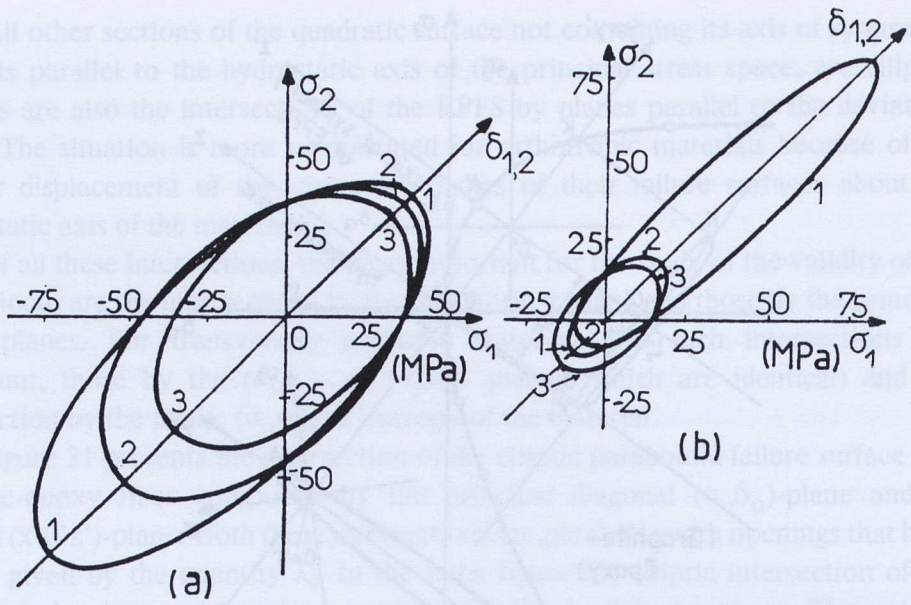

Fig. 33 - The intersections of the EPFSs for C-strong oriented polycarbonate (a) and T-strong oriented polypropylene (b) by the plane of isotropy (σ_1,σ_2). Curve 1 corresponds to the actual transtropic case, curve 2 to the isotropic case with strength differential effect ($\sigma_C>\sigma_T$) and curve 3 to the isotropic case without strength differential effect ($\sigma_T=\sigma_C$).

pairs of curves for the isotropic and the orthotropic cases with strength differential effects, the points corresponding to uni-axial loading $|\sigma_1|\neq 0$, $\sigma_2=0$ or $|\sigma_2|\neq 0$, $\sigma_1=0$ are coincident, there is a large difference between the two cases for biaxial equal loading and especially for bi-axial equal compression for the C-strong material or for biaxial equal tension for the T-strong material.

This fact suggests an interesting test for the evaluation of the failure properties of the transversely isotropic materials, according to which a thin or thick plate, cut along the transverse isotropic plane of the fiber composite, is subjected to biaxial equal tension or compression. By comparing the failure stress for this case with the respective test for a plate made of the same material as the matrix of the composite, important information is gathered concerning the amount of anisotropy of the composite. For a complete study of the results of such biaxial tests on the isotropic transverse plane of symmetry (σ_1,σ_2) of a transversely isotropic material the reader is referred to recent publications of the author in refs.[85] and [86], where it was shown that there is a clear difference between criteria based on the same failure tensor polynomials but accepting different assumptions for defining their coefficients, sufficient to distinguish which one of them is closer to reality. In these references the comparison is restricted to the most common used criteria of Tsai-Wu with the

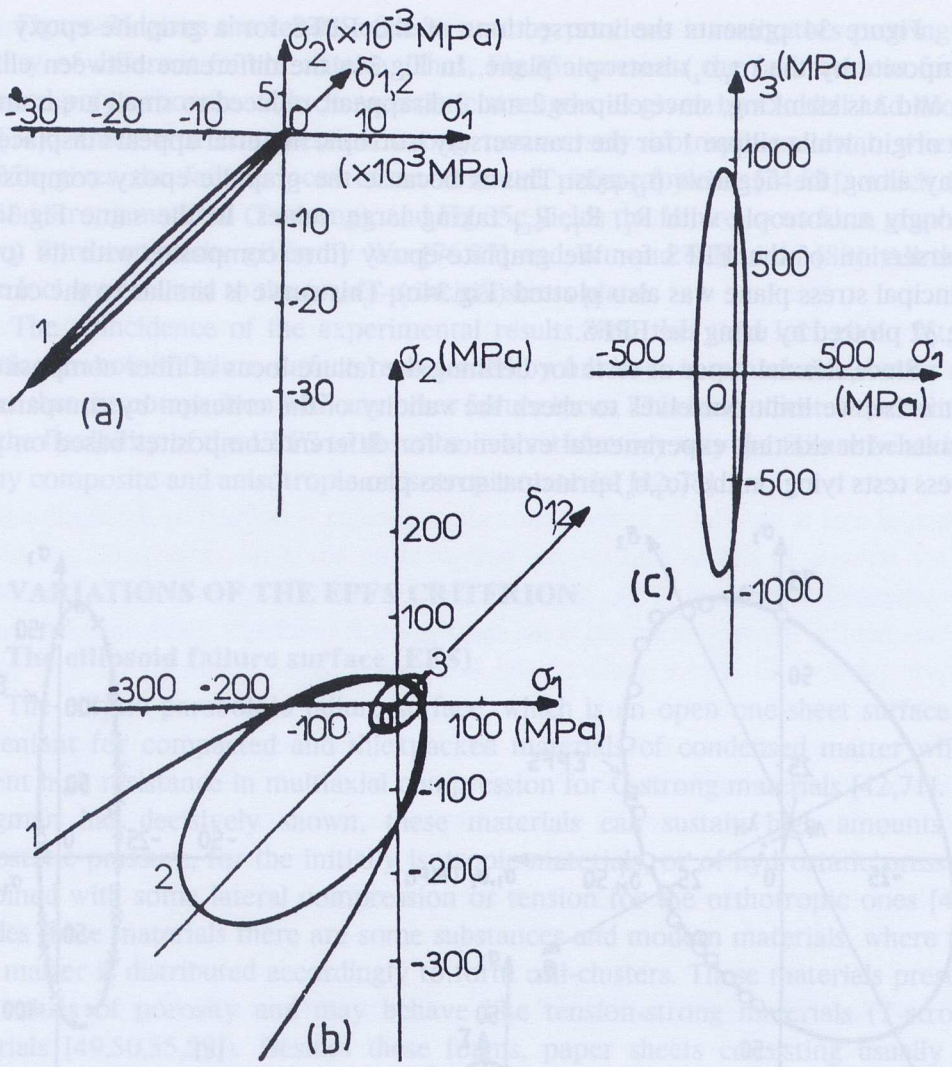

Fig.34 - (a) The intersections of the EPFS for the graphite-epoxy fiber composite of Fig.31 by the (σ_1,σ_2)-principal stress plane of isotropy (normal to the fibre direction).(b) is the detail around the origin of the three respective intersections for the fibre composite (curve 1), for the isotropic case with strength differential effect the same as previously (curve 2) and for the totally isotropic case (curve 3). and (c) the intersection of EPFS with the (σ_1,σ_3)-plane.

assumption made in ref.[81] that $H_{ij}=0$ for $i\neq j$, as well as for the Tsai-Hahn criterion [80], where it is arbitrarily assumed that $H_{ij}=-1/2(H_{ii}\,H_{jj})^{1/2}$, which were compared with the EPFS-criterion.

Figure 34 presents the intersections of the EPFS for a graphite-epoxy fibre composite by the (σ_1,σ_2)-isotropic plane. In Fig.34a the difference between ellipses 1,2 and 3 is strinking, since ellipses 2 and 3 disappear, reduced to small areas around the origin, while ellipse 1 for the transversely isotropic material appears displaced far away along the negative δ_{12}-axis. This is because the graphite-epoxy composite is strongly anisotropic with R_L, R_T, R_{LT} taking large values. In the same Fig.34 the intersection of the EPFS for the graphite-epoxy fibre composite with its (σ_3,σ_1)-principal stress plane was also plotted (Fig.34c). This curve is similar to the curve of Fig.32 plotted by using the EPFS.

Since triaxial types of tests for defining the failure locus of fiber composites do not exist, we limit ourselves to check the validity of the criterion by comparing its results with existing experimental evidence for different composites based on plane stress tests lying on the (σ_3,σ_1)-principal stress plane.

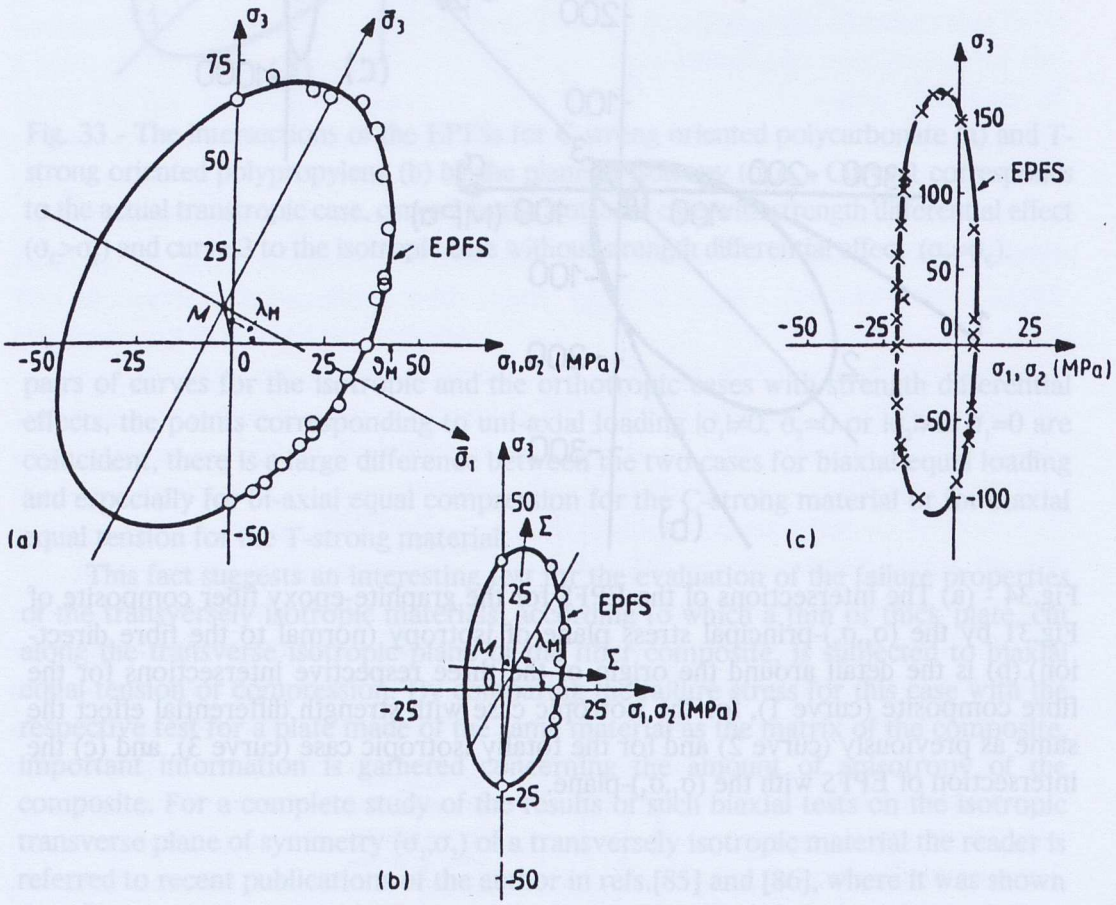

Fig.35 - A comparison of the failure loci along the (σ_3,σ_1)-stress plane for (a) an oriented polycarbonate (C-strong), (b) an oriented polypropylene and (c) Morganite II (carbon fibre-epoxy composite) and the existing experimental evidence.

Figure 35 gives the results of tests used by previous investigators proving the validity of different failure criteria. Thus, Fig.35a presents the failure locus for an oriented polycarbonate with characteristic strengths as given by Caddell and Woodliff [74], which is a compression strong transversely isotropic material, whereas Fig.35b gives the failure locus of an oriented polypropylene [74,81], which is a tension strong material (T-strong), and Fig.35c yields the failure locus for a graphite-epoxy fibre composite given by Wu [76,87] and Wu and Scheublin [88]. All these three loci are referred to the (σ_3,σ_1)-principal stress plane.

The coincidence of the experimental results with the yield loci given by the elliptic paraboloid failure surface represented by full lines is remarkable, better and higher that the comparison with any other failure locus. This fact indicates the validity and the flexibility of the EPFS to describe in a satisfactory way the failure behaviour of any composite and anisotropic or isotropic material [42,78].

4. VARIATIONS OF THE EPFS CRITERION

4.1 The ellipsoid failure surface (EFS)

The elliptic paraboloid failure surface, which is an open one-sheet surface, is convenient for compacted and thickpacked materials of condensed matter which present high resistance in multiaxial compression for C-strong materials [42,71]. As Bridgman has decisively shown, these materials can sustain high amounts of hydrostatic pressure, for the initially isotropic materials, or of hydrostatic pressure combined with some lateral compression or tension for the orthotropic ones [40]. Besides these materials there are some substances and modern materials, where the solid matter is distributed accordingly to form cell-clusters. These materials present high values of porosity and may behave like tension-strong materials (T-strong materials [49,50,55,59]). Besides these foams, paper sheets consisting usually of complicated conglomerations of fibriles with many voids between them present a definite T-strong behavior [59]. Similarly, oriented polypropylene is a T-strong material, since the geometric configuration of the individual polymer molecules in the unit cell of a polymeric crystallite of this high polymer depends strongly on the repulsion of the methyl groups in the planar zig-zag conformation. Then, the molecules assume positions at 120° out of the plane of the chain and are therefore forming helical conformations within the unit cell. This results in a low density for the oriented polypropylene, which is influenced by the spring-like cells and creates a tension strong behavior [11,53].

The principal mechanism of failure of all these materials is based on the cell-wall bending. It has been established that their failure mode can be satisfactorily described by the elliptic paraboloid failure surface for the general orthotropic body [55,59]. Besides, since these materials fail in the compression-compression-compression

octant of the principal stress space (or in the tension-tension-tension octant for the T-strong materials) by elastic buckling (or general collapse of their foamy structure for the T-strong ones) there is a need to take into consideration this also mode of failure. In previous publications by the author [55,59] it was established intuitively that the EPFS-criterion should be complemented by an ellipsoid surface, whose principal major axis coincides with the EPFS-axis of symmetry. This ellipsoid can be defined by the existing evidence for the definition of the EPFS complemented by one triaxial test. The best and simplest such test is either a hydrostatic pressure p_c, or a hydrostatic tension p_t. Comparison of this two surface criterion with experimental evidence with foams showed a good agreement of theory and experiments.

It is therefore possible to generalize the elliptic paraboloid failure surface, associated together with a congruent ellipsoid describing the buckling behavior of such materials, by a unique failure surface defined by an ellipsoid, whose major principal axis is parallel to hydrostatic axis and which is defined by the three pairs of failure stresses in simple tension and compression along the three principal axes of the material combined with a single failure test in hydrostatic compression. Consequently, this new criterion is the most general criterion, which includes also the elliptic paraboloid failure surface, and it is much more versatile, since it can be adapted to any type of material.

For a closed-end surface, as it should be the ellipsoid failure surface EFS, relations (57) defining the three off-diagonal terms of the fourth-rank tensor **H** do not hold anymore. They should be replaced by other substitutes. For this purpose we consider the principal diagonal intersection of the ellipsoid by the (σ_3,δ_{12})-plane, which for the general orthotropic body is expressed by :

$$\frac{1}{2}(H_{11}+H_{22}+2H_{12})\,\delta_{12}^2+H_{33}\sigma_3^2+\sqrt{2}(H_{13}+H_{23})\delta_{12}\sigma_3+\frac{\sqrt{2}}{2}(h_1+h_2)\delta_{12}+h_3\sigma_3-1=0 \qquad (90)$$

Relation (90) for the transversely isotropic material, which is of interest here, because of its simplicity and almost general application in orthotropic materials of the praxis, becomes:

$$(H_{11}+H_{12})\delta_{12}^2+H_{33}\sigma_3^2+2\sqrt{2}H_{13}\delta_{12}\sigma_3+\sqrt{2}h_1\delta_{12}+h_3\sigma_3-1=0 \qquad (91)$$

In order Eq.(91) to express an elliptic intersection for the new criterion, instead of a parabolic as it is for the EPFS, it is necessary to satisfy the following inequality [78] :

$$\det \mathbf{A_2} = \det \begin{pmatrix} (H_{11}+H_{12}) & \sqrt{2}H_{13} \\ \sqrt{2}H_{13} & H_{33} \end{pmatrix} > 0$$

The determinant $\mathbf{A_2}$ yields the inequality :

$$(H_{11}+H_{12})H_{33} > 2H_{13}^2 \tag{92}$$

We apply now the first general constraint on eq.(91) that the major axis of the elliptic intersection is parallel to the hydrostatic axis of the system, i.e.,

$$\sigma_3 = \sqrt{2}/2\ \delta_{12} \tag{93}$$

This relation implies that angle θ, subtended by the hydrostatic axis and the δ_{12}-diagonal, is equal to $\theta=35.26°$. On the other hand, the angle θ subtended by the symmetry axis of the surface of Eq.(91) and the δ_{12}-axis is given by [78] :

$$\tan 2\theta = 2h/(a-b) \tag{94}$$

where 2h, a and b are the coefficients of the terms $\delta_{12}\sigma_3$, δ_{12}^2 and σ_3^2 respectively of the polynomial of Eq.(91). Then it is vald that :

$$\tan 2\theta = \frac{2\sqrt{2}\,H_{13}}{(H_{11}+H_{12}-H_{33})} = 2\sqrt{2} \tag{95}$$

Relation (95) yields :

$$IH_{12}=H_{13}-H_{11}+H_{33} \tag{96}$$

Since both relations (92) and (96) must be valid, substituting Eqs. (96) into (92), we derive that :

$$2H_{13}^2-H_{33}H_{13}-H_{33} < 0 \tag{97}$$

Relation (97) when solved, yields :

$$-1/2H_{33}<H_{13}<H_{33} \tag{98}$$

Then, Eq. (91) represents an ellipse in the principal diagonal plane (σ_3,δ_{12}), whose an axis of symmetry (major or minor) is parallel to the hydrostatic axis. Therefore, the set of relations (96) and (98) defines a family of ellipses.

It can be readily shown that these ellipses, which constitute central intersections of the failure surface, belong to an ellipsoid surface, symmetric to the (σ_3,δ_{12}) plane for the transversely isotropic bodies. From the infinite family of ellipsoids corres-

ponding to values of the term H_{13} lying inside the interval (98) we have now to choose the convenient one which fits the particular properties of the material under study. This can be decided by a single test. As the most convenient, simplest and most reliable test, a failure test in hydrostatic compression, p_c , is suggested. A second choice may be a test of a lateral pressure $-p_l$ in the plane (σ_1,σ_2) combined with a simple tension or compression up to failure along the σ_3-direction, p_e.

The inequality (98) may be written as follows :

$$H_{13} = \varkappa H_{33} \tag{99}$$

where the factor $\varkappa$ for ellipsoids moves inside the interval :

$$-0.5 < \varkappa < 1.0 \tag{100}$$

Then Eq. (96) yields the value of the coefficient H_{12} as follows :

$$H_{12} = [(1+\varkappa)H_{33}-H_{11}] \tag{101}$$

The expression for the symmetric ellipsoid valid for the transversely isotropic body is given by :

$$H_{11}(\sigma_1^2+\sigma_2^2)+H_{33}\sigma_3^2+2[H_{33}(1+\varkappa)-H_{11}]\sigma_1\sigma_2+2\varkappa H_{33}(\sigma_1\sigma_3+\sigma_2\sigma_3)+ \\ +h_1(\sigma_1+\sigma_2)+h_3\sigma_3=1 \tag{102}$$

This surface represents :

1) A paraboloid when : $H_{13} = -1/2\ H_{33}$,
2) An ellipsoid when : $-1/2\ H_{33} < H_{13} < H_{33}$,
3) A two-sheet hyperboloid when : $H_{13} < -H_{33}/2$. This hyperboloid has its two sheets symmetrically placed on either side of an axis parallel to the hydrostatic axis, and
4) A two-sheet hyperboloid, whose either sheet is pierced by the hydrostatic axis, if $H_{13}>H_{33}$.

Cases (3) and (4), defining failure surfaces which are two-sheet surfaces, violate the principle of uniqueness and therefore may be rejected.
Relation (102) is the most general expression for a failure surface belonging to the tensor polynomial functions for the transversely isotropic bodies. It can be readily generalized for the orthotropic materials according to the theory developed in previous papers [68]. Indeed, by giving to the factor $\varkappa$ the value $\varkappa$=-0.5 we derive the

expression of the elliptic paraboloid failure surface, which is a powerful criterion for all compacted and thickpacked anisotropic materials of condensed matter, which present a very high strength in the compression-compression-compression octant of the principal stress space [42-50,68].

For values of $\varkappa$ in the interval $-0.5<\varkappa<0$ the failure surface becomes an ellipsoid. For values close to the low limit $\varkappa=-0.5$ the respective ellipsoid coincides almost with the corresponding elliptic paraboloid in the important zone of moderate loadings near the origin of the stress space. The discrepancies between the two surfaces start to appear at very high compressive loads, where the ellipsoid deviates from the respective paraboloid tending to close at some high value of compression.

The renowned experiments by Bridgman [40] indicated clearly that all isotropic materials can sustain high amounts of hydrostatic pressure without failure and, consequently, the orthotropic materials present safe paths for loading modes along the symmetry axes of their failure loci [51]. These types of loading consist of a hydrostatic pressure, superimposed by tensile or compressive lateral loads defined by the displacement of the symmetry axis from the hydrostatic axis [83]. However, some anisotropic materials may fail at high pressures by complicated fracture modes. In these cases a suitable failure criterion is the ellipsoid failure surface (EFS) with values of $\varkappa$ approaching the limiting value of $\varkappa=-0.50$.

Besides these compacted materials, there are some substances and modern materials where the solid matter is distributed accordingly either to form cell-clusters, or to form porous materials. The high porosity of these materials makes them to behave like tension strong materials (T-strong). Such typical material is the oriented polypropylene [87].

A material may become a tension-strong one when its porosity overpasses some critical value. Thus, polyurethane foams of a density below $d_1=96$ kg/m^3 become T-strong materials, whereas for densities above this limit-density they behave like normal compression-strong substances. At the limit of approximately $d_1=96$ kg/m^3 the polyurethane foam behaves as a quasi-isotropic substance [59]. Then, the amount of porosity plays a role in the behavior of the material, by changing it from compression strong to tension strong.

Similarly, paper sheets present a definite T-strong behavior, as well as oriented polypropylene is also a T-strong material [40,53]. Failures of these materials may be conveniently represented by ellipsoids, which present a closed-end surface. In all these cases values of the factor $\varkappa$ are approaching usually the limit value of $\varkappa=-0.50$.

Finally, rigid-cell foams, which fail normally as compression strong materials, are conveniently represented by elliptic paraboloid failure surfaces. However, if these materials present a premature cut-off failure by internal buckling at moderate compression stresses, this failure type may be represented by an ellipsoid failure surface of the family of ellipsoids corresponding to values of the factor $\varkappa$, either

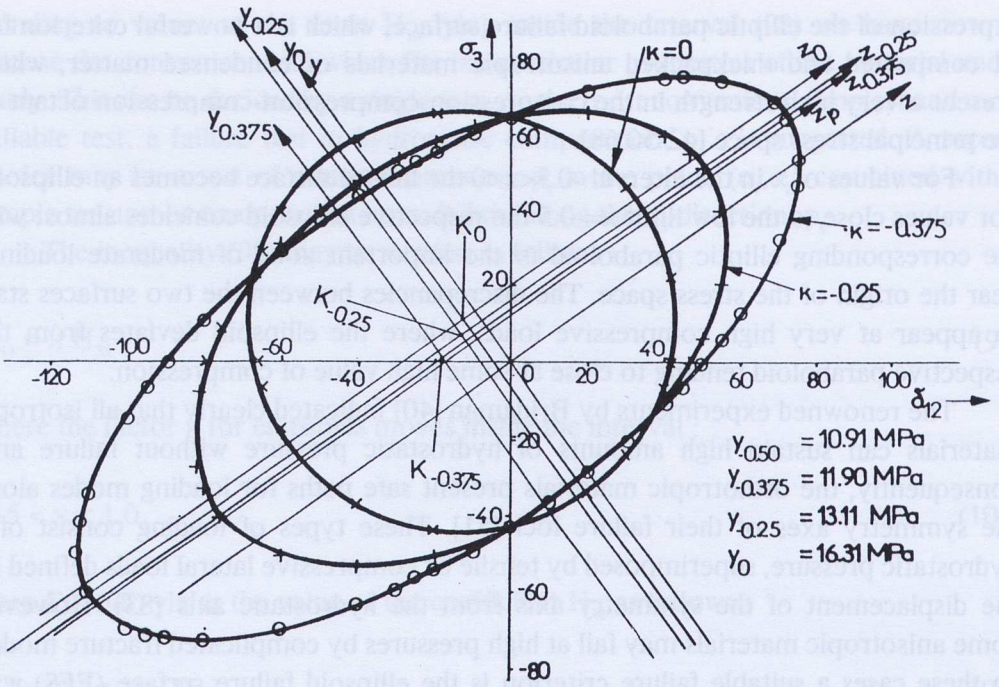

Fig.36 - The intersections of the EFS by the principal diagonal (σ_3,δ_{12})-plane (σ_3-axis, the strong stress-axis) for values of the factor $\varkappa$=-0.375, -0.25, and 0, corresponding to a fictitious oriented polycarbonate having these values for the $\varkappa$-factor.

negative ones approaching the value $\varkappa$=0, or positive values lying in the interval $0<\varkappa<1.0$. The first case yields prolate ellipsoids, whose principal diagonal intersections are rounded-off thus approaching a circle, whereas the second case yield oblate ellipsoids relatively to the symmetry axis parallel to the hydrostatic one.

Figure 36 presents a series of intersections of the family of ellipsoids by the (σ_3,δ_{12})-principal diagonal plane, where σ_3 is the direction of the strongest principal failure stress (fiber-deriction) and δ_{12} is the bisector of the right angle $\sigma_1 0\sigma_2$ subtended by the principal σ_1-and σ_2-directions in the isotropic plane, corre-sponding to an oriented polycarbonate, studied previously, where it was assumed that, instead of $\varkappa$=-0.50, the factor $\varkappa$ takes the arbitrary values $\varkappa$=-0.375, $\varkappa$=-0.25 and finally the value $\varkappa$=0. For this latter value the respective ellipsoid becomes a special one having a circular intersection by the principal diagonal plane (σ_3,δ_{12}). For positive values of $\varkappa$ the prolate ellipsoids along the hydrostatic axis become oblate, having their symmetry- axes parallel to the hydrostatic axis, rapidly receding from it, thus presenting a strong asymmetry and tending to become two-sheet hyperboloids. Figure 37 presents the cases for $\varkappa$=0.50 and $\varkappa$=0.875 for the same material of polycarbonate.

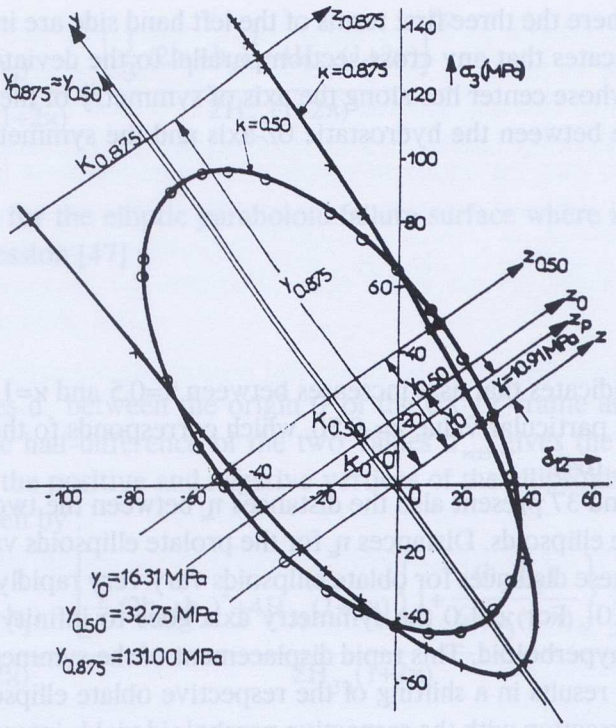

Fig.37 - The (σ_3,δ_{12})-principal diagonal intersections of the EFS corresponding to the same material as in Fig.36 but with positive values of the $\varkappa$-factor ($\varkappa$=0.50, 0.875).

It is clear from these ellipses that their major axes, which are parallel (for -0.5<$\varkappa$<0) or normal (for 0<$\varkappa$<1.0) to the hydrostatic axis, are receding from the hydrostatic axis or its normal, as $\varkappa$ is increasing. For $\varkappa$-negative the ellipsoids are prolate relatively to the hydrostatic axis. For $\varkappa$=0 the (σ_3,δ_{12}) intersection of the ellipsoid becomes circle and for $\varkappa$-positive the ellipsoids change to oblate ones.

It is worthwhile referring the ellipsoids to a Cartesian system 0xyz, where the 0z-axis coincides with the hydrostatic axis and the 0xy-plane coincides with the deviatoric π-plane. The 0y-axis lies on the (σ_3,δ_{12})-plane, whereas the 0x-axis is normal to it. Moreover, it is of interest to define also the 0'x'y'z'-system of coordinates, where the 0'z'-axis is the axis of the ellipsoid which is parallel to the hydrostatic axis, 0z, and the 0'x'y'-plane is parallel to the deviatoric plane, whose 0'x'- and 0'y'-axes correspond to the minor and the intermediate principal axes of the ellipsoid. For the transversely isotropic material it reduces to :

$$[2H_{11}-H_{33}(1+\varkappa)]x^2+H_{33}(1-\varkappa)y^2-\sqrt{\frac{2}{3}}(h_1-h_3)y+H_{33}(1+2\varkappa)z^2+\frac{1}{\sqrt{3}}(2h_1+h_3)z-1=0 \quad (103)$$

Relation (103), where the three first terms of the left hand side are independent of the z-coordinate, indicates that any cross-section parallel to the deviatoric plane, where z=0 is an ellipse whose center lies along the axis of symmetry of the ellipsoid.

The distance between the hydrostatic 0z-axis and the symmetry axis 0'z', $\eta_\varkappa$, is expressed by :

$$\eta_\varkappa = \frac{(h_1-h_3)}{\sqrt{6}\,(1-\varkappa)H_{33}} \tag{104}$$

Equation (104) indicates that as $\varkappa$ increases between $\varkappa$=0.5 and $\varkappa$=1.0 the distance $\eta\varkappa$ increases. For the particular value $\varkappa$=-0.50, which corresponds to the EPFS-criterion, $\eta\varkappa$ is given by Eq. (64).

Figures 36 and 37 present also the distances $\eta_\varkappa$ between the two parallel axes for prolate and oblate ellipsoids. Distances $\eta_\varkappa$ for the prolate ellipsoids vary imperceptibly with $\varkappa$, whereas these distances for oblate ellipsoids vary very rapidly as $\varkappa$ is increasing from $\varkappa$=0 to $\varkappa$=1.0 . For $\varkappa$=1.0 the symmetry axis goes to infinity and the ellipsoid degenerates to a hyperboloid. This rapid displacement of the symmetry axis 0'y' of the ellipsoids for $\varkappa$>0 results in a shifting of the respective oblate ellipsoid along the 0'y'-axis. Thus its intersection with the respective paraboloid yields intersections which are progressively asymmetric. This pheno-menon corroborates the experimental results of failures of different foams by internal buckling, where the curves traced by the experiments in the (σ_3,δ_{12})-plane are progressively asymmetric as the buckling failure loads are approaching the origin [39].

The intersection of the ellipsoid by the (σ_3,δ_{12})-principal diagonal plane referred to the $(0\sigma_1\sigma_2\sigma_3)$-system of coordinates is expressed by [57] :

$$H_{33}(1+\varkappa)\delta_{12}^2+H_{33}\sigma_3^2+2\sqrt{2}\,\varkappa H_{33}\delta_{12}\sigma_3+\sqrt{2}\,h_1\delta_{12}+h_3\sigma_3-1=0 \tag{105}$$

Equation (103) or (105) may be used for the definition of any cross-section of the ellipsoid. A detailed description of these failure surfaces was presented in ref.[57]. Here we are limited to give the characteristic dimensions of these ellipsoids.

Equation (103) indicates that the intersections of the ellipsoid by planes z=p parallel to the deviatoric plane z=0 have their centers along the 0'z'-axis of symmetry, so that the coordinates of these centers are [45,78] :

$$x'_p = \xi_p = 0, \qquad y'_p = \eta_\varkappa \qquad \text{and} \qquad z'_p = \zeta_p = p \tag{106}$$

Other interesting dimensions of the ellipsoids are :

1) The distances $d_\varkappa$ between the deviatoric plane and the points of piercing the ellispoids by the hydrostatic axis, 0z : These distances are expressed by relation (103) by putting x=y=0. They are given by :

$$d_{\varkappa(\pm)} = -\frac{(2h_1+h_3)}{2\sqrt{3}\,H_{33}(1+2\varkappa)} \pm \frac{\left[\frac{1}{3}(2h_1+h_3)^2+4H_{33}(1+2\varkappa)\right]^{1/2}}{2H_{33}(1+2\varkappa)} \tag{107}$$

Expression (107) for the elliptic paraboloid failure surface where $\varkappa$=-0.50 yields the well-known expression [47] :

$$d_{\varkappa} = \sqrt{3}/(2h_1+h_3) \tag{108}$$

2) The distances $d'_{\varkappa}$ between the origin 0' of the 0'x'y'z'-frame and the vetrices of the ellipsoids: The half-difference of the two values $d'_{\varkappa(\pm)}$ gives the distances $\zeta_{\varkappa}$. The distances $d'_{\varkappa(\pm)}$ of the positive and negative vertices of the ellipsoids from the deviatoric plane are given by :

$$d_{\varkappa(\pm)} = \frac{-\frac{1}{\sqrt{3}}(2h_1+h_3)}{2H_{33}(1+2\varkappa)} \pm \frac{\left[\frac{1}{3}(2h_1+h_3)^2+4H_{33}(1+2\varkappa)\left\{1+\frac{(h_1-h_2)}{6H_{33}(1-\varkappa)}\right\}\right]^{1/2}}{2H_{33}(1+2\varkappa)} \tag{109}$$

Then, the distance between the deviatoric plane and the center of the ellipsoid is given by :

$$\zeta_{\varkappa} = (d_{\varkappa(+)} - d_{\varkappa(-)})/2 = (d'_{\varkappa(+)} - d'_{\varkappa(-)})/2 \tag{110}$$

3) The dimensions of the major and minor semi-axes of the maximum elliptic intersection of the ellipsoid which is parallel to the deviatoric plane: The length of the minor semi-axis of the ellipse along the 0'x'-axis is derived from the equation of the ellipsoid referred to the 0'x'y'z'-system by putting y'=0. Then, it can be readily found the expression for $x'_{\varkappa}$:

$$[2H_{11}-H_{33}(1-\varkappa)]x'^2_{\varkappa} = 1+\frac{(h_1-h_3)}{6H_{33}(1-\varkappa)} - \zeta^2_{\varkappa}H_{33}(1+2\varkappa)+\zeta_{\varkappa}\frac{(2h_1+h_3)}{\sqrt{3}} \tag{111}$$

The ratio $x'_{\varkappa}/y'_{\varkappa}$ of the principal semi-axes of any intersection of the ellipsoid by planes parallel to the deviatoric plane is given by :

$$\lambda_{\varkappa} = \frac{x_{\varkappa}}{y'_{\varkappa}} = \left\{\frac{H_{33}(1-\varkappa)}{2H_{11}-H_{33}(1+\varkappa)}\right\}^{1/2} \tag{112}$$

which is independent of the coordinate $z'_{\varkappa}$ and therefore remains constant along the length of the major symmetry axis of the ellipsoid.

It is of great interest to define the position, orientation and the shape of the intersection of the ellipsoid by the principal stress plane (σ_1,σ_3), since this failure locus corresponds to two-dimensional failure loci of plates. It has been shown [57] that the coordinates of the centers of such intersections are expressed by :

$$(\sigma_{01},\sigma_{03})=\left\{-\frac{(h_1-\varkappa h_3)}{2(H_{11}-\varkappa^2 H_{33})},\ -\frac{(h_3H_{11}-\varkappa h_1H_{33})}{2H_{33}(H_{11}-\varkappa^2H_{33})}\right\} \tag{113}$$

The angle θ_1 subtended by the polar radius 0M connecting the origin 0 and the center of the ellipse is expressed by :

$$\tan 2\theta_1 = -\,[2\varkappa H_{33}/(H_{11}-H_{33})] \tag{114}$$

whereas the angle λ_1 subtended by the minor axis σ_1 of the elliptic intersection and the σ_1-axis is given by :

$$\tan\lambda_1 = -\frac{(h_3H_{11}-\varkappa h_1H_{33})}{H_{33}(h_1-\varkappa h_3)} \tag{115}$$

The lengths of the semi-axes of this ellipse, denoted by α_{1M} and α_{3M} respectively, are given by relations (25) to (29). In these relations the respective quantities for the ellipsoid failure surface corresponding to the $\varkappa$-factor are given by :

$$\det\mathbf{A}_2 = (H_{11}H_{33} - \varkappa^2 H_{33}^2) \tag{116}$$

$$\det\mathbf{A}_3 = -\det\mathbf{A}_2 - 1/4\{h_3^2H_{11}+h_1^2H_{33}-2\varkappa h_1h_3H_{33}\} \tag{117}$$

$$\left.\begin{matrix}\delta_1\\ \delta_2\end{matrix}\right\} = \frac{1}{2}\{(H_{11}+H_{33})\pm[(H_{11}-H_{33})^2+4\varkappa^2H_{33}^2]^{1/2}\} \tag{118}$$

It has been shown [57,59] that, as the factor $\varkappa$ is increasing from its lower bound of $\varkappa$=-0.50 to the upper bound $\varkappa$=0, the intersections of the ellipsoid by the principal-stress planes become more and more rounded off, whereas the principal axes of the elliptic intersections rotate anti-clockwise tending to become parallel to the principal stress axes σ_1 and σ_3.

Another important observation is that the differences in the positions and shapes of the intersections for various values of $\varkappa$ are rather small and, to a good approximation, the theory of elliptic paraboloid failure surface remains valid even for materials failing in the compression-compression-compression octant of the principal stress space.

For the ellipsoid failure surface the three pairs of normal stresses in simple tension and compression are not anymore sufficient for its definition. An extra information is necessary in order to define the as yet non-defined factor $\varkappa$. The easiest and the most reliable test is the hydrostatic pressure test up to failure, since there exist special arrangements in the testing machines for such a failure test which yield safe and imperceptibly scattered data. Assume that the failure test under hydrostatic pressure yields a value $-p_c$.

Setting $\sigma_1=\sigma_2=\sigma_3=p_c$ we defined a value for $\delta_{12}=-p_c\sqrt{2}$. When these values are introduced into eq.(112) yield :

$$\varkappa=\left\{\frac{1}{6H_{33}p_c^2}+\frac{(2h_1+h_3)}{6H_{33}p_c}-\frac{1}{2}\right\} \tag{119}$$

Equation (119) defines the value for $\varkappa$ corresponding to the hydrostatic failure pressure $(-p_c)$. As soon as the factor $\varkappa$ is evaluated the respective ellipsoid failure surface is completely defined.

For thickpacked materials of condensed matter, failing under very high hydrostatic pressure (for isotropic materials), or high hydrostatic pressure superimposed with a lateral stress (for anisotropic materials) the ellipsoid failure surface is efficient to describe the failure mode of these materials under any combination of external loads. Now, in order to prove the validity of the proposed ellipsoid failure surface criterion, we checked the experimental results of failure stresses of a typical C-strong rigid foam material with the failure locus derived by the intersection of this ellipsoid failure surface by the principal (σ_1,σ_3)-stress plane. As such material we have used a polyurethane foam with a density 192 kg/m^3 (PUR 192). The failure stresses of this material were given by [59] :

$$\sigma_{T1}=\sigma_{T2}=1.58\ \text{MPa} \qquad \sigma_{T3}=2.44\ \text{MPa}$$
$$\sigma_{c1}=\sigma_{c2}=2.56\ \text{MPa} \qquad \sigma_{c3}=3.35\ \text{MPa} \tag{120}$$

Based on these failure stresses in simple tension and compression the elliptic paraboloid failure surface was completely defined. In order to define the respective ellipsoid failure surface for this material it is necessary to measure the hydrostatic compression failure stress $(-p_c)$ corresponding to a general collapse of the specimen by elastic buckling through plastic hinges developed inside the members of the cell walls composing the foam. This value was found to be $p_c=-2.52$MPa. Then, using Equation (119) the value of the $\varkappa$-factor is found to be $\varkappa=-0.658$. The symmetric ellipsoid traced by using the values (120) as well as the value for $\varkappa=-0.658$ is much different in general shape as the respective elliptic paraboloid defined by the values given in (120) alone. These differences are indicated in ref. [59]. However, the intersection of the EPFS and the respective EFS for the same material by the (σ_1,σ_3)-

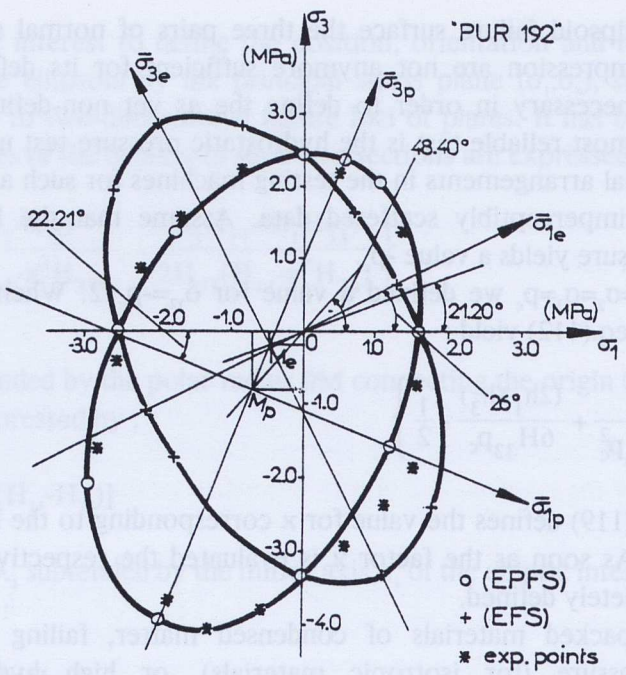

Fig. 38 - The (σ_1,σ_3)-principal stress intersections of the failure elliptic paraboloid and the ellipsoid loci for polyurethane PUR 192.

principal stress plane give two ellipses which are very close to each other. Fig. 38 presents these intersections by the (σ_1,σ_3)-plane for polyurethane foam (PUR 192). It is to be pointed out that the experimental evidence and the two ellipses are all close together, with the one ellipse angularly displaced by a greater angle than the other.

4.2 The generalized elliptic paraboloid failure surface (GEPFS)

In the generalized elliptic paraboloid failure surface (GEPFS) we dispense the failure criterion from the postulate that the safest loading path is along an axis parallel to the hydrostatic axis [88]. Instead, this postulate is replaced by the postulate that the safest loading path for an anisotropic material is the loading path yielding a spherical strain tensor [88].

Denoting by **s** this safe symmetric stress tensor it can be determined by :

$$\mathbf{s} = \mathbf{C} \cdot \mathbf{1} \tag{121}$$

or, otherwise, in the natural form of Cartesian indices as :

$$s_{ij} = C_{ijkl}\delta_{kl} = C_{ijkk} \tag{122}$$

The analytic expressions of the safe stress tensor are given in compacted form as:

$$s_i = C_{i1} + C_{i2} + C_{i3} \qquad (i=1,2...,6)$$

Then, the failure criterion for the GEPFS is expressed by :

$$\mathbf{H} \cdot \mathbf{s} = \lambda \mathbf{s} = 0 \tag{123}$$

or because of Eq. (121) it is valid that :

$$\mathbf{H} \cdot \mathbf{C} \cdot \mathbf{1} = 0 \tag{124}$$

Equation (124) interrelates the components of the failure tensor **H** with the components of the elastic stiffness tensor **C** of the material and indicates an intimate relationship between the elastic properties and the failure properties of an anisotropic material.

Then, while relations (51) to (53), expressing the diagonal terms of the tensor **H** and the differential strength tensor **h**, remain valid, only the off-diagonal terms of the **H**-tensor are influenced by the new postulate.

Developing equation (124) and taking into consideration that we are concerned only with materials presenting an orthotropic symmetry we obtain a system of three equations with three unknown quantities, the terms H_{ij} $(i \neq j)$, in terms of the elastic constants of the material. The solution of this system yields the following three equations [88] :

$$H_{ij} = \frac{1}{2} \left\{ H_{\varkappa\varkappa} \frac{\lambda_{\varkappa}^2}{\lambda_i \lambda_j} - H_{ii} \frac{\lambda_i}{\lambda_j} - H_{jj} \frac{\lambda_j}{\lambda_i} \right\} \tag{125}$$

Comparing equations (57), valid for the EPFS, and (125) valid for the GEPFS we derive at once that both relations become identical when $\lambda_1 = \lambda_2 = \lambda_3$.

It can be readily found that the solution of the system (124) of the three equations for the transversely isotropic material, with the strong elastic modulus as E_L and the transverse one as E_T and the respective Poisson's ratios denoted by ν_L and ν_T, respectively, yields :

$$\lambda_1 = \lambda_2 = (1+\nu_T)\,(1+\nu_L)\,E_T$$

and :

$$\lambda_3 = (1+\nu_T)\,\{2E_T\nu_L + E_L(1-\nu_T)\} \tag{126}$$

where, as always, the 3-direction is the strong direction and the 1,2-plane is the isotropic one.

Equations (125) for the transversely isotropic materials can be simplified and

take the form :

$$H_{12}=\left\{\frac{\lambda_3^2}{2\lambda_1^2}H_{33}-H_{11}\right\}$$

$$H_{13}=H_{23}=-\frac{\lambda_3}{2\lambda_1}H_{33} \qquad (127)$$

or, introducing the elastic constants of the material, we obtain that :

$$H_{12}=\frac{1}{2}\left\{\frac{2E_T\nu_L+E_L(1-\nu_T)}{E_T(1+\nu_L)}\right\}^2 H_{33}-H_{11}$$

$$H_{13}=H_{23}=-\left\{\frac{2E_T\nu_L+E_L(1-\nu_T)}{E_T(1+\nu_L)}\right\}H_{33} \qquad (128)$$

The new GEPFS-criterion for transversely isotropic materials with safe stress tensor s causing a spherical strain tensor is completely determined by equations (51) to (53) and (128).

In the principal stress space the GEPFS-criterion is again represented by a quadric elliptic paraboloid having as a symmetry axis a line subtending an angle θ_G with the principal (σ_1,σ_2)-plane expressed by :

$$\tan 2\theta_G=\frac{2\sqrt{2}\,E_T(1+\nu_L)\{2E_T\nu_L+E_L(1-\nu_T)\}}{2E_T^2(1+\nu_L)^2-[2E_T\nu_L-E_L(1-\nu_T)]^2} \qquad (129)$$

Therefore, the angle θ_d subtended between the symmetry axis of the GEPFS and the hydrostatic axis equals.

$$\theta_d=(1/2\ \arctan 2\theta_G-35.26°) \qquad (130)$$

Equations (126) to (128) indicate that there is a correlation between the components of the failure tensor **H** and the engineering elastic constants of the material, fact suggesting directly that initial failure depends on the elastic anisotropic properties of the material, since initial failure is a limiting elastic state. However, the same interrelation, but indirect, is implied by the postulate for the EPFS. Equations (127) suggest, furthermore, that the off-diagonal failure tensor components depend on the ratio of the two factors (λ_3/λ_1) and not on their absolute values. This means that the degree of anisotropy of the material is the regulating factor defining the failure tensor **H** of the material.

For moderately anisotropic materials, as it is the oriented polycarbonate (PC) [30], the predictions of the two alternative versions of the elliptic paraboloid failure surface do not differ considerably, the angle θ_d between their symmetry axes being equal to :

$\theta_{d(PC)} = (37.50° - 35.26°) = 2.24°$

whereas for highly anisotropic substances, as it is the carbon fiber-epoxy matrix composite Morganite II [86] the differences are significant. Indeed, in this case angle $\theta_{d(C/E)}$ is given by :

$$\theta_{d(C/E)} = (76.65° - 35.26°) = 41.39° \qquad (131)$$

Apart the difference in angles subtended by the symmetry axes of the two versions of this failure locus, that is the EPFS-criterion and the GEPFS-one, there is a similarity in shape of both surfaces. Another characteristic difference between them is the fact that the EPFS-criteria become progressively shallower as the anisotropy of the material is increased. On the contrary, the GEPFS-criterion remains always a deep paraboloid, but with increasing angle of orientation with respect to the hydrostatic axis.

Introducing the values for the off-diagonal terms H_{ij} ($i \neq j$) given by relations (127) for the transversely isotropic material into the general expression (59) for the failure locus we derive the expression :

$$\left(2H_{11} - \frac{\lambda_3^2}{2\lambda_1^2} H_{33}\right)x^2 + \left(2 + \frac{\lambda_3}{\lambda_1}\right)^2 \frac{H_{33}}{6} y^2 + \frac{\sqrt{2}}{3}\left(1 - \frac{\lambda_3}{\lambda_1}\right)\left(2 + \frac{\lambda_3}{\lambda_1}\right) H_{33} yz -$$

$$- \sqrt{\frac{2}{3}}(h_1 - h_3)y + \frac{1}{3}\left(1 - \frac{\lambda_3}{\lambda_1}\right)^2 H_{33} z^2 + \frac{(2h_1 + h_3)}{\sqrt{3}} z - 1 = 0 \qquad (132)$$

The principal diagonal (σ_3, δ_{12})-intersection of the generalized elliptic paraboloid failure surface is derived by putting into eq.(132) the value x=0.

Similarly, for x=0 and y=0 we derive the distances between the origin of the coordinates and the points where the symmetry axis of the paraboloid is piercing the failure surface. These distances are given by :

$$d'_\chi = \frac{-\frac{(2h_1 + h_3)}{\sqrt{3}} \pm \sqrt{\frac{(2h_1 + h_3)^2}{3} + \frac{4}{3} H_{33}\left(1 - \frac{\lambda_3}{\lambda_1}\right)^2}}{\frac{2}{3} H_{33}\left(1 - \frac{\lambda_3}{\lambda_1}\right)^2} \qquad (133)$$

The equation of the intersection of the failure locus by the deviatoric π-plane is given by putting into Eq.(132) the value z=0. Then we have :

$$2\{H_{11}-(\lambda_3/2\lambda_1)^2H_{33}\}x^2+(H_{33}/6)\{2+(\lambda_3/\lambda_1)\}^2y^2-\div 2/3\,(h_1-h_3)y-1=0 \tag{134}$$

yields the values for the major and minor semi-axes of the elliptic cross-section as follows :

$$y_{1,2}=\frac{\sqrt{\frac{2}{3}}\,(h_1-h_3)\pm\left\{\frac{2}{3}\left[(h_1-h_3)^2+\left(2+\frac{\lambda_3}{\lambda_1}\right)^2 H_{33}\right]\right\}^{1/2}}{\frac{H_{33}}{3}\left\{2+\frac{\lambda_3}{\lambda_1}\right\}^2} \tag{135}$$

and

$$x_{1,2}=\left\{2\left[H_{11}-\left(\frac{\lambda_3}{2\lambda_1}\right)^2 H_{33}\right]\right\}^{1/2} \tag{136}$$

The distance between the symmetry axis of the paraboloid from a parallel to it axis passing through the origin of the coordinates is expressed by :

$$\eta_\kappa=\frac{y_1+y_2}{2}=\frac{\sqrt{6}\,(h_1-h_3)}{H_{33}\left(2+\frac{\lambda_3}{\lambda_1}\right)^2} \tag{137}$$

The expression of the principal diagonal (σ_3,δ_{12})-plane intersection of the generalized elliptic paraboloid failure surface is given by :

$$\frac{\lambda_3^2}{2\lambda_1^2}H_{33}\delta_{12}^2+H_{33}\sigma_3^2-\sqrt{2}\,\frac{\lambda_3}{\lambda_1}H_{33}\delta_{12}\sigma_3+\sqrt{2}\,h_1\delta_{12}+h_3\sigma_3-1=0 \tag{138}$$

which for $\delta_{12}=0$, that is the distances $\sigma_3^{(\pm)}$ of the points of piercing the paraboloid by the σ_3-strong principal axis are given by :

$$\sigma_3^{(\pm)}=\frac{-h_3\pm\sqrt{h_3^2+4H_{33}}}{2H_{33}}=\begin{cases}\sigma_{T3}\\ \sigma_{C3}\end{cases} \tag{139}$$

as it should be expected.

The relation expressing the elliptic intersection of the generalized elliptic paraboloid failure surface by the (σ_1,σ_3)-principal stress plane is given by :

$$H_{11}\sigma_1^2+H_{33}\sigma_3^2-\frac{\lambda_3}{\lambda_1}H_{33}\sigma_1\sigma_3+h_1\sigma_1+h_3\sigma_3-1=0 \tag{140}$$

The center of this ellipse is defined by the coordinates $(\sigma_{3M}^G, \sigma_{1M}^G)$ expressed by :

$$(\sigma_{3M}^G\ ,\ \sigma_{1M}^G) = \left\{ -\frac{\left(\frac{\lambda_3}{\lambda_1}h_3+2h_1\right)}{\left(4H_{11}-\frac{\lambda_3^2}{\lambda_1^2}H_{33}\right)}\ ,\ -\frac{\left(\frac{\lambda_3}{\lambda_1}h_1H_{33}+h_3H_{11}\right)}{H_{33}\left(4H_{11}-\frac{\lambda_3^2}{\lambda_1^2}H_{33}\right)} \right\} \tag{141}$$

In order to define the major and the minor semi-axes of this elliptic cross-section we need the following determinants [68] :

$$\det\mathbf{A}_2^G = \begin{pmatrix} H_{11} & -\lambda_3/2\lambda_1\ H_{33} \\ -\lambda_3/2\lambda_1\ H_{33} & H_{33} \end{pmatrix} = [H_{11}H_{33}-(\lambda_3/2\lambda_1)^2H_{33}-\lambda_3/2\lambda_1H_{33} \tag{142}$$

$$\det\mathbf{A}_3^G = \begin{pmatrix} H_{11} & -\lambda_3/2\lambda_1\ H_{33} & h_1/2 \\ -\lambda_3/2\lambda_1\ H_{33} & H_{33} & h_3/2 \\ h_1/2 & h_3/2 & -1 \end{pmatrix} \tag{143}$$

and the roots $\delta_{1,2}$ of the characteristic equation :

$$\delta^2 - \mathrm{tr}A_{ii}^G\delta + \det\mathbf{A}_2^G = 0 \tag{144}$$

Then, the semi-axes of the elliptic (σ_1,σ_3)-principal stress plane intersection are given by [68] :

$$(\alpha_{1M}^G, \alpha_{3M}^G) = \left(\frac{C}{\delta_{1,2}}\right)^{1/2} \tag{145}$$

with

$$C = -(\det\mathbf{A}_3/\det\mathbf{A}_2) \tag{146}$$

Equation (143) yields :

$$\det\mathbf{A}_3^G = -\det\mathbf{A}_2 - \frac{1}{4}\left\{\frac{\lambda_3}{2\lambda_1} H_{33}h_1^2 + H_{11}h_3^2 + \left(1+\frac{\lambda_3}{2\lambda_1}\right) H_{33}h_1h_3\right\} \tag{147}$$

and the solution of the characteristic (144) yields the roots :

$$\delta_{1,2} = \frac{1}{2}(H_{11}+H_{33}) \pm \left\{(H_{11}+H_{33})^2 - 4H_{33}\left[H_{11} - \left(\frac{\lambda_3}{2\lambda_1}\right)^2 H_{33}\right]\right\}^{1/2} \tag{148}$$

Finally, in order to define the intersection of the GEPFS-locus by the (σ_1,σ_2) isotropic principal-stress plane we use the expression for the elliptic paraboloid in the $(\sigma_1,\sigma_2,\sigma_3)$-principal stress system, where we introduce the value $\sigma_3=0$ and we derive :

$$H_{11}(\sigma_1^2+\sigma_2^2) + \left[\left(\frac{\lambda_3}{\lambda_1}\right)^2 H_{33} - 2H_{11}\right]\sigma_1\sigma_2 + h_1(\sigma_1+\sigma_2) - 1 = 0 \tag{149}$$

which for $\sigma_1=\sigma_2$ yields :

$$\left(\frac{\lambda_3}{\lambda_1}\right)^2 H_{33}\sigma_1^2 + 2h_1\sigma_1 - 1 = 0 \tag{150}$$

and for $\sigma_1=-\sigma_2$ gives :

$$\left[4H_{11} - \left(\frac{\lambda_3}{\lambda_1}\right)^2 H_{33}\right]\sigma_1^2 = 1 \tag{151}$$

We use all three last equations in order to trace the elliptical intersection of the GEPFS-locus by the (σ_1,σ_2)-isotropic plane.

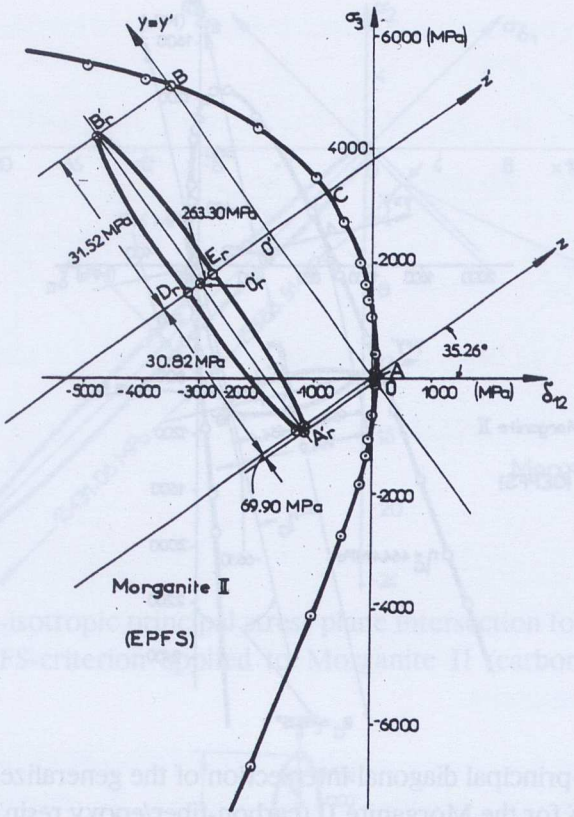

Fig.39 - The (σ_3,δ_{12})-principal diagonal intersection of the elliptic paraboloid failure surface EPFS for the Morganite II (carbon-fiber/epoxy resin) composite.

This completes the description of this type of failure locus.

In order to check the loci derived from this form of the GEPFS-criterion we use the experimental evidence with a carbon fiber-epoxy resin composite under the nomination of Morganite II studied by Wu and others [86]. The experimental evidence with this composite gave the following failure stresses in simple tension and compression along the three principal stress axes :

$\sigma_{T3} = 1065.93$ MPa $\qquad \sigma_{T1} = \sigma_{T2} = 42.40$ MPa

$\sigma_{C3} = 615.01$ MPa $\qquad \sigma_{C1} = \sigma_{C2} = 143.20$ MPa

Figures 39 and 40 present the principal diagonal (σ_3,δ_{12})-intersections of the EPFS and the GEPFS for the Morganite II composite presented in refs.[82 and 86]. While this (σ_3,δ_{12})-intersections of the EPFS for this material is a shallow parabola, the respective parabola for the GEPFS is a significantly deep parabola, differently oriented that the previous one.

Figures 41 and 42 present the intersections of the elliptic paraboloid failure surface EPFS by the (σ_1,σ_3)-principal stress plane and the (σ_1,σ_2)-principal stress isotropic plane. Both elliptic intersections present the typical shapes of oblong cigar-like types of curves. Similarly, figures 43 and 44 present the same intersections but for the generalized elliptic paraboloid failure surface.

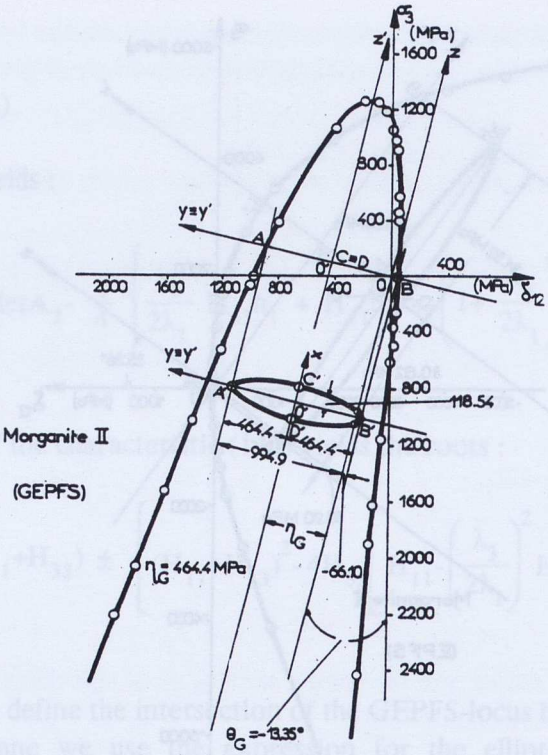

Fig.40 - The (σ_3,δ_{12})-principal diagonal intersection of the generalized elliptic paraboloid failure surface GEFS for the Morganite II (carbon-fiber/epoxy resin) composite.

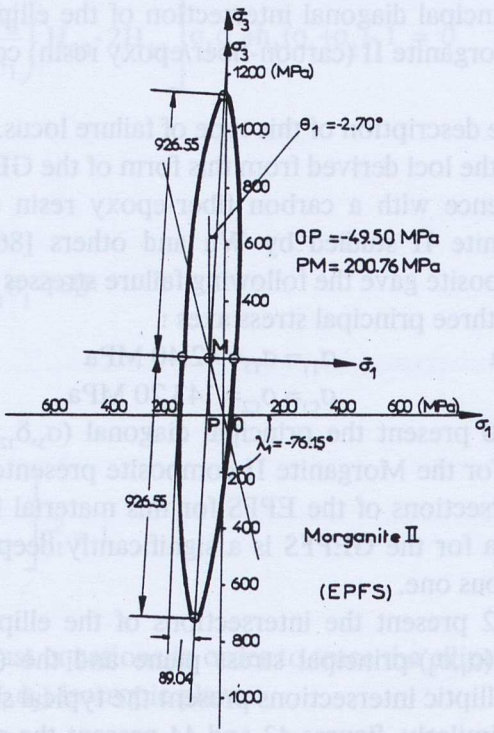

Fig.41 - The (σ_3,σ_1)-principal stress plane intersection for the elliptic paraboloid failure surface EPFS-criterion applied to Morganite II (carbon-fiber/epoxy resin) composite.

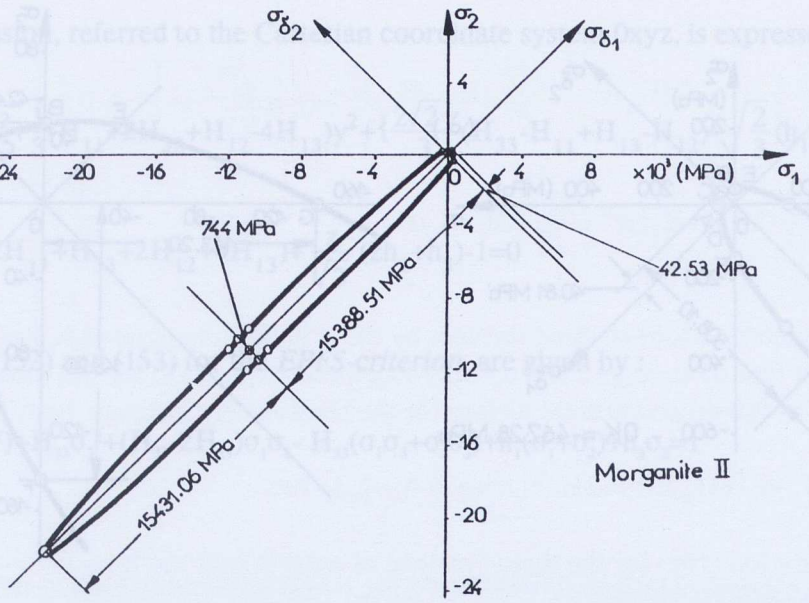

Fig.42 - The (σ_1,σ_2)-isotropic principal stress plane intersection for elliptic paraboloid failure surface EPFS-criterion applied to Morganite II (carbon-fiber/epoxy resin) composite.

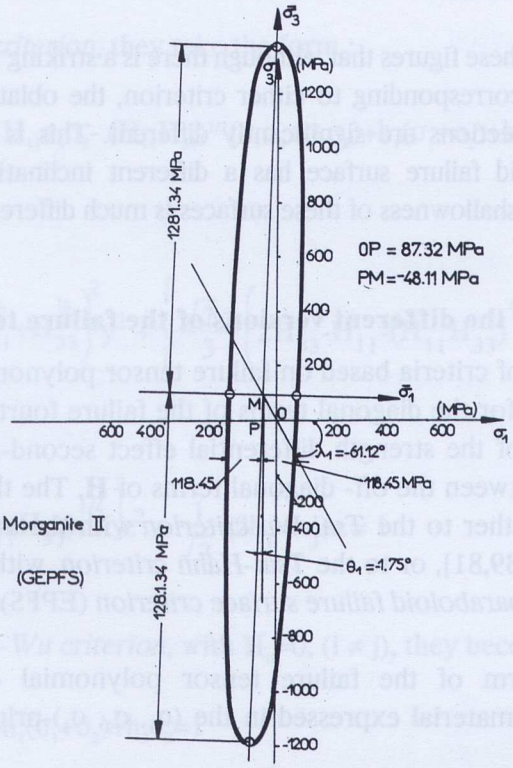

Fig.43 The (σ_1,σ_2)-principal stress plane intersection for the generalized elliptic paraboloid failure surface GEPFS-criterion applied to Morganite II composite (a) and a detail of this intersection (b).

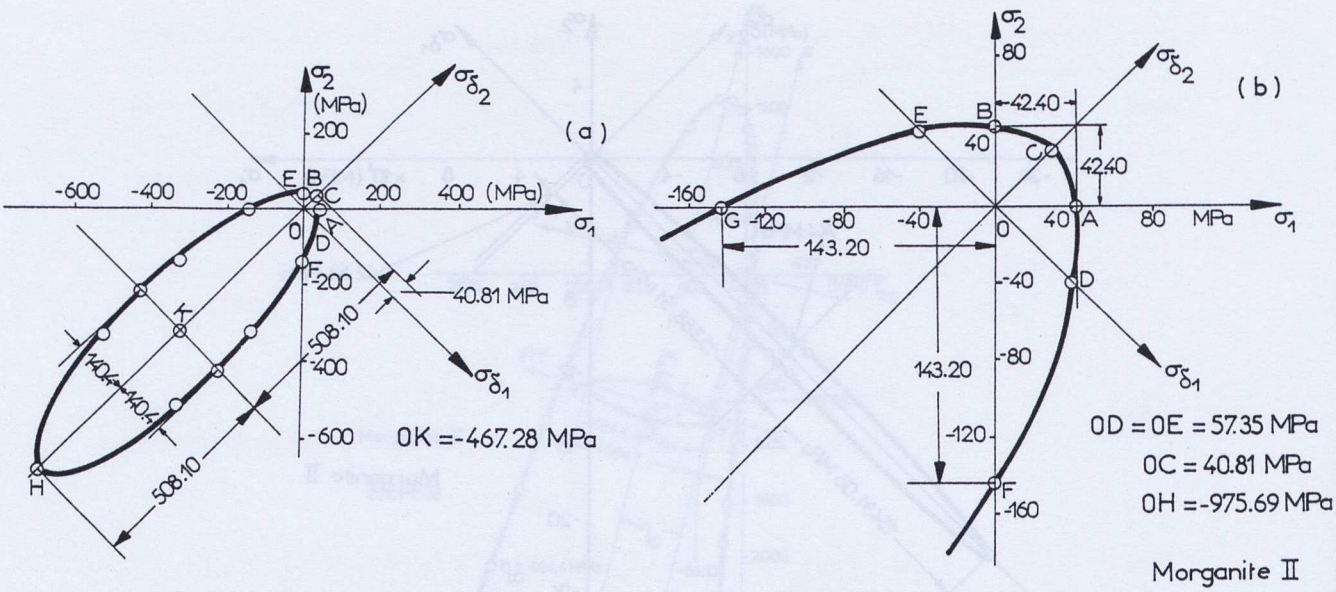

Fig. 44 - The (σ_1,σ_2)-isotropic principal stress plane intersection for generalized elliptic paraboloid failure surface GEPFS-criterion applied to Morganite II (carbon-fiber/epoxy resin) composite.

It is clear from all these figures that, although there is a striking resemblence between both groups of curves corresponding to either criterion, the oblateness and the extent of the respective intersections are significantly different. This is due to the fact that either elliptic paraboloid failure surface has a different inclination relatively to the hydrostatic axis and the shallowness of these surfaces is much different.

4.3 A comparison of the different versions of the failure tensor polynomial

Several versions of criteria based on failure tensor polynomials (FTP), whereas define identical values for the diagonal terms of the failure fourth-rank tensor, **H**, as well as for the terms of the strength differential effect second-rank tensor, **h**, they present differences between the off- diagonal terms of **H**. The three most important versions correspond either to the *Tsai-Wu criterion* with the additional assumption that $H_{ij} = 0$, for $i \neq j$, [39,81], or to the *Tsai-Hahn criterion*, with$H_{ij} = -1/2\ (H_{ii}\ H_{jj})^{1/2}$ [80], or to the *elliptic paraboloid failure surface criterion* (EPFS), with $H_{ij} = 1/2\ (H_{kk} - H_{ii} - H_{jj})$ [42-71].

The simplest form of the failure tensor polynomial corresponding to a transversely isotropic material expressed in the $(\sigma_1, \sigma_2, \sigma_3)$-principal stress space is expressed by :

$$H_{11}(\sigma_1^2+\sigma_2^2)+H_{33}\sigma_3^2+2H_{12}\sigma_1\sigma_2+2H_{13}(\sigma_1\sigma_3+\sigma_2\sigma_3)+h_1(\sigma_1+\sigma_2)+h_3\sigma_3=1 \qquad (152)$$

This expression, referred to the Cartesian coordinate system 0xyz, is expressed by :

$$H_{11}\text{-}H_{12})x^2+\frac{1}{3}(H_{11}+2H_{33}+H_{12}-4H_{13})y^2+\{\frac{2\sqrt{2}\,z}{3}(H_{33}\text{-}H_{11}+H_{13}\text{-}H_{12})\text{-}\sqrt{\frac{2}{3}}(h_1\text{-}h_3)y+$$

$$+\frac{z^2}{3}(2H_{11}+H_{33}+2H_{12}+4H_{13})+\frac{z}{\sqrt{3}}(2h_1+h_3)\text{-}1=0 \qquad (153)$$

Relations (152) and (153) for the *EPFS-criterion*, are given by :

$$H_{11}(\sigma_1^2+\sigma_2^2)+H_{33}\sigma_3^2+(H_{33}\text{-}2H_{11})\sigma_1\sigma_2\text{-}\ H_{33}(\sigma_1\sigma_3+\sigma_2\sigma_3)+h_1(\sigma_1+\sigma_2)+h_3\sigma_3=1 \qquad (154)$$

and :

$$(2H_{11}\text{-}\frac{1}{2}H_{33})x^2+\frac{3}{2}H_{33}y^2\text{-}\sqrt{\frac{2}{3}}(h_1\text{-}h_3)y+\frac{1}{\sqrt{3}}(2h_1+h_3)z=1 \qquad (155)$$

For the *Tsai-Hahn criterion*, they take the form :

$$H_{11}(\sigma_1^2+\sigma_2^2)+H_{33}\sigma_3^2\text{-}H_{11}\sigma_1\sigma_2\text{-}\ (H_{11}H_{33})^{1/2}(\sigma_1\sigma_3+\sigma_2\sigma_3)+h_1(\sigma_1+\sigma_2)+h_3\sigma_3=1 \qquad (156)$$

and :

$$\frac{3}{2}H_{11}x^2+\frac{2}{3}\left(\frac{1}{2}H_{11}^{1/2}+H_{33}^{1/2}\right)^2y^2+\left\{\frac{\sqrt{2}\,z}{3}\left(2H_{33}\text{-}H_{11}\text{-}(H_{11}H_{33})^{1/2}\right)\text{-}\sqrt{\frac{2}{3}}(h_1\text{-}h_3)\right\}y+$$

$$+\frac{1}{3}\left[H_{11}+H_{33}\text{-}2(H_{11}H_{33})^{1/2}\right]z^2+\frac{1}{\sqrt{3}}(2h_1+h_3)z=1 \qquad (157)$$

Finally, for the *Tsai-Wu criterion*, with $H_{ij}=0$, $(i \neq j)$, they become:

$$H_{11}(\sigma_1^2+\sigma_2^2)+H_{33}\sigma_3^2+h_1(\sigma_1+\sigma_2)+h_3\sigma_3=1 \qquad (158)$$

and :

$$H_{11}x^2+\frac{1}{3}(H_{11}+2H_{33})y^2-\left[\frac{2\sqrt{2}}{3}(H_{11}-H_{33})z+\sqrt{\frac{2}{3}}(h_1-h_3)\right]y+$$

$$+\frac{1}{3}(2H_{11}+H_{33})z^2+\frac{1}{\sqrt{3}}(2h_1+h_3)z=1 \qquad (159)$$

For the intersections of these surfaces by the principal diagonal $(\sigma_3\delta_{12})$-plane, we must put that $\sigma_1=\sigma_2=\delta_{12}/\div 2$ and $\sigma_3=\sigma_3$. The general expression for this intersection of the tensor failure polynomial surface for the transversely isotropic body is given by :

$$(H_{11}+H_{12})\delta_{12}^2+H_{33}\sigma_3^2+2\div 2H_{13}\delta_{12}\sigma_3+\div 2h_1\delta_{12}+h_3\sigma_3-1=0 \qquad (160)$$

Relation (160) for the three versions of criteria take the form :
For the (EPFS)-criterion :

$$1/2(H_{33}\delta_{12}^2)+H_{33}\sigma_3^2-\div 2H_{33}\delta_{12}\sigma_3+\div 2h_1\delta_{12}+h_3\sigma_3-1=0 \qquad (161)$$

for the Tsai-Hahn criterion :

$$1/2(H_{11}\delta_{12}^2)+H_{33}\sigma_3^2-\div 2(H_{11}H_{33})^{1/2}\delta_{12}\sigma_3+\div 2h_1\delta_{12}+h_3\sigma_3-1=0 \qquad (162)$$

and the Tsai-Wu with H_{ij}=0 criterion :

$$H_{11}\delta_{12}^2+H_{33}\sigma_3^2+\div 2h_1\delta_{12}+h_3\sigma_3-1=0 \qquad (163)$$

The curves (161) to (163) corresponding to the $(\sigma_3\delta_{12})$-principal diagonal intersections of the quadric surface representing the FTP criteria delineate either an ellipse or a parabola depending on the signs of the following matrices [78] :

(i) $\det\mathbf{A}_2>0$ or $\det\mathbf{A}_2=0$
(ii) $\det\mathbf{A}_3\neq 0$ and
(iii) $(\det\mathbf{A}_3\ \mathrm{tr}\ \mathbf{A}_2)<0$ (164)

(i) *For the EPFS-criterion :*

$$\det\mathbf{A}_2=\begin{pmatrix}\frac{1}{2}H_{33} & -\frac{H_{33}}{\sqrt{2}}\\ -\frac{H_{33}}{\sqrt{2}} & H_{33}\end{pmatrix}$$

$$\det \mathbf{A}_3 = \begin{vmatrix} \frac{1}{2}H_{33} & -\frac{H_{33}}{\sqrt{2}} & \frac{h_1}{\sqrt{2}} \\ \frac{H_{33}}{\sqrt{2}} & H_{33} & \frac{h_3}{2} \\ \frac{h_1}{\sqrt{2}} & \frac{h_3}{2} & -1 \end{vmatrix} = -\frac{H_{33}}{2}\left(h_1 + \frac{h_3}{2}\right)^2 \tag{165}$$

$$\mathrm{tr}\mathbf{A}_2 = \frac{3}{2}H_{33}$$

The equation of the symmetry axis $O'z'_p$ of the parabolic intersection of the EPFS by the $(\sigma_3\delta_{12})$-plane is given by the second rank eigentensor corresponding to the zero eigenvalue of the fourth-order tensor **H** and it is given by :

$$\frac{1}{2}H_{33}\delta_{12} - \frac{H_{33}}{\sqrt{2}}\sigma_3 = 0$$

which yields :

$$\sigma_3 = \frac{1}{\sqrt{2}}\delta_{12}$$

and

$$\tan\theta_p = 35.26^\circ \tag{166}$$

Relations (165) indicate that the $(\sigma_3\delta_{12})$-intersection of the EPFS-criterion for transversely isotropic materials is a parabola whose symmetry axis is parallel to the hydrostatic axis $\sigma_1=\sigma_2=\sigma_3$ lying at a distance η_p given by Eq.(64) :

(ii) *For the Tsai-Hahn criterion it is valid :*

$$\det\mathbf{A}_2 = \begin{vmatrix} \frac{H_{11}}{2} & -\left(\frac{H_{11}H_{33}}{2}\right)^{1/2} \\ \left(\frac{H_{11}H_{33}}{2}\right)^{1/2} & H_{33} \end{vmatrix} = 0$$

$$\mathbf{A}_3 = \begin{pmatrix} \frac{H_{11}}{2} & -\left(\frac{H_{11}H_{33}}{2}\right)^{1/2} & \frac{h_1}{\sqrt{2}} \\ \left(\frac{H_{11}H_{33}}{2}\right)^{1/2} & H_{33} & \frac{h_3}{2} \\ \frac{h_1}{\sqrt{2}} & \frac{h_3}{2} & -1 \end{pmatrix} = -\left(\sqrt{H_{33}}\,h_1 + \frac{1}{2}\sqrt{H_{11}}\,h_3\right)^2 \qquad (167)$$

$$\mathrm{tr}\mathbf{A}_2 = \left(\frac{1}{2}H_{11} + H_{33}\right)$$

The zeroing of the determinant of the matrix A_2 yields the angle θ_p ,which is expressed by :

$$\theta_p = \tan^{-1}\left(\frac{H_{11}}{2H_{33}}\right)^{1/2} \qquad (168)$$

By a straightforward analysis based on the properties of the parabola [78], it can be deduced that the distance η_p of the symmetry axis of the parabolic intersection from the hydrostatic Oz-axis is given by:

$$\eta_p = -\sqrt{2}\left\{\frac{h_1h_3(H_{11}-2H_{33}) + \sqrt{H_{11}H_{33}}\,(h_3^2 - 2h_1^2)}{\left(\sqrt{\frac{H_{11}}{H_{33}}}\,h_3 + 2h_1\right)(H_{11}-2H_{33})^{3/2}}\right\} \qquad (169)$$

(iii) *for the Tsai-Wu* criterion with $H_{ij}=0$ $(i\neq j)$ it can be deduced that the intersection of the surface expressing this criterion by the $(\sigma_3\delta_{12})$-principal diagonal plane is an ellipse, whose coordinates of its center are given by :

$$(y^0_{TW}, z^0_{TW}) = \left(-\frac{h_1}{\sqrt{2}\,H_{11}}, -\frac{h_3}{2H_{33}}\right) \qquad (170)$$

the equation of the ellipse is expressed by :

$$H_{11}z_{TW}^2 + H_{33}y_{TW}^2 = \left(1 + \frac{h_3^2}{4H_{33}} + \frac{h_1^2}{2H_{11}}\right) \tag{171}$$

where the (z_{TW}, y_{TW})-principal axes of the ellipse are parallel to the $(\sigma_3\delta_{12})$-axes respectively.

Figure 45 presents the intersections by the $(\sigma_3\delta_{12})$-plane of the three versions of the failure tensor polynomial criterion for the oriented polycarbonate, whose failure properties are given in table 1 as material A.

It is evident from these plottings that the EPFS-criterion and the TH-criterion yield open-ended surfaces, whose $(\sigma_3\delta_{12})$-intersections, which are symmetric to the failure surfaces, present the following differences. The EPFS-intersection has its symmetry axis parallel to the hydrostatic axis, whereas the TH-intersection is strongly inclined to this axis.

The TW-intersection is an ellipse, whose principal axes are parallel to the σ_3- and δ_{12}- axes and its center is displaced inside the second quadrant of the $(\sigma_3\delta_{12})$-plane at a polar distance derived from relation (171).

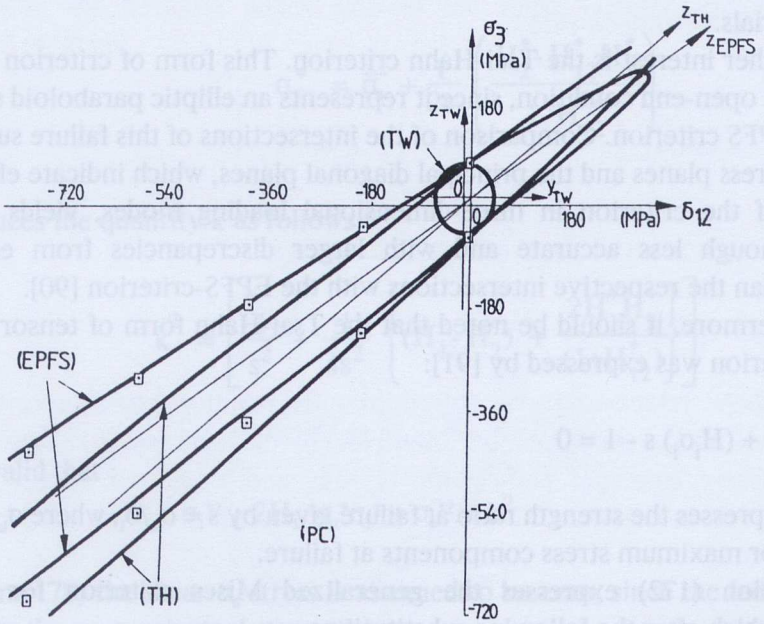

Fig.45 - The (σ_3,δ_{12})-principal diagonal intersections for oriented polycarbonate according to the three versions of failure tensor polynomial criterion EPFS : The elliptic paraboloid failure surface, (TH) : The Tsai-Hahn criterion and (TW) : The Tsai-Wu with $H_{ij}=0$ $(i\neq j)$ criterion.

Experiments executed by Bridgman [40,107] have definitely established that the resistance to failure of all materials (isotropic and orthotropic) is much higher than their resistance to failure in simple compression. This fact implies the principle that the failure strength of materials to a loading mode approaching the hydrostatic pressure should be very high, so that their failure surfaces should be open. Then, the TW-criterion with $H_{ij}=0$, which yields a failure stress under hydrostatic pressure, which is of the same order of magnitude with the failure stress in simple compression is unacceptable, as it is also any other criterion represented in the stress space by a closed surface. Furthermore, the Tsai-Wu criterion stating that all interaction (off-diagonal) terms H_{ij} are independent and should be determined experimentally constitutes, instead of a failure criterion, a curve fitting process, not based on any phenomenological trend, and establishing only a failure condition with statistical features.

The difficulty in executing complicated tests to define the failure characteristics of anisotropic materials explains the paucity of such tests in the literature. The only triaxial tests with anisotropic materials existing in the literature are those executed with mildly anisotropic high-polymers, mechanically or thermally deformed, to lend them some amount of orientation as it is the oriented polycarbonate (PC) [12,13,18]. There exist also some triaxial tests with foams and porous materials, as well as with sands and rocks, but all these results are not sufficient for studying the failure loci of these materials.

Of higher interest is the Tsai-Hahn criterion. This form of criterion satisfies the single sheet open-end condition, since it represents an elliptic paraboloid surface, as it does the EPFS criterion. Comparison of the intersections of this failure surface by the principal stress planes and the principal diagonal planes, which indicate efficiently the behavior of the criterion in three-dimensional loading modes, yields satisfactory results although less accurate and with larger discrepancies from experimental evidence than the respective intersections with the EPFS-criterion [90].

Furthermore, it should be noted that the Tsai-Hahn form of tensor polynomial failure criterion was expressed by [91]:

$$(H_{ij}\sigma_i\sigma_j)\, s^2 + (H_i\sigma_i)\, s - 1 = 0 \qquad (172)$$

where s expresses the strength ratio at failure given by $s = \sigma_{ia}/\sigma_i$, where σ_{ia} denotes the allowable or maximum stress components at failure.

Equation (172) expresses the generalized Mises criterion for orthotropic materials which after the following substitutions :

$$\bar{\sigma}_i = H_{ii}^{1/2}\sigma_i \qquad (i=1,2,6) \qquad (173)$$

takes the form :

$$(\bar{\sigma}_1^2+2H_{12}^*+\bar{\sigma}_2^2+\bar{\sigma}_6^2)\ s^2+\ (H_1^*\bar{\sigma}_1+H_2^*\bar{\sigma}_2)\ s\ -\ 1\ =\ 0 \tag{174}$$

with :

$$H_{12}^* = \frac{H_{12}}{(H_{11}H_{22})^{1/2}} \qquad H_1^* = \frac{H_1}{(H_{11})^{1/2}} \qquad H_2^* = \frac{H_2}{(H_{22})^{1/2}} \tag{175}$$

Then, Tsai [91] simplifies equation (174) by an appropriate coordinate translation, in order to eliminate the linear terms in Eq.(174) using the following relations :

$$\sigma_1^* = \bar{\sigma}_1 + \frac{1}{2s}\left(\frac{H_1^*-H_{12}^*H_2^*}{1-H_{12}^{*2}}\right) \tag{176}$$

$$\sigma_2^* = \bar{\sigma}_2 + \frac{1}{2s}\left(\frac{H_2^*-H_{12}^*H_1^*}{1-H_{12}^{*2}}\right)$$

and introduces the quantity k as follows :

$$k^2 = \left[\frac{1}{s^2} + \frac{1}{4s^2}\left\{(H_1^*-H_2^*) + \frac{2H_1^*H_2^*}{(1+H_{12}^*)}\right\}\right] \tag{177}$$

Then it is valid that :

$$\sigma_1^{*2} + 2H_{12}^*\sigma_1^*\sigma_2^* + \sigma_2^{*2} = k^2 \tag{178}$$

In Equation (178) the shear σ_6-stress is assumed to be zero, since the failure loci are considered in the σ_1,σ_2-principal stress plane.

Now, Tsai comparing relation (178) with the typical Mises failure criterion in the principal stress plane derives readily that it should be valid that :

$$H_{12}^* = -1/2 \tag{179}$$

Equation (179) introduced into the first of relations (175) yields :

$$H_{12} = -\frac{1}{2}(H_{11}H_{22})^{1/2} \tag{180}$$

However, this relationship is only valid for the translated coordinate system (σ_1^*,σ_2^*) and not for the initial one (σ_1,σ_2)-frame, as it is accepted by Tsai [91]. This could be valid for both systems only if $H_1=H_2=0$ that is, if the strength differential effect is neglected, fact which leads this criterion to the previous criteria of the Mises-Hill type.

Therefore, the Tsai-Hahn criterion, which indicates an inclination of the respective failure surface to the hydrostatic axis, should also by rejected for the additional reason that this failure surface, leaning toward the one side of the hydrostatic axis presents some unbalance, approaching an instability condition.

It is worthwhile indicating that although large differences exist between the various versions of criteria based on the failure tensor polynomial, the respective failure loci for a biaxial loading mode of the materials do not differ significantly between them. Indeed, the intersections of the quadric failure surface by the principal stress plane is an ellipse whose coordinates of its center are expressed by relations (79), whereas the inclination of its principal axes relatively to the principal stress axes is given by Eq. (81): Furthermore, the lengths of its principal semi-axes are derived from relations (83) :

$$\alpha_{1M} = \left[-\frac{\det \mathbf{A}_3}{\lambda_1 \det \mathbf{A}_2} \right]^{1/2} \quad \text{and} \quad \alpha_{3M} = \left[-\frac{\det \mathbf{A}_3}{\lambda_2 \det \mathbf{A}_2} \right]^{1/2} \tag{181}$$

and λ_1, λ_2 are the roots of the characteristic equation :

$$\lambda_2 - (H_{ii}+H_{jj})\lambda + (H_{ii}H_{jj}-H_{ij}^2) = 0 \tag{182}$$

Using the above relationships for determining the positions, orientations and shapes of the intersections of the respective failure loci by the principal $(\sigma_3\sigma_1)$-stress plane for the transversely isotropic body with $H_{11}=H_{22}$ and $h_1=h_2$ we readily derive the coordinates for the centers of the elliptic intersections of the respective failure surfaces given by :

i) For EPFS :

$$(\sigma_1^0,\sigma_3^0) = \left[-\frac{2h_1+h_3}{4H_{11}H_{33}}, -\frac{h_1H_{33}+2h_3H_{11}}{H_{33}(4H_{11}-H_{33})} \right]$$

ii) For TH :

$$(\sigma_1^0, \sigma_3^0) = \left[-\frac{h_3(H_{11}H_{33})^{1/2}+2h_1H_{33}}{3H_{11}H_{33}}, \; -\frac{h_1(H_{11}H_{33})^{1/2}+2h_3H_{11}}{3H_{11}H_{33}} \right]$$

and

iii) For TW :

$$(\sigma_1^0, \sigma_3^0) = \left[-\frac{h_1}{2H_{11}}, \; -\frac{h_3}{2H_{33}} \right] \tag{183}$$

Using the above relationships we have plotted in Fig. 46 the (σ_1,σ_3)-intersections for oriented polycarbonate based on the values of failure stresses of this material in simple tension and compression along each of the principal directions. In the same figure we have also plotted the experimental results from the tests of refs. [74] and [92]. All intersections for the three distinct versions of the tensor polynomial criterion should pass through the points A,A' and B,B'. Therefore, there is not much ground for differing these three ellipses. Furthermore, the expected scatter of the experimental results, added to the previous property of the ellipses, does not leave enough ground for deciding which one of the three criteria corroborates the experimental evidence.

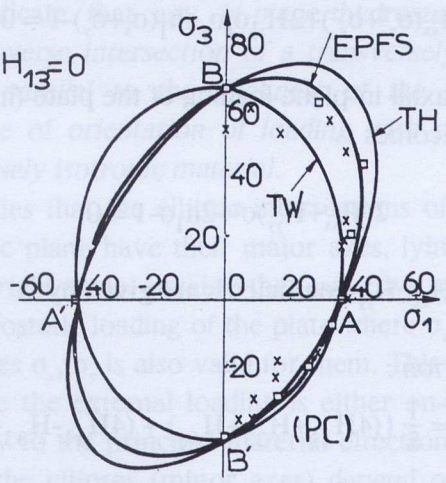

Fig.46 - The (σ_3,σ_1)-principal stress intersections for oriented polycarbonate according to the three versions of failure tensor polynomial criterion EPFS : The elliptic paraboloid failure surface, (TH) : The Tsai-Hahn criterion and (TW) : The Tsai-Wu with $H_{ij}=0$ $(i\neq j)$ criterion.

We examine the failure loci in the transverse $(\sigma_1\sigma_2)$-plane of symmetry for the three versions of the criterion. The transverse intersection of the general quadric surface, by the plane of symmetry of the material, in the $(\sigma_1\sigma_2)$-principal stress coordinate frame, is given by :

$$H_{11}(\sigma_1^2+\sigma_2^2)+2H_{12}\sigma_1\sigma_2+h_1\sigma_1+h_2\sigma_2-1=0 \tag{184}$$

where the diagonal coefficient H_{12} is expressed by :

(i) *For the EPFS:*

$$H_{12}=\frac{1}{2}(H_{33}-2H_{11})$$

(ii) *For TH:* (185)

$$H_{12}=-\frac{H_{11}}{2} \quad \text{and}$$

(iii) *For TW with H_{ij}=0 for $i\neq j$:*

$$H_{12}=0$$

For an arbitrary biaxial in-plane loading mode of the plate with $\sigma_x\neq\sigma_y$ relation (184) becomes:

$$H_{xx}(\sigma_x^2+\sigma_y^2)+2H_{xy}\sigma_x\sigma_y+h_1(\sigma_x+\sigma_y)-1=0 \tag{186}$$

whereas, for an equal biaxial in-plane loading of the plate (hydrostatic loading), with $\sigma_x=\sigma_y=\sigma$ relation (186) becomes :

$$2(H_{xx}+H_{yy})\sigma^2+2h_1\sigma-1=0 \tag{187}$$

where the values of the H_{xx}, H_{yy}-coefficients are given by :

(i) *For the EPFS-criterion :*

$$H_{xx}=\frac{1}{8}\{(4H_{11}+H_{33}+H_{66})+(4H_{11}-H_{33}-H_{66})\cos4\theta\}$$

$$H_{xy}=\frac{1}{8}\{(3H_{33}-4H_{11}-H_{66})-(4H_{11}-H_{33}-H_{66})\cos4\theta\} \tag{188}$$

(ii) *For the TH-criterion :*

$$H_{xx} = \frac{1}{8}\{(5H_{11}+H_{66}) + (3H_{11}-H_{66})\cos 4\theta\}$$
$$H_{xy} = -\frac{1}{8}\{(H_{11}+H_{66}) + (3H_{11}-H_{66})\cos 4\theta\} \quad (189)$$

and

(iii) *For the (TW)-criterion with* $H_{ij}=0$ $(i\neq j)$ *:*

$$H_{xx} = \frac{1}{8}\{(6H_{11}+H_{66}) + (2H_{11}-H_{66})\cos 4\theta\}$$
$$H_{xy} = \frac{1}{8}(2H_{11}-H_{66})(1-\cos 4\theta) \quad (190)$$

where θ is the angle subtended by the 0xy-system and the $0\sigma_1\sigma_2$-system.

Relation (187) for the three different criteria studied becomes :

(i) *For the EPFS :* $H_{33}\sigma^2 + 2h_1\sigma - 1 = 0$
(ii) *For the TH :* $H_{11}\sigma^2 + 2h_1\sigma - 1 = 0$ (191)
(iii) *For the TW:* $2H_{11}\sigma^2 + 2h_1\sigma - 1 = 0$

Relations (191) indicate that any *in-plane hydrostatic loading of a plate corresponding to a transverse intersection of a transversely isotropic material, so that its strong axis is parallel to the thickness of the plate, is invariant and independent of the angle of orientation of loading with respect to the principal directions of the transversely isotropic material.*

Relation (186) implies that the elliptic intersections of the failure loci by the $(\sigma_1\sigma_2)$-transverse isotropic plane have their major axes, lying along the bisector of the first quadrant $(\sigma_1 0\sigma_2)$-right angle, equal to the respective major axes of the ellipses corresponding to an hydrostatic loading of the plate where $\sigma_x = \sigma_y = \sigma$, since the same equality of applied stresses σ_x, σ_y is also valid for them. This is valid for any loading mode of the plate, where the external loading is either on-axis ($\theta=0°$), or off-axis ($\theta\neq 0°$) oriented, relatively to the principal material directions. On the contrary, the other principal axes of the ellipses (minor axes) depend on the θ-angle with the maximum deviations appearing at $\theta=45°$.

Figures 47 and 48 present the elliptic intersections of the three failure loci studied for the oriented polycarbonate. Figure 47 corresponds to angle $\theta=0°$, whereas Fig.48 to angle $\theta=45°$.

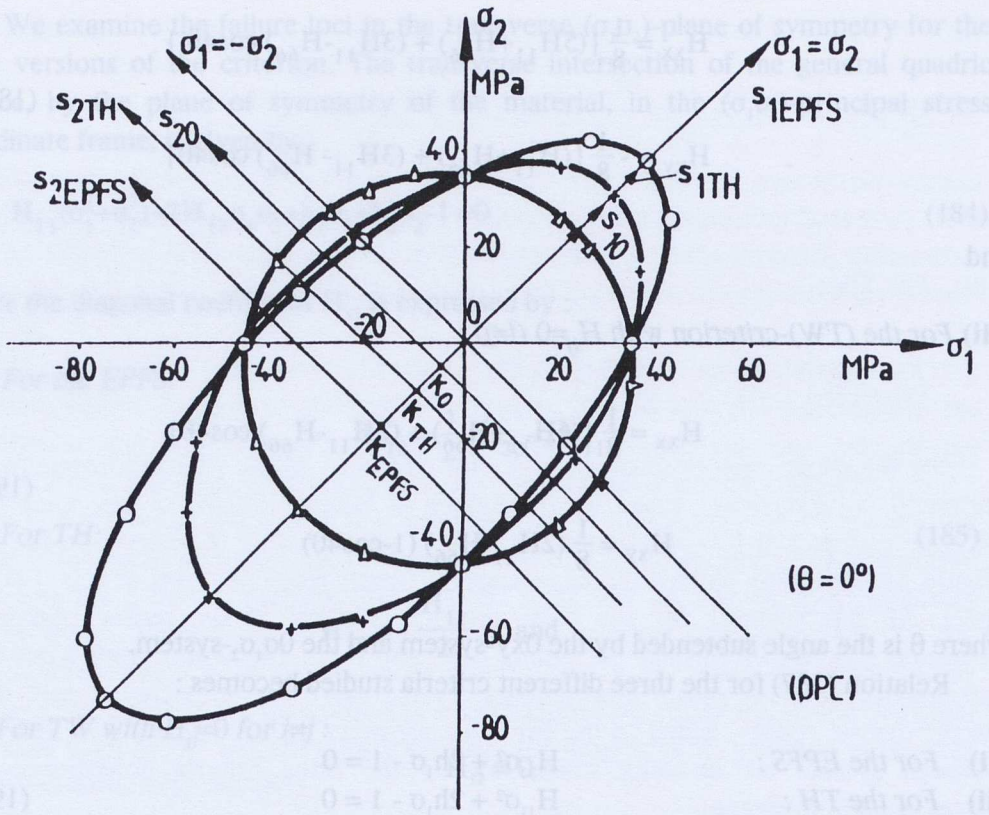

Fig. 47 - The (σ_1,σ_2)-principal stress intersections with $\theta=0°$ for oriented polycarbonate according to the three versions of failure tensor polynomial criterion EPFS : The elliptic paraboloid failure surface, (TH) : The Tsai-Hahn criterion and (TW) : The Tsai-Wu with $H_{ij}=0$ $(i\neq j)$ criterion.

By comparing the ellipses of the pair of figures one may realize at once the coincidence of the major axes of the respective ellipses, for different θ-angles, whereas their minor axes differ significantly. It is wothwhile remarking that the oriented polycarbonate is a compression strong material ($tr\mathbf{h}=(h_3+2h_1)>0$) and the larger differences in the failure stresses between the various criteria appear in the third quadrant, where this material presents its maximum strength.

By comparing the failure stresses for hydrostatic loading of the plates of the materials corresponding to their transverse isotropic planes it is obvious that the ratios of these stresses for the various versions of the failure tensor polynomial criterion are considerable. These ratios are stronger for the mode of loading for which the material is more resistant, that is this difference in failure stresses under hydrostatic in-plane loading becomes higher in the compression-compression zone of

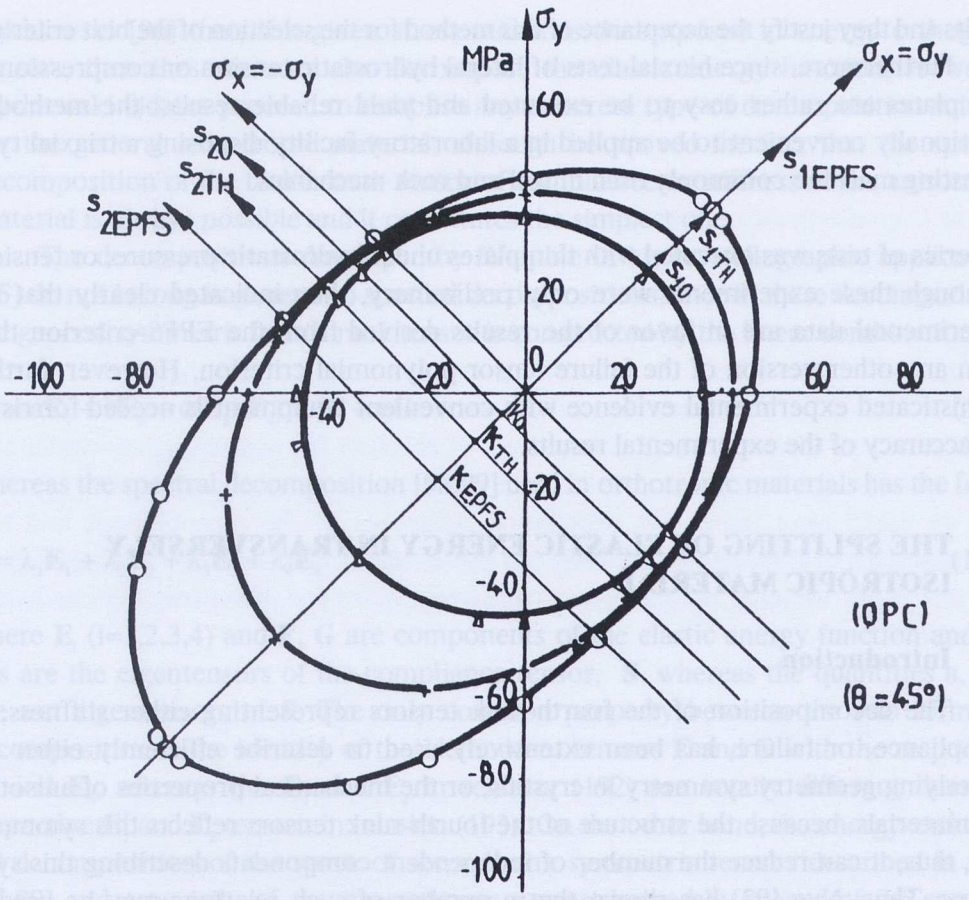

Fig. 48 - The (σ_x,σ_y)-transverse isotropic plane intersections with $\theta=45°$ for oriented polycarbonate according to the three versions of failure tensor polynomial criterion EPFS : The elliptic paraboloid failure surface, (TH) : The Tsai-Hahn criterion and (TW) : The Tsai-Wu with $H_{ij}=0$ $(i\neq j)$ criterion.

loading for compression-strong materials and in the tension-tension quadrant for the tension-strong materials. Thus, for the oriented polycarbonate the ratios of failure stresses under hydrostatic in-plane compression is given by :

$$\sigma_{(EPFS)} : \sigma_{(TH)} : \sigma_{(TW)} = (-73.10) : (-51.12) : (-33.64) \text{ MPa}$$

These large differences in strengths given by the different versions of the tensor failure polynomial criterion in plates corresponding to transverse cross-sections on the isotropic plane of a transversely isotropic material constitute a certain technique for deciding which version corresponds to reality, corroborating existing experimental

results and they justify the acceptance of this method for the selection of the best criterion.

Furthermore, since biaxial tests of lateral hydrostatic tension or compression in thin plates are rather easy to be executed and yield reliable results, the method is additionally convenient to be applied in a laboratory facility disposing a triaxial type of testing machine commonly used in soil and rock mechanics.

A series of tests was executed with thin plates under hydrostatic pressure, or tension. Although these experiments were only preliminary, they indicated clearly that the experimental data are in favor of the results derived from the EPFS-criterion than from any other version of the failure tensor polynomial criterion. However, further sophisticated experimental evidence with convenient equipment is needed for rising the accuracy of the experimental results.

5. THE SPLITTING OF ELASTIC ENERGY IN TRANSVERSELY ISOTROPIC MATERIAL

5.1 Introduction

The decomposition of the fourth-rank tensors representing either stiffness, or compliance, or failure, has been extensively used to describe efficiently either the underlying geometry symmetry in crystals, or the mechanical properties of anisotropic materials, because the structure of the fourth-runk tensors reflects this symmetry and, thus, it can reduce the number of independent components describing this symmetry. Thus, Nye [93] has shown that a number of such relations may be used to introduce fourth-rank tensors describing the elastic stiffnesses and compliances, elasto-optical and piezo-optical coefficients and other properties in crystals. More recently Srinivasan and Nigam [94] have introduced appropriate decompositions of the tensor structure in order to reflect a valuable insight and simultaneously to achieve simplifications in the calculations of their inverses and their inner products. Similarly, Walpole [95] has presented a reduction of the algebra of the fourth-rank tensors to irreducible subalgebras, which were simpler than the initial one and, therefore, they facilitated operations between these tensors. In this general form of decomposition Walpole included also the spectral decomposition of the fourth-rank tensor and applied these decompositions to define the properties of various crystalline systems. However, the decompositions used by Walpole in his applications do not correspond to spectral ones, except the trivial cases of the isotropic and the cubic-system fourth-rank tensors. Rychlewski [96,97] has shown the possibility to decompose the elastic stiffness and compliance fourth-rank tensors by using the spectral decomposition. Indeed, the definition of energy orthogonal stress states was anticipated by Rychlewski [97]. This term denotes stress tensors mutually orthogonal and at the same time collinear with their respective strain tensors. It was also shown by

Rychlewski [96] that, if a given stress tensor is decomposed in energy orthogonal tensors, then these tensors also decompose the elastic energy function. However, Rychlewski did not proceed to establish any concrete type of decomposition suitable for the general anisotropic material, although he proved the fact that the spectral decomposition of the fourth-rank tensor of compliance or stiffness of the anisotropic material is always possible and it constitutes the simplest one.

The decompositions developed by Walpole in his crystallographic applications [95] do not belong in general to spectral decompositions,since in these decompositions the general symmetric fourth-rank tensor is constructed by the linear combination :

$$\mathbf{S} = a\mathbf{E}_1 + b\mathbf{E}_2 + c(\mathbf{E}_3+\mathbf{E}_4) + f\mathbf{F} + g\mathbf{G} \tag{192}$$

whereas the spectral decomposition [98,99] used in orthotropic materials has the form:

$$\mathbf{S} = \lambda_1\mathbf{E}_1 + \lambda_2\mathbf{E}_2 + \lambda_3\mathbf{E}_3 + \lambda_4\mathbf{E}_4 \tag{193}$$

where $\mathbf{E}_i$ (i=1,2,3,4) and $\mathbf{F}$, $\mathbf{G}$ are components of the elastic energy function and the λ_i's are the eigentensors of the compliance tensor, $\mathbf{S}$, whereas the quantities a, b, c are not eigentensors of $\mathbf{S}$. The only common property between the two forms of decomposition is the identity of the idempotent tensors $\mathbf{F}$ and $\mathbf{G}$ with the respective $\mathbf{E}_3$ and $\mathbf{E}_4$, whereas the $\mathbf{E}_1$ and $\mathbf{E}_2$ in relation (192) are totally different than the respective $\mathbf{E}_1$ and $\mathbf{E}_2$ tensors in relation (193). On the other hand, the energy-orthogonal decomposition of the space of second rank symmetric tensors described in refs. [84,98] and especially of the stress tensor $\boldsymbol{\sigma}$, was derived by means of the spectral decomposition of the symmetric fourth-rank tensor, $\mathbf{S}$, which defines, in an unambiguous manner, the positive definite elastic energy function:

$$2T = \boldsymbol{\sigma} \cdot \mathbf{S} \cdot \boldsymbol{\sigma} \tag{194}$$

The decomposition of tensor $\boldsymbol{\sigma}$, for the transversely isotropic solid, gave four orthogonal stress states, which decompose the elastic energy function in a clear and radical manner. Two of them, i.e., $\boldsymbol{\sigma}_1$ and $\boldsymbol{\sigma}_2$, are solely associated with a distortional elastic energy, whereas the remaining two denote in general both voluminal and distortional elastic energies [99-101]. In this way it is succeeded to establish energy orthogonal stress- and strain-states for the general orthotropic and particularly for the transversely isotropic material, based on the spectral decomposition of the compliance and stiffness tensors and to separate the SED into well-defined components. Similar decompositions were recently introduced by the author [58,102], based on geometric properties of the stress- and strain- vectors of the transversely isotropic body, which, however, do not possess the generality and the elegance of the spectral decomposition presented here.

Previous efforts were spent to extend the splitting process valid for the isotropic elastic body, where the elastic energy density can be separated into two energy-orthogonal subspaces of loading, that is to the spherical and the deviatoric tensors, which constitute eigentensors of the isotropic **S**-compliance tensor. These components correspond to the eigenvalues 1/3K and 1/2G respectively. However, it becomes evident from the theory of the spectral analysis that this type of decomposition of the elastic energy density for the general anisotropic elastic body into a component contributing to the volume change exclusively and another component corresponding to a distortional type of energy is impossible. The necessary condition for this decomposition to be valid is that the strain-eigentensor representing the volume variation should be an eigentensor of the compliance tensor **S**. This means that the spherical tensor **1** should be an eigentensor of **S**. Then the orthogonality conditions imply that the remaining eigentensors of **S** should be deviatoric tensors. Only in this case we could have these two orthogonal subspaces of the eigentensors, and the decomposition of SED into the dilatational and the distortional component is possible. But, this is not the case for the anisotropic body, since for the anisotropic body the decomposition :

$$T(\boldsymbol{\sigma}) = T(\boldsymbol{\sigma}_P) + T(\boldsymbol{\sigma}_D) = \frac{1}{18K}(\mathrm{tr}\,\boldsymbol{\sigma})^2 + \frac{1}{2G}\left[\mathrm{tr}\boldsymbol{\sigma}^2 - \frac{1}{3}(\mathrm{tr}\,\boldsymbol{\sigma})^2\right] \tag{195}$$

is not possible, as it is for the isotropic body.

However, the spectral decomposition of the energy density for the transversely isotropic body presented here is equally general and is based on the same principle. Indeed, it is futile to search for a decomposition of the type (195) for the general anisotropic body, since this decomposition holds only for isotropic bodies, as well as for cubic crystals. Thus, the great efforts spent by Olszak and his coworkers [103,104], motivated by the possibility of introducing a generalization of the Huber-Mises-Hencky criterion to anisotropic bodies and aimed to establish the distortional component of the strain energy density as a critical failure quantity, did not succeed for the abovementioned reasons and it was abandoned by its inspirers.

A theory will be presented here, which succeeds to decompose spectrally the compliance (or stiffness or failure) tensor for a transversely isotropic material, and to evaluate its characteristic values. Based on the properties of this decomposition, energy-orthogonal stress states were established.

5.2 Spectral decomposition for the transversely isotropic fourth-rank tensor

Consider the decomposition of the compliance tensor **S** of a transversely isotropic linear elastic solid. Of course, any other similar tensor related with different material properties will decompose in the same manner. We suppose the Cartesian coordinate system, which the stress and strain tensor components are referred to, being oriented

along the principal material directions, with 3-axis being of infinite symmetry of the material and it is normal to the isotropic (transverse) plane. Using engineering constants with subscript (T) to denote elastic properties on the isotropic plane and subscript (L) the corresponding ones on the normal (longitudinal) plane, components of the **S**-tensor associated with the adopted Cartesian system are given by:

$$
\begin{aligned}
&S_{1111} = S_{2222} = 1/E_T, \qquad S_{3333}=1/E_L \\
&S_{1122} = S_{2211} =- \nu_T/E_T \\
&S_{1133} = S_{3311} = S_{2233} = S_{3322} = -\nu_L/E_L \\
&S_{2323} = S_{2332} = S_{3223} = S_{3232} = 1/4G_L \\
&S_{1313} = S_{1331} = S_{3113} = S_{3131} = 1/4G_L \\
&S_{1212} = S_{1221} = S_{2112} = S_{2121} = 1/4G_T
\end{aligned}
\tag{196}
$$

All remaining S_{ijkl} are zero. Moreover, between the engineering constants of the transverse plane the following well-known isotropic relation holds :

$$
\frac{1}{2G_T} = \frac{(1+\nu_T)}{E_T} \tag{197}
$$

The eigenvalues of the associated square matrix of the rank six to tensor **S** defined by (196) are expressed by [100] :

$$
\lambda_1 = \frac{(1+\nu_T)}{E_T} = \frac{1}{2G_T}
$$

$$
\lambda_2 = \frac{1}{2G_L}
$$

$$
\lambda_3 = \frac{(1-\nu_T)}{2E_T} + \frac{1}{2E_L} + \left\{ \left[\frac{(1-\nu_T)}{2E_T} - \frac{1}{2E_L} \right]^2 + \frac{2\nu_L^2}{E_L^2} \right\}^{1/2}
$$

$$
\lambda_4 = \frac{(1-\nu_T)}{2E_T} + \frac{1}{2E_L} - \left\{ \left[\frac{(1-\nu_T)}{2E_T} - \frac{1}{2E_L} \right]^2 + \frac{2\nu_L^2}{E_L^2} \right\}^{1/2} \tag{198}
$$

with the two first eigenvalues λ_1 and λ_2 being of multiplicity two.

The minimum polynomial of tensor **S** is a quartic and has as roots the eigenvalues λ_1, λ_2, λ_3 and λ_4. The associated form idempotent tensors $\mathbf{E}_m$ (m=1÷4) of

the spectral decomposition of **S** are given by relations (29) of ref. [101]. It is further valid for the eigenvalues (198) and the corresponding idempotent tensors $\mathbf{E}_1$, $\mathbf{E}_2$, $\mathbf{E}_3$ and $\mathbf{E}_4$, to whom the unit tensor **I** is spectrally decomposed, that :

$$\mathbf{E}_1 + \mathbf{E}_2 + \mathbf{E}_3 + \mathbf{E}_4 = \mathbf{I} \tag{199}$$

and the tensor **S** is expressed by relation (193).

Furthermore, the eigenangle ω, defined in ref.[100], is expressed by :

$$\tan 2\omega = \frac{-\dfrac{\sqrt{2}\,\nu_L}{E_L}}{\left[\left(\dfrac{1-\nu_T}{2E_T}\right)-\dfrac{1}{2E_L}\right]} \tag{200}$$

If the stress states $\boldsymbol{\sigma}_m$ constitute the eigenstates of tensor **S** they satisfy the relationship:

$$\mathbf{S}\cdot\boldsymbol{\sigma}_m = \lambda_m\boldsymbol{\sigma}_m \tag{201}$$

with the index m varying between 1 and 4 and the λ_m-values given by relations (198). These stress states are defined by :

$$\boldsymbol{\sigma}_m = \mathbf{E}_m\cdot\boldsymbol{\sigma} \tag{202}$$

where $\boldsymbol{\sigma}$ is the contracted stress tensor written as follows :

$$\boldsymbol{\sigma} = [\sigma_1, \sigma_2, \sigma_3, \sigma_4, \sigma_5, \sigma_6]^T \tag{203}$$

Relations (202) imply a series of calculations which finally yield :

$$\boldsymbol{\sigma}_1 = \left[\frac{1}{2}(\sigma_1-\sigma_2),\ -\frac{1}{2}(\sigma_1-\sigma_2),\ 0,\ 0,\ 0,\ \sigma_6\right]^T$$

$$\boldsymbol{\sigma}_2 = [0,\ 0,\ 0,\ \sigma_4,\ \sigma_5,\ 0]^T \tag{204}$$

$$\boldsymbol{\sigma}_3 = \left(\frac{1}{\sqrt{2}}\cos\omega(\sigma_1+\sigma_2) + \sin\omega\sigma_3\right)\left[\frac{1}{\sqrt{2}}\cos\omega,\ \frac{1}{\sqrt{2}}\cos\omega,\ \sin\omega,\ 0,\ 0,\ 0\right]^T$$

$$\boldsymbol{\sigma}_4 = \left(\frac{1}{\sqrt{2}}\sin\omega(\sigma_1+\sigma_2) - \cos\omega\sigma_3\right)\left[\frac{1}{\sqrt{2}}\sin\omega,\ \frac{1}{\sqrt{2}}\sin\omega,\ -\cos\omega,\ 0,\ 0,\ 0\right]^T \quad (16)$$

with :

$$\boldsymbol{\sigma}_1 + \boldsymbol{\sigma}_2 + \boldsymbol{\sigma}_3 + \boldsymbol{\sigma}_4 = \boldsymbol{\sigma} \quad (205)$$

Relations (204) imply that the stress eigenstates corresponding to spectral decomposition of the compliance tensor **S** for the transversely isotropic materials brake down the generic stress tensor $\boldsymbol{\sigma}$ into four elements. The states $\boldsymbol{\sigma}_1$ and $\boldsymbol{\sigma}_2$ are shears, simple together with pure, and pure ones respectively and they are independent of the eigenangle ω. The $\boldsymbol{\sigma}_3$-state represents an equilateral stress state in the isotropic plane together with a superposed tension along the infinite symmetry axis of the material, whereas the $\boldsymbol{\sigma}_4$-state replaces the uniaxial tension by uniaxial compression along the symmetry axis. The sum $(\sigma_3+\sigma_4)$ is the supplement of the $(\sigma_1+\sigma_2)$-state as it is indicated by relation (205).

To these four stress-tensors $\boldsymbol{\sigma}_1$ to $\boldsymbol{\sigma}_4$ are associated four strain tensors $\boldsymbol{\varepsilon}_1$, $\boldsymbol{\varepsilon}_2$, $\boldsymbol{\varepsilon}_3$ and $\boldsymbol{\varepsilon}_4$. The two first strain tensors correspond to a pure distortion of the solid without any volume change. Therefore the following part of the elastic energy for the transversely isotropy body

$$2T_d = \lambda_1[(\sigma_1-\sigma_2)^2 + 4\sigma_6^2] + 4\lambda_2[\sigma_4^2+\sigma_5^2] \quad (206)$$

is purely distortional.

Then :

$$2T_d = \frac{(1+\nu_T)}{2E_T}[(\sigma_1-\sigma_2)^2+4\sigma_6^2] + \frac{2}{G_L}[\sigma_4^2+\sigma_5^2] \quad (207)$$

The remaining states $\boldsymbol{\sigma}_3$ and $\boldsymbol{\sigma}_4$ of the decomposition correspond to mixtures of distortional and dilatational components of elastic energy. Therefore, the corresponding strain tensors $\boldsymbol{\varepsilon}_3$ and $\boldsymbol{\varepsilon}_4$ produce both volume changes and distortions of shape. Then, we have :

$$2T_m = T(\boldsymbol{\sigma}_3)+T(\boldsymbol{\sigma}_4) = \left\{\left[\frac{1-\nu_T}{2E_T}+\frac{1}{2E_L}\right] + \left[\left(\frac{1-\nu_T}{2E_T}-\frac{1}{2E_L}\right)^2 + \frac{2\nu_L^2}{E_L^2}\right]^{1/2}\right\} \times$$

$$x\left\{\frac{\sqrt{2}}{2}\cos\omega(\sigma_1+\sigma_2)+\sin\omega(\sigma_3)\right\}^2+\left\{\left[\frac{1-\nu_T}{2E_T}+\frac{1}{2E_L}\right]-\left[\left(\frac{1-\nu_T}{2E_T}-\frac{1}{2E_L}\right)^2+\frac{2\nu_L^2}{E_L^2}\right]^{1/2}\right\}x$$

$$x\left\{\frac{\sqrt{2}}{2}\sin\omega(\sigma_1+\sigma_2)-\cos\omega(\sigma_3)\right\}^2 \qquad (208)$$

This part of the elastic energy depends on the value of the eigenangle ω for each particular orthotropic material and is associated with shape and volume changes of the material.

5.3 A generalization of Beltrami's ellipsoid for the anisotropic material

If we project the eigentensors $\boldsymbol{\sigma}_m$, given by relations (204), where they are referred as they stand to a generic Cartesian system $(0\text{-}\sigma_1\sigma_2\sigma_3)$, on the principal stress space $(0\text{-}\sigma_1^*\sigma_2^*\sigma_3^*)$ indicated in Figs. 49 & 50, it can be readily derived that the projection of the eigentensor $\boldsymbol{\sigma}_2$, which is expressed as a pure shear loading, becomes equal to zero in the principal stress space. On the other hand, the projections of the stress eigentensors $\boldsymbol{\sigma}_1$, $\boldsymbol{\sigma}_3$ and $\boldsymbol{\sigma}_4$ are generally represented by a tri-orthogonal frame of vectors, which are associated with the respective unit strain-vectors $\mathbf{e}_1$, $\mathbf{e}_3$ and $\mathbf{e}_4$ defined as follows :

$$\mathbf{e}_1 : \left[\frac{1}{\sqrt{2}}, \frac{1}{\sqrt{2}}, 0\right]^T$$

$$\mathbf{e}_3 : \left[\frac{\cos\omega}{\sqrt{2}}, \frac{\cos\omega}{\sqrt{2}}, \sin\omega\right]^T \qquad (209)$$

$$\mathbf{e}_4 : \left[\frac{\sin\omega}{\sqrt{2}}, \frac{\sin\omega}{\sqrt{2}}, -\cos\omega\right]^T$$

It can be readily derived from the second and third of relations (209) that the vectors $\mathbf{e}_3$ and $\mathbf{e}_4$ lie on the principal diagonal $(\sigma_3\delta_{12})$-plane, since they are equally inclined with respect to the principal stress axes $0\sigma_1^*$ and $0\sigma_2^*$. Furthermore, vector $\mathbf{e}_3$ subtends an angle equal to $(\omega\text{-}\pi/2)$ with the positive σ_3^*-axis. Similarly, the vector $\mathbf{e}_4$ subtends an

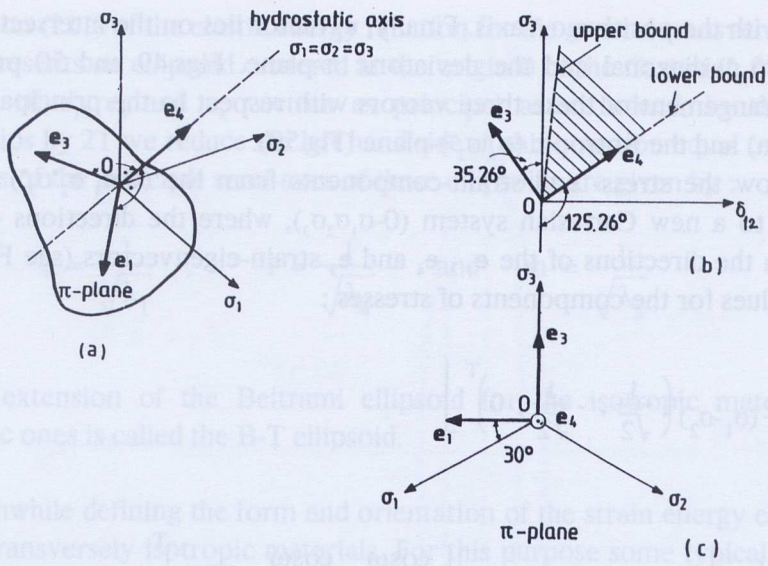

Fig. 49 - Representation of the eigentensors of the transversely isotropic compliance tensor in the principal stress space $(0\sigma_1\sigma_2\sigma_3)$ (α) their projection on the $(\sigma_3\delta_{12})$-plane (b) and the projection of the idempotent tensors **σ** and **e** on the π- plane (c).

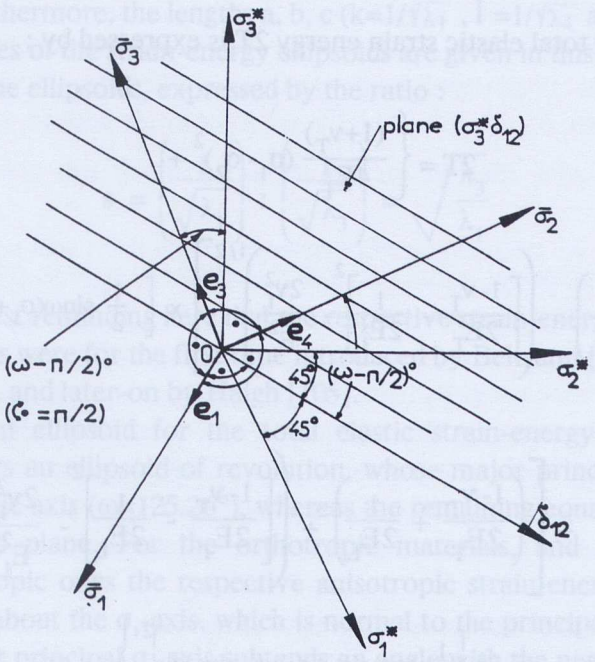

Fig. 50 - Characteristic stress states in the $0\sigma_1\sigma_2\sigma_3$-frame related to the principal stress frame $(0\sigma_1^*\sigma_2^*\sigma_3^*)$ for the transversely isotropic material.

angle (π-ω) with the positive σ_3^*-axis. Finally, $\mathbf{e}_1$ vector lies on the intersection of the principal ($\sigma_3^*\delta_{12}^*$)-diagonal and the deviatoric π-plane. Figs.49 and 50 present the geometric arrangement of these three vectors with respect to the principal diagonal plane (Fig.49a) and the isotropic ($\sigma_1^*\sigma_2^*$)-plane (Fig.50).

Referring now the stress- and strain-components from the (0-$\sigma_1^*\sigma_2^*\sigma_3^*$) principal-stress frame to a new Cartesian system (0-$\sigma_1\sigma_2\sigma_3$), where the directions σ_1, σ_2, σ_3 coincide with the directions of the $\mathbf{e}_1$, $\mathbf{e}_4$ and $\mathbf{e}_3$ strain-eigenvectors (see Fig.50), we derive the values for the components of stresses :

$$\bar{\sigma}_1 = \left[\frac{1}{2}(\sigma_1-\sigma_2)\left(\frac{1}{\sqrt{2}}, -\frac{1}{\sqrt{2}}, 0 \right)^T \right] \tag{210}$$

$$\bar{\sigma}_3 = \left[\frac{1}{2}\cos\omega(\sigma_1+\sigma_2) + \sin\omega\sigma_3 \right] \left[\frac{\cos\omega}{\sqrt{2}}, \frac{\cos\omega}{\sqrt{2}}, \sin\omega \right]^T$$

$$\bar{\sigma}_4 = \left[\frac{1}{2}\sin\omega(\sigma_1+\sigma_2) - \cos\omega\sigma_3 \right] \left[\frac{\sin\omega}{\sqrt{2}}, \frac{\sin\omega}{\sqrt{2}}, -\cos\omega \right]^T$$

Therefore, the total elastic strain energy 2T is expressed by :

$$2T = \left\{ \frac{(1+\nu_T)}{4E_T}(\sigma_1-\sigma_2)^2 + \right.$$

$$+ \left[\left(\frac{(1-\nu_T)}{2E_T} + \frac{1}{2E_L} \right) - \left(\left[\frac{1-\nu_T}{2E_T} - \frac{1}{2E_L} \right]^2 - \frac{2\nu_L^2}{E_L^2} \right)^{1/2} \right] x \left[\frac{1}{2}\sin\omega(\sigma_1+\sigma_2) - \cos\omega\sigma_3 \right]^2 +$$

$$+ \left[\left(\frac{1-\nu_T}{2E_T} + \frac{1}{2E_L} \right) + \left(\left[\frac{1-\nu_T}{2E_T} - \frac{1}{2E_L} \right]^2 - \frac{2\nu_L^2}{E_L^2} \right)^{1/2} \right] x$$

$$\left. x \left[\frac{1}{2}\cos\omega(\sigma_1+\sigma_2) + \sin\omega\sigma_3 \right]^2 \right\} \tag{211}$$

Expression (211) of the elastic energy function for the general transversely isotropic body, represents an ellipsoid centered at the origin 0 of the Cartesian frame with the directions of $\mathbf{e}_1$, $\mathbf{e}_3$ and $\mathbf{e}_4$ vectors as principal axes. Indeed, by dividing these relationships by 2T we reduce the left hand side of this equation equal to unity. Then, the lengths of the principal semi-axes of these ellipsoids are given by :

$$k = \frac{1}{\sqrt{\lambda_1}} \quad , \qquad l = \frac{1}{\sqrt{\lambda_4}} \qquad \text{and} \qquad m = \frac{1}{\sqrt{\lambda_3}} \tag{212}$$

The extension of the Beltrami ellipsoid for the isotropic materials to the anisotropic ones is called the B-T ellipsoid.

It is worthwhile defining the form and orientation of the strain energy ellipsoid for a series of transversely isotropic materials. For this purpose some typical composites, which are strongly anisotropic and therefore ideal for tests, are examined. Their mechanical properties are given in refs. [58] and [100]. Table 4 contains the materials compiled from the literature and given in ref. [58] indicated with a star. In the same table some woven fabric composites, studied in ref.[58], are given [100], and indicated with a double star. In this table the ratios $E_L/2G_L$, of the longitudinal elastic and the double of shear moduli are given, as well as the corresponding values of the eigenangle ω.Furthermore, the lengths a, b, c ($k=1/\sqrt{\lambda_1}$, $l=1/\sqrt{\lambda_4}$ and $m=1/\sqrt{\lambda_3}$) of the principal semi-axes of the strain-energy ellipsoids are given in this table, as well as the *slenderness* s of the ellipsoids, expressed by the ratio :

$$s = \left(\frac{1}{\sqrt{\lambda_1}}\right) : \left(\frac{1}{\sqrt{\lambda_3}}\right) = \sqrt{\frac{\lambda_3}{\lambda_1}} \tag{213}$$

It is of interest reminding here that the respective strain-energy ellipsoids for the isotropic materials were for the first time introduced by Beltrami [104] some hundred and ten years ago, and later-on by Haigh [105].

The Beltrami ellipsoid for the total elastic strain-energy for the isotropic materials is always an ellipsoid of revolution, whose major principal axis coincides with the hydrostatic axis ($\omega=125.26°$), whereas the remaining equal principal axes lie on the deviatoric plane. For the orthotropic materials, and especially for the transversely isotropic ones the respective anisotropic strain-energy ellipsoids (B-T ellipsoids) rotate about the σ_1-axis, which is normal to the principal diagonal $(\sigma_3\delta_{12})$-plane, so that their principal σ_2-axis subtends an angle with the negative σ_3-axis equal to the respective eigenangle ω of the material.

Figure 51 presents the B-T ellipsoid for *Thornel 75S* graphite fiber-epoxy matrix

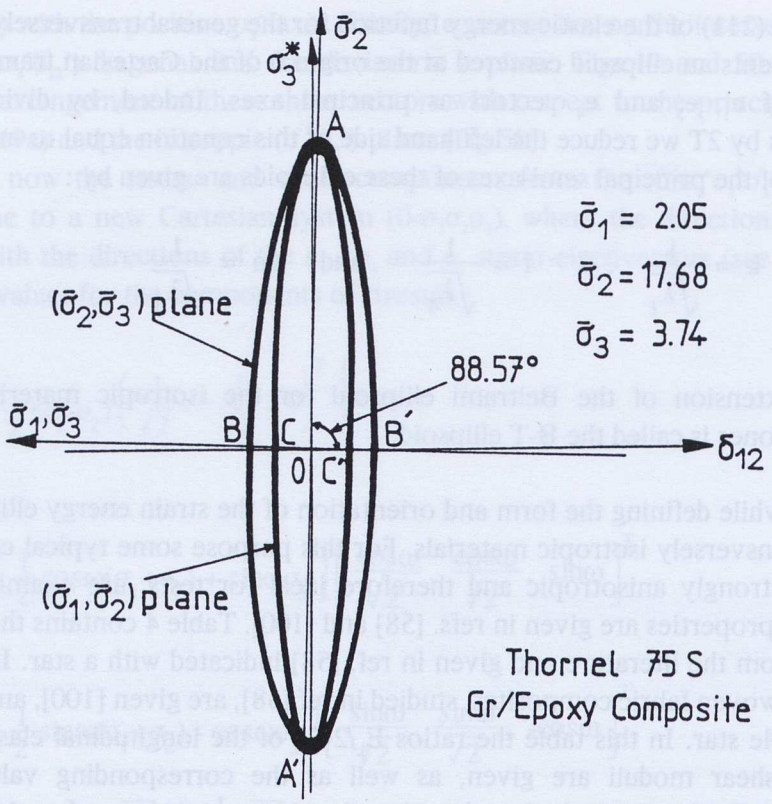

Fig.51 - The normalized to total strain energy 2T (B-T)-strain-energy ellipsoids for a strongly anisotropic fiber reinforced composite (Thornel 75 S graphite-epoxy composite) (Planes (σ_1,σ_2) are folded up by $\pi/2$ to coincide with (σ_2,σ_3) planes).

composite. The σ_2-principal stress axis for this ellipsoid is now subtending an angle with the isotropic (σ_1,σ_2)-stress plane equal to $(\omega-\pi/2)=88.57°$, that is this axis coincides almost with the σ_3-axis. It is interesting remarking that the B-T ellipsoids for the family of transversely isotropic materials with the σ_3-axis as the strong one, whose eigenangle $\boldsymbol{\omega}$ varies in the interval 125.26° and 180°, are slender ellipsoids having a direction of slenderness normal to the principal diagonal (σ_3,δ_{12})- plane. This fact can be confirmed by the values of the principal semi-axis $k=1/\sqrt{\lambda_1}$ of this family of ellipsoids, which are always smaller than the lengths of semi-axes $m=1/\sqrt{\lambda_3}$.

5.4 The isotropic and the quasi-isotropic material

For the isotropic materials, where $E_L=E_T$, $G_L=G_T$, and $\nu_L=\nu_T$, relations (198) and (200) together with Eq.(193) yield to the spectral decomposition of the isotropic elastic body the already well-known relationship :

$$\mathbf{S} = \frac{1}{3K}\left(\frac{1}{3}\mathbf{1}\otimes\mathbf{1}\right) + \frac{1}{2G}\left(\mathbf{I} - \frac{1}{3}\mathbf{1}\otimes\mathbf{1}\right) \tag{214}$$

where K and G are the elastic bulk and shear moduli of the material. Furthermore, we could decompose an arbitrary loading $\boldsymbol{\sigma}$ as the sum of a spheric and a deviatoric tensor as follows :

$$\boldsymbol{\sigma} = \boldsymbol{\sigma}_P + \boldsymbol{\sigma}_D \tag{215}$$

where :

$$\boldsymbol{\sigma}_P = \frac{1}{3}(\mathrm{tr}\,\boldsymbol{\sigma})\,\mathbf{1}$$

and tr$\boldsymbol{\sigma}$ is the first invariant of $\boldsymbol{\sigma}$-tensor, whereas the unit tensor **1** in Cartesian form is represented by the Krönecker delta. Then, using relations (214) and (215), the following relationship can be shown :

$$\boldsymbol{\sigma}_P \cdot \mathbf{S} \cdot \boldsymbol{\sigma}_D = \boldsymbol{\sigma}_D \cdot \mathbf{S} \cdot \boldsymbol{\sigma}_P = 0 \tag{216}$$

Therefore, for the isotropic body **S** the following relationship holds :

$$T(\boldsymbol{\sigma}_P + \boldsymbol{\sigma}_D) = T(\boldsymbol{\sigma}_P) + T(\boldsymbol{\sigma}_D) \tag{217}$$

which indicates that the applied loading $\boldsymbol{\sigma}$ can be split into a spherical and a deviatoric loading.

However, the above sketched spectral decomposition of the elastic energy density is not exclusive only to the elastic isotropic material. It may be extended to a broader category of materials, the *quasi-isotropic materials.* These materials are characterized by the property to possess a value of the eigenangle ω approaching the limiting value for ω_i,valid for isotropic materials (ω_i =125.26°).

Relation (200), expressing the tangent of the double of the eigenangle $\boldsymbol{\omega}$, suggests a particular relationship between E_L , E_T and ν_L , ν_T , in order to yield the angle ω_i=125.26°. This relationship is expressed by :

$$\frac{(1-\nu_L)}{E_L} = \frac{(1-\nu_T)}{E_T} \tag{218}$$

Relation (218) is derived by introducing into relation (200) the value for the

$\tan(2\omega_i)=-2\sqrt{2}$. Indeed, this value for ω_i is the only root for angle ω, yielding positive values for Poisson's ratios, which are, of course, the only acceptable values for Poisson's ratios of usual engineering materials. Introducing eq.(218) into the eigenvalues relations (198) we derive the following eigenvalues for the *quasi-isotropic material*:

$$\lambda_1 = \frac{1}{2G_T} \quad , \quad \lambda_2 = \frac{1}{2G_L} \tag{219}$$

$$\lambda_3 = \frac{1}{2G_L} \qquad \& \qquad \lambda_4 = \frac{(1-2\nu_L)}{E_L}$$

It may be concluded from the above relationships that only the first eigenvalue λ_1 depends on the transverse shear modulus, whereas the remaining three eigenvalues depend exclusively on the longitudinal elastic modulus and Poisson's ratio.

Moreover, the eigentensors $\boldsymbol{\sigma}_m$ of the symmetric stress tensor $\boldsymbol{\sigma}$ are given now by:

$$\boldsymbol{\sigma}_1 = \left[\frac{\sigma_1-\sigma_2}{2}\ ,\ -\frac{\sigma_1-\sigma_2}{2}\ ,\ 0,\ 0,\ 0\ \sigma_{12}\right]^T$$

$$\boldsymbol{\sigma}_2 = \left[0,\ 0,\ 0,\ \sigma_{23},\ \sigma_{13},\ 0\right]^T \tag{220}$$

$$\boldsymbol{\sigma}_3 = \frac{1}{6}\,(\sigma_1+\sigma_2-2\sigma_3)\ [1,\ 1,\ -2,\ 0,\ 0,\ 0]^T$$

$$\boldsymbol{\sigma}_4 = \frac{1}{3}\,(\sigma_1+\sigma_2+\sigma_3)\ [1,\ 1,\ 1,\ 0,\ 0,\ 0]^T$$

Relations (220) indicate that the characteristic states of stress corresponding to the spectral decomposition of the compliance tensor **S** for the transversely isotropic materials, satisfying also the relationship (218) decompose the generic stress tensor $\boldsymbol{\sigma}$ in four distinct states. The three first are either simple, or pure shears, whereas the fourth state ($\boldsymbol{\sigma}_4$) is a hydrostatic stress producing a dilatational strain energy, whereas the strain energies of all the other three components are distortional. Thus, this class of transversely isotropic materials, called *quasi-isotropic materials*, maintains the property of real isotropic substances, which for a certain orientation of loading, admit a clear separation of the total strain energy into two distinct components, a distortional, and a dilatational one.

Furthermore, relations (209) for the class of quasi-isotropic materials, satisfying Eq.(218) become :

$$\mathbf{e}_1 : \left[\frac{1}{\sqrt{2}} , \frac{1}{\sqrt{2}} , 0 \right]^T$$

$$\mathbf{e}_3 : \frac{1}{\sqrt{2}} \left[- \frac{1}{\sqrt{3}} , - \frac{1}{\sqrt{3}} , \frac{2}{\sqrt{3}} \right]^T \qquad (221)$$

$$\mathbf{e}_4 : \left[\frac{1}{\sqrt{3}} , \frac{1}{\sqrt{3}} , \frac{1}{\sqrt{3}} \right]^T$$

Relations (221) indicate that the $\mathbf{e}_1$-tensor represents a shear, the $\mathbf{e}_3$-vector corresponds to a deviatoric strain component, whereas the $\mathbf{e}_4$-vector is a spherical strain-tensor, corresponding to a dilatational mode of deformation. For this frame of eigenvectors the angles subtended by the respective vectors and the $\boldsymbol{\sigma}_3^*$-principal stress direction are : (i) for the $\mathbf{e}_3$-vector the angle is 35.25° and (ii) for the $\mathbf{e}_4$-vector the angle is 54.74°. This means that the direction of the $\mathbf{e}_4$-vector coincides with the positive hydrostatic axis.

Moreover,the components of the stress tensor $\boldsymbol{\sigma}_m$ in the principal stress frame (0- σ_1, σ_2, σ_3) and the total elastic strain energy density are deduced from relations (210) and (211) respectively, and they are given by :

$$\bar{\sigma}_1 = \left[\frac{1}{2}(\sigma_1 - \sigma_2) \left(\frac{1}{\sqrt{2}} , - \frac{1}{\sqrt{2}} , 0 \right)^T \right]$$

$$\bar{\sigma}_3 = \left[\frac{1}{6}(\sigma_1 + \sigma_2 - 2\sigma_3) (1, \ 1, \ -2)^T \right] \qquad (222)$$

$$\bar{\sigma}_4 = \left[\frac{1}{3}(\sigma_1 + \sigma_2 + \sigma_3) (1 , \ 1 , \ 1)^T \right]$$

The total elastic strain energy density is then expressed by :

$$2T = \left\{ \frac{1+\nu_T}{4E_T} (\sigma_1 - \sigma_2)^2 + \right\}$$

$$+\left[\left(\frac{(1-\nu_T)}{2E_T}+\frac{1}{2E_L}\right)-\left(\left[\frac{1-\nu_T}{2E_T}-\frac{1}{2E_L}\right]^2-\frac{2\nu_L^2}{E_L^2}\right)^{1/2}\right]\left[\frac{1}{36}(\sigma_1+\sigma_2-2\sigma_3)^2\right]+$$

$$+\left[\left(\frac{(1-\nu_T)}{2E_T}+\frac{1}{2E_L}\right)+\left(\left[\frac{1-\nu_T}{2E_T}-\frac{1}{2E_L}\right]^2-\frac{2\nu_L^2}{E_L^2}\right)^{1/2}\right]\left[\frac{1}{9}(\sigma_1+\sigma_2+\sigma_3)^2\right] \quad (223)$$

In relation (223) the two first terms represent distortional strain-energy components, whereas the third one is a dilatational one.

Then, all the advantages valid for the isotropic materials, are extended to this class of transversely isotropic substances, besides the particular properties derived from the anisotropy of the material.

The possibilities of modern technology to create new composite materials by acting upon the selection of the particular elastic moduli of the reinforcements and the matrix and choosing the appropriate density of inclusions, allowed to form a series of new composites with selected mechanical and other physical properties convenient for special uses in industry. For this procedure, the definition of the particular eigenangle $\boldsymbol{\omega}$ of the composite plays an important role, since it constitutes *the criterion* for the proper selection of the composite. It has been shown that composites with eigenangles lying at the vicinity of the critical value for the eigenangle, ω_i, for the isotropic materials [100] behave like *quasi-isotropic* materials, with equilibrated properties along the principal axes of anisotropy, fact which has a direct influence on an increase of the adhesion between phases and therefore an increase of their toughness.

Furthermore, it has been proved in a recent study [106] that the possibility of disposing orthotropic plates with particular properties interconnecting their mechanical properties improves considerably their mechanical behavior, by reducing drastically the stress concentration factors in discontinuities (holes or cracks) existing eventually in the structures. These stress concentration factors are considerably reduced when the respective composite has properties approaching the respective values for isotropic materials [106]. Then, it is worthwhile seeking convenient types of composites, which, not only are highly reinforced by their anisotropy, but also they are favorably designed to develop the lowest possible stress concentration factors at eventual discontinuities of structures made of these materials. It was further indicated that the minimum of such concentration factors can be achieved by the respective

isotropic material, if such a material existed with the same mechanical properties of the respective anisotropic material.

Since for modern composites a vast possibility exists to arrange conveniently the selection of the quantities and the properties of their constituent phases, it becomes feasible to produce convenient composites approaching this simple condition (218). Then, for quasi-isotropic composites it is possible to split the total elastic strain energy into a distortional and a dilatational component, a property which has beneficial repercursions in designing optimal structures. Indeed, it has been shown previously [106] that such materials, whose properties approach those of an isotropic material, present very reduced stress-concentration and stress-intensity factors. Thus, a structure made of such materials presents a superiority over a similar one made by a strong anisotropic composite, since for the same mode and intensity of loading the first type of structure can hold much larger loadings.

It seems that this phenomenon has been detected intuitively by the designers of advanced research centers based on their long experience in practical applications, since they have established by a long practice and a trial and error procedure, that it is advantageous to introduce in structures convenient materials, whose elastic constants approach better relation (218). Indeed it has been shown that the values of the eigen-angle ω in modern strong-matrix composites, approach the critical value ω_i for the isotropic materials, in contrast to the old glass-epoxy or graphite-epoxy composites, whose angles ω approach the limiting value $\omega=90°$. Reference [107] gives the variation of the $E_L/2G_L$-ratio versus the eigenangle ω for a large number of tested fiber reinforced materials which was plotted in a universal diagram. This figure is here reproduced as Fig.52. It is clear from this figure that, as the ω-angle recedes from $\omega_i=125.26°$ to its limits $\omega=90°$ or 180°, the values of the $E_L/2G_L$-ratio increase asymptotically, indicating that the respective composites present a very high SCF at holes or cracks thus behaving very anisotropically [106].

On the contrary, strong matrix composites present values of ω in the intermediate zone, where the variation of the $E_L/2G_L=f(\omega)$ is smooth and almost flat indicating a quasi-isotropic behavior. Similarly, woven-fabric composites lie to the left of the ω_i-value and in the zone of almost constant ω-values, indicating again their quasi-isotropic behaviour. Indeed, the transversely isotropic materials with a weak σ_3-principal stress axis, which correspond to composites with eigenangles ω varying between 90° and 125.26°, in which all the woven fabric materials are included, present a direction of slenderness along the σ_3-principal stress axis. Again, the values, for this group of materials given in table 4 for $k= 1/\sqrt{\lambda_1}$ are always larger than the respective values of the other transverse principal semi-axis $m=1/\sqrt{\lambda_3}$. Figure 53 presents the B-T ellipsoids for two typical substances, the glass-epoxy woven fabric composite with $v_f=0.50$ in simple weave, which behaves like a quasi-isotropic material (IR=1.00) and the compression annealed pyrolytic graphite, whose eigenangle is equal to $\omega=90.84°$, thus approaching the lower limit of its variation [108].

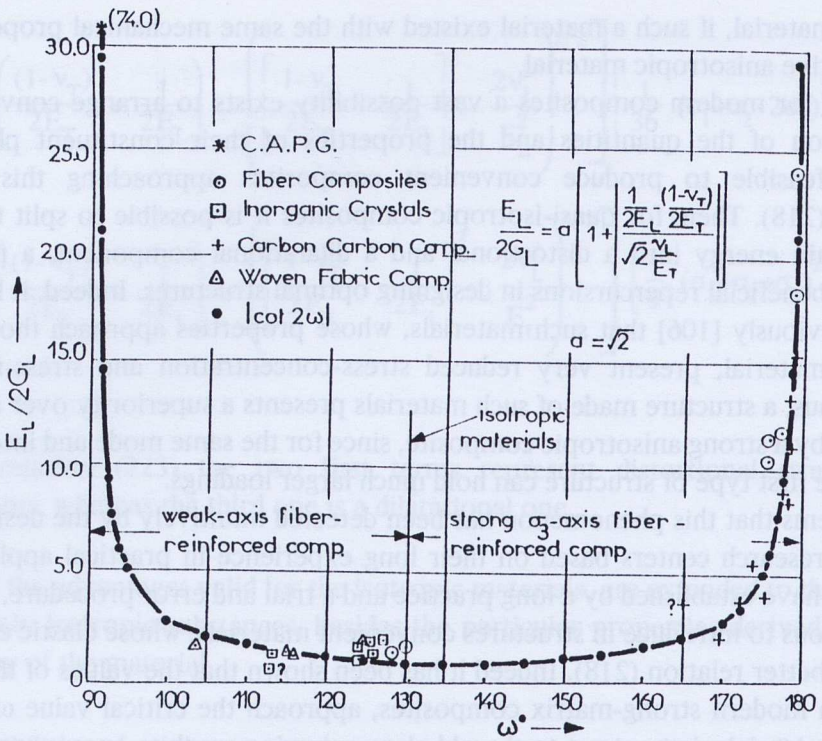

Fig. 52 - The variation of the $E_L/2G_L$-ratio for a series of transversely isotropic materials versus their eigenangle ω and the well-fitting curve expressed by $E_L/2G_L=\sqrt{2}[1+|\cot 2\omega|]$.

In Figures 51 and 53 both principal intersections of each ellipsoid were plotted together by rotating the intersections by the $0\sigma_1\sigma_2$-plane by an angle of $\pi/2$ so that this plane will coincide with the $0\sigma_2\sigma_3$-principal plane. The ratios of the respective semi-axes $0\sigma_3$ and $0\sigma_1$ represent the slenderness of each ellipsoid. It is worthwhile indicating that the last column in table 4 presents the values of the slenderness s for the different materials examined in this table. While the slenderness for the category of materials lying in the range $125.26°<\omega<180°$ is smaller than unity, the slenderness of materials in the range $90°<\omega<125.26°$ is higher than unity. Moreover, it is clear from table 4 that the values of slenderness in the range $90°<\omega<125.26°$ increase rapidly at the zone near the limit of 90°, whereas in the range $125.26°\leq\omega\leq180°$ the slenderness remain constant with smaller variations. Thus, for the compression annealed pyrolytic graphite s=4.63, whereas for Thornel 75s graphite- epoxy with $\omega=178.57°$, s=0.548.

Thus, the possibility of decomposing spectrally either the elastic stiffness, or compliance, or failure tensors in elementary fourth-rank tensors allowed an energy orthogonal decomposition of the stress tensor for transversely isotropic bodies. The powerful properties of the spectral decomposition allowed, among others, to extend the advantageous properties of linearity and coincidence of the components of

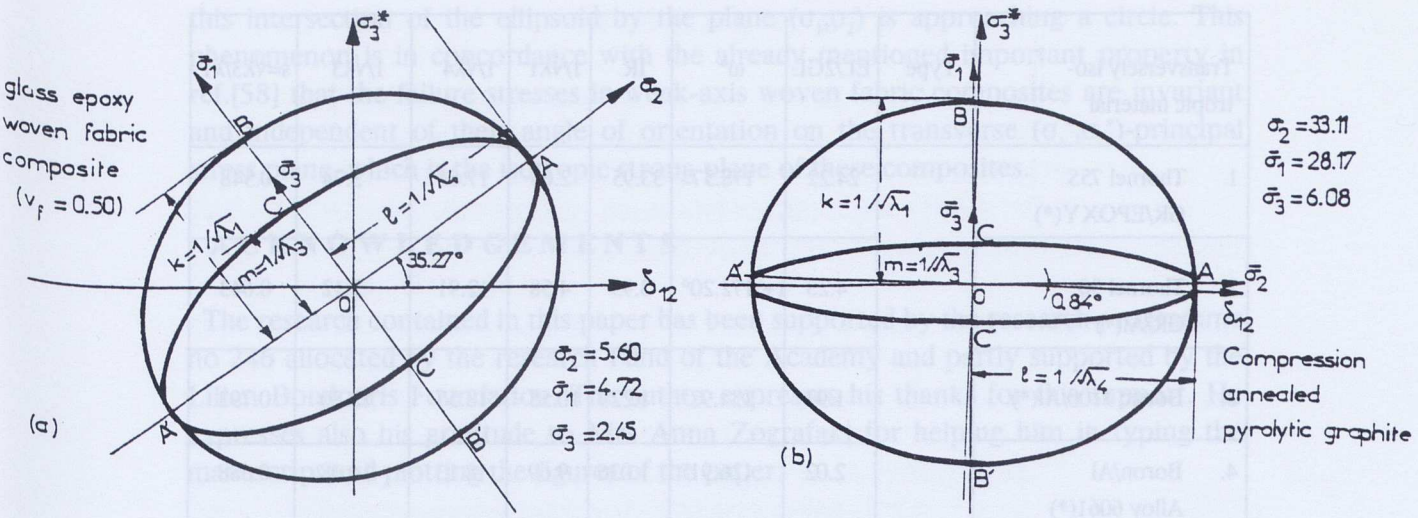

Fig. 53 - The normalized to total strain energy 2T(B-T) strain-energy ellipsoids for a weak-axis woven fabric composite with ω=125.26° and the compression annealed pyrolitic graphite with ω=90.84° (Planes (σ_1,σ_2) are folded up by $\pi/2$ to coincide with (σ_2,σ_3) planes).

principal stresses and strains, holding up-to-now only for isotropic materials, to a broader category of transversely isotropic materials.

By exploiting the advantages of spectral type decomposition of the fourth-rank tensor, a privileged Cartesian frame was defined by the three *indempotent tensors* of the fourth-rank strain tensor. In this system the total elastic strain energy, is represented by an ellipsoid having as center the origin of the coordinates 0 and lengths of the three principal semi-axes the inverse square roots of the respective eigenvalues of the strain tensor. The longest principal semi-axis of the strain-energy ellipsoid, called B-T ellipsoid, is always the σ_3-axis, which subtends with the negative σ_3^*-axis an angle ω equal to the respective eigenangle of the material. This strain energy ellipsoid degenerates into the Beltrami ellipsoid valid for isotropic materials. Thus, the notion of the total elastic strain energy ellipsoid, valid up-to-now only for isotropic materials, was extended through the B-T ellipsoid for all transversely isotropic materials.

Finally, an interesting property concerning the materials, whose eigenangles ω are included in the interval $90°<\omega<125.26°$, is derived from the values of the lengths of the principal semi-axes of the B-T ellipsoids and the representations in Figs. 53. It is clear from these results that the variation of the total elastic strain energy along the (σ_1,σ_2)-plane, which is normal to the principal (σ_3^*,δ_{12})-diagonal plane and consequently to the (σ_3,σ_2)-plane, is generally insignificant and therefore the shape of

Transversely isotropic material	Type	EL/2GL	ω°	IR	$1/\sqrt{\lambda 1}$	$1/\sqrt{\lambda 4}$	$1/\sqrt{\lambda 3}$	$s=\sqrt{\lambda 3}/\lambda 1$
1. Thornel 75S GR/EPOXY(*)		24.22	178.57°	33.95	2.05	17.68	3.74	0.548
2. Thornel 50 GR/Al(*)		4.23	(+)172.20°	3.95	4.58	12.91	7.12	0.643
3. Borsic 1100/Al(*)		1.93	134.92°	1.229	10.55	18.57	13.30	0.793
4. Boron/Al Alloy 6061(*)		2.02	126.91°	1.036	9.69	18.13	14.08	0.688
5. Water (-16°C)(*)	element	1.85	125.26°	1.00	2.60	5.20	2.53	1.00
6. Glass-Epoxy(**) (υf=0.50),ω=125.27°		1.66	125.27°	1.00	4.72	5.60	2.45	1.927
7. Glass/Epoxy (ω=114.96°)(**)		1.27	114.96°	0.49	4.29	8.81	3.45	1.243
8. T300 Gr-Epoxy (5208)(**)		1.36	114.20°	0.15	5.94	6.33	2.08	2.856
9. Glass/Epoxy (**)		1.93	103.45°	0.315	4.38	6.58	3.10	1.413
10. Comp.Annealed(*) Pyrolytic Graphite	element	74.00	90.84°	0.034	28.17	33.11	6.08	4.633

(+) corrected value for $\nu_L=0.21$

Table 4 - The values for the eigenangle ω, the ratios $E_L/2G_L$ and $IR=(1-\nu_T)E_L/(1-\nu_T)E_T$ and the lengths of the principal semi-axes of the respective B-T total elastic strain energy ellipsoids for a series of composites.

this intersection of the ellipsoid by the plane (σ_1,σ_2) is approaching a circle. This phenomenon is in concordance with the already mentioned important property in ref.[58] that the failure stresses in weak-axis woven fabric composites are invariant and independent of their angle of orientation on the transverse (σ_1^*,σ_2^*)-principal stress plane, which is the isotropic strong plane of these composites.

ACKNOWLEDGEMENTS

The research contained in this paper has been supported by the research programme no 246 allocated by the research Fund of the Academy and partly supported by the Lilian Boudouris Foundation. The author expresses his thanks for this support. He expresses also his gratitude to Mrs Anna Zografaki for helping him in typing the manuscript and plotting the figures of the paper.

REFERENCES

[1] M.T.Huber, Czasopismo Techniczne, Vol.**22**, (1904), 81.

[2] R.von Mises, Nachr.Göttingen Akad. Wiss., Math-physik. Kl., (1913), 582.

[3] F. Schleicher, Zeitsch. ang. Math. und Mech., Vol.**5**, (1925),478.

[4] H.Hencky, Zeitsch. ang. Math. und Mech., Vol.**4**, (1924), 323.

[5] H.Tresca, Compt. Rendus hebd. Acad. Sci., Paris, Vol.**59**, (1864), 754 and Vol.**64**, (1867), 89.

[6] R.Hill, *Mathematical Theory of Plasticity,* Oxford at the Clarendon Press, (1956).

[7] C.A.Coulomb, Mémoires de Mathématiques et de Physique,Acad,Roy. des Sciences par divers savants, Vol.**7**, (1773), 343.

[8] O. Mohr, Zeitsch.Verein Deutsch-Ing., Vol.**44**, (1990), 1254.

[9] B.Paul, Intern.Jnl.Sol.Struct., Vol.**4**(2), (1968),175.

[10] N.W.Tschoegl, Jnl. Polymer Sci.,Part C, Polymer Symposia 32, H.H.Kausch Editor, Interscience, N.York, (1971), 239.

[11] P.S.Theocaris, Theoretical and Applied Mechanics (Theoretichna i Prilojnia Mekhanika), Proc. Bulg. Acad. Sciences, Vol.**19**, (1987), 74.

[12] A. Nadai, 2nd Edition McGraw-Hill, N.York, (1950), 207.

[13] D.C.Drucker, Jnl. Mech.Phys. Solids, Vol.**1**, (1953), 217.

[14] P.S.Theocaris and J. Prassianakis, Magazine for Concr. Res, Vol.**26**(87), (1974), 73.

[15] L.F.Coffin Jr., Jnl. Appl. Mech., Vol.**17**, No. 3, (1950), 233 ; see also : R.C. Grassi and I. Cornet, Jnl. Appl. Mech., Vol. **16**, (1949),178.

[16] G.I.Taylor and H.Quinney, Phil. Trans. Roy.Soc. London, Ser. A, Vol. **230**, (1931), 323.

[17] W.Lode, Zeitsch.der Physik, Vol.**36**, (1926), 913.

[18] P.S.Theocaris, Intern.Jnl.Mech.Sci., Vol.**18**, No.4, (1976), 171.

[19] W. Spitzig., A.R.J.Sober and O.Richmond, Acta Metallurgica, Vol.**23**, (1975), 885.

[20] J.C. Bauwens, Jnl.Polymer Sci., A-2, Vol.**5**, (1967), 1145.

[21] S. Sternstein and L. Ongchin, A.C.S. Polymer Rep. Vol.**10**, (1969),1117.

[22] R. Raghava, R.M. Caddell and G.S.Y.Yeh, Jnl. Mat.Sci., Vol.**8**, 225-232, (1973).

[23] W.A.Spitzig and O.Richmond, Polymer Engng. and Sci., Vol.**19**, No.16, (1979), 1129.

[24] D.C.Drucker and W. Prager, Quart. Appl. Math., Vol.**10**, (1952), 157.

[25] F.Stassi, F.d'Alia, Meccanica, Vol.**3**, (1967),178.

[26] E. E. Thotokoglou, G. Tsamasphyros and P. S. Theocaris, Materials Sic. Monographs No 21. Interrelations between Processing, Structure and Properties of Polymeric Materials, J. C. Seferis and P. S. Theocaris Editors, Elsevier Publ., (1984), 423.

[27] F. McClintock, Jnl.Appl.Mech., Trans. ASME, Vol.**35**, No.2, (1968), 363.
[28] A.L.Gurson, Jnl.Engng.Mat.and Technology, Vol.**99**, (1977), 2.
[29] L.M. Brown and J.D. Embury, 3rd Int. Conf. of Strength of Metals and Alloys, Inst.of Metals, London, (1973), 164.
[30] P.S. Theocaris, Int. Jnl. Solids and Struct., Vol.**22**, (4), (1986), 445.
[31] P.S. Theocaris, *Mechanics of Fracture*, Vol.VII, G.C.Sih Editor, Martinus Nijhoff Publ., Hague, Chapt.3, (1981), 189.
[32] R.J. Bourcier and D.A.Koss, Proc. Fifth Int.Congr. Fract., Cannes, France 1981, D.Francois Editor, Pergamon Press, Oxford Publ., Vol.I, (1981), 187.
[33] V. Nagpal, F. McClintock, C.A. Berg and M. Subudhi, Proc. Intern. Symp. on Foundations of Plasticity, A. Sawczuk Editor, Vol. I, (1973), 365.
[34] A.L. Gurson, Proc. 4th Int. Conf. Fracture, D.Taplin Ed., Pergamon Press, Vol.2A, (1977), 357.
[35] V. Tvergaard, Intern. Jnl. Solid 1 and Struct., Vol. **30** (4), (1982), 265.
[36] P.S. Theocaris, Proc. Nat. Acad.Athens, Vol.**58**(1), (1983), 641.
[37] P.S. Theocaris, Meccanica, Vol.**21** (2), (1986), 97.
[38] O. Hoffman, Jnl. Comp. Mat., Vol. **1**, (1967), 200.
[39] S.W. Tsai and E.M. Wu, Jnl. Comp. Materials, Vol. **5**, (1971), 58.
[40] P.W. Bridgman, *Studies in Large Plastic Flow and Fracture with Special Emphasis on the Effects of Hydrostatic Pressure,* Mac Graw Hill Book Co., N. York, (1952).
[41] R. Hill, Proc. Royal Soc. London, Ser. A, Vol. **193**, (1948), 281.
[42] P.S. Theocaris, Proc. Nat. Acad. Athens, Vol. **61**, (1986), 84.
[43] P.S. Theocaris, Advances in Mechanics, (Uspechi Mekhanikii), Vol.**10**, (1987), 83.
[44] P.S. Theocaris, Proc. Nat. Acad. Athens, Vol.**62**, (1987), 129.
[45] P.S. Theocaris and T. Philippidis, Jnl. Reinf. Plast. & Comp., Vol.**6**, (1987), 378.
[46] P.S. Theocaris, Proc. Intern. Conf. on Meas. of Static and Dyn. Parameters of Struct. and Mat., Pilzen Checol. Vol. **2**, (1987), 547.
[47] P.S. Theocaris, Rheologica Acta, Vol. **27**, (1988), 451.
[48] P.S. Theocaris, Proc. Third Conf. on Composite Materials (Amer. Soc. Comp. U.S.A.), Vol. **1**, (1988), 451.
[49] P.S. Theocaris, Jnl. Reinf. Plast. Comp., Vol. **8**, (1989), 451.
[50] P.S. Theocaris, Engn. Fract. Mech., Vol. **33**, (1989), 451.
[51] P.S. Theocaris & T. Philippidis, Intrn. Jnl. Fract. ; Reports on Current Res., Vol.**41** R6, (1989).
[52] P.S. Theocaris, Proc. of Prof. Kouyoumtzelis' anniversary volume, **1**, 25, (1989).
[53] P.S. Theocaris, Jnl. Mat. Science, Vol. **25**, (1990), 1076.
[54] P.S. Theocaris, Durability of Polymer Based Comp. Systems for Struct. Appl., A.Cardon & G. Verchery Edit., Elsevier Appl. Sci. Publ., London, (1991), 169.

[55] P.S. Theocaris, Acta Mechanica, Vol. **89**, (1991), 93.
[56] P.S. Theocaris, Advances in Polymer Technology, Vol. **11**, (1991), 27.
[57] P.S. Theocaris, Acta Mechanica, Vol. **92**, (1992), 35.
[58] P.S. Theocaris, Acta Mechanica, Vol. **95**, (1992), 69.
[59] P.S. Theocaris, Int. Jnl. of Fracture, Vol. **56**, (1992), 353.
[60] P.S. Theocaris, Int. Jnl. Damage Mechanics, Vol. **1**, (1992), 4.
[61] P.S. Theocaris, Proc. Third Panhellenic Congr. Theor. & Appl. Mech. Vol.**1** (1992).
[62] P.S. Theocaris, Acta Mechanica, Vol. **96**(2), (1993), 163.
[63] P.S. Theocaris, Acta Mechanica, Vol.**97**, (1993) in print.
[64] P.S. Theocaris, Polymers and Polymer Composites, Vol.**1**(1), (1993), 3.
[65] P.S. Theocaris, Composites Science and Technology, Vol.**42** (1993) in print.
[66] P.S. Theocaris, Proc. 8th Intrn. Conf. on Fract., Kiev, Ukraine (1993).
[67] P.S. Theocaris, Int. Jnl. Composites Engng., (1994), in print.
[68] P.S. Theocaris, Acta Mechanica, Vol.**79**, (1989), 53.
[69] P.S. Theocaris, Rheologica Acta, Vol.**28**, (1989), 154.
[70] P.S. Theocaris, Proc. Nat. Acad. Athens, Vol.**64**, (1989), 80.
[71] P.S. Theocaris, Proc. Nat. Acad. Athens, Vol.**64**, (1989), 298.
[72] R. von Mises, Zeitsch. ang. Math. & Mech., Vol. **8**, (1928), 161.
[73] P.W. Bridgman, Mechanical Engineering, 107, (Febr. 1939).
[74] R.M. Caddell and A.R. Woodliff, Jnl. Mat. Sci., Vol.**12**, (1977), 2028.
[75] E.M. Wu, *Mechanics of Composite Materials*, Edited by G.P.Sendeckyj, Academic Press, N.York, Vol.**2**, Chapter 9, (1974), 353.
[76] E.M. Wu, Jnl. Comp. Mat., Vol.**6**(5), (1972), 472.
[77] P.S. Theocaris and T. Philippidis, Comp. Sci. & Techn., Vol. **40**(2), (1991), 181.
[78] F.J. Murnagham, *Analytic Geometry,* Prentice Hall Inc., N.York, (1946).
[79] R.M. Caddell and J.W. Kim, Int. Jnl. Mech. Sci., Vol.**23**(2), (1981), 99.
[80] S.W.Tsai and H.T. Hahn, *Introduction to Composite Materials*, Lancaster Penn. Technomik (1958).
[81] R. Narayanaswami and H.M. Adelman, Jnl. Comp. Mat., Vol.**11**, (1977), 366.
[82] P.S. Theocaris, Engn. Fract. Mech., Vol.**33**(3), (1989), 335.
[83] P.S. Theocaris, Acta Mechanica, Vol. **77**(1-2), (1989), 69.
[84] P.S. Theocaris, Jnl. Reinf. Plast. & Comp., Vol.**8**(6), (1989), 565.
[85] R.B. Pipes and B.W. Cole, Jnl. Comp. Mat., Vol.**7**, (1973), 246.
[86] E.M. Wu and J.K. Scheublin, in *Composite Materials : Testing and design,* ASTM STP 546, ASTM Publ., Phil. USA, (1974), 186.
[87] P.S. Theocaris, Engn. Fract. Mech., Vol. **33**, (1988),185.
[88] P.S. Theocaris and T. Philippidis, Zeit. angw. Math. & Mech., Vol. **72**(11), (1992), 549.
[89] P.S. Theocaris and T. Philippidis, Comp. Sci. & Techn., Vol.**40**(2), (1991), 181.
[90] P.S. Theocaris and T. Philippidis, Proc. 3rd Intern. Symp. "COMP 90" AMATEC Publ., Patras Greece, (1991), 89.

[91] S.W. Tsai, Proc. Euromech. Coll. 115, *Mechanical Behavior of Anisotropic Solids*, J.P. Boehler ed., Nijhoff Hague, 435.
[92] R.S. Raghava and R.M. Caddell, Jnl. Mat. Sci., Vol.**12**, (1977), 2028.
[93] J.F. Nye, *Physical properties of crystals : Their representation by tensors and matrices,* Oxford at the Clarendon Press (1957).
[94] T.P. Srinivasan and S.D. Nigam, Jnl. Math. and Mech. Vol.**19**(5), (1969), 411.
[95] L.J. Walpole, Proc. Roy. Soc. London, Vol.**A391**, (1984), 149.
[96] J. Rychlewski, Prikl. Matem. i Mekh., Vol.**48**(3), (1984), 303.
[97] J. Rychlewski, Advances in Mechanics (Uspechi Mekhanikii), Vol.**10**(3), (1987), 83.
[98] P.S. Theocaris, Proc. Nat. Acad. Athens, Vol.**64**(1), (1989), 80.
[99] P.S. Theocaris and T.P. Philippidis, Archives of Mechanics (Archiwum Mekh. Stosowanej) Vol.**41**(5), (1989), 717.
[100] P.S. Theocaris and T.P. Philippidis, Acta Mechanica, Vol.**85**(1), (1990), 13.
[101] P.S. Theocaris and T.P. Philippidis, Zeit. angew. Math. & Mech., Vol.**71**(3), (1991), 161.
[102] W. Olszak and W. Urbanowski, Arch. Mekh. Stos., Vol.**8**, (1956), 671.
[103] W. Olszak and J. Ostrowska-Maciejewska, Engn. Fract. Mech., Vol.**21**(4), (1985), 625.
[104] E. Beltrami, Opere Matematice IV (1920) : see also Rendiconti del R. Istituto Lombardo di Scienze Lettere e Arti, Vol.**18**, (1885), 704.
[105] R.P. Haigh, Engineering CX, (1920), 158.
[106] P.S. Theocaris and T.P. Philippidis, Acta Mechanica, Vol.**80**(2), (1989), 95.
[107] P.S. Theocaris, Acta Mechanica, Vol. **96**(2), (1993), 163.
[108] P.S. Theocaris, Acta Mechanica, Vol. **97**(2), (1993), 75.